THE UNIVERSITY OF MANITOBA

AN EXPERIMENTAL AND THEORETICAL STUDY OF TRANSIENT LIQUID PHASE BONDING OF NICKEL BASED MATERIALS

BY

MOHAMED ABDELFATTAH

A thesis submitted to the Faculty of Graduate Studies in partial fulfilment of the requirements for the degree of Master of Science

DEPARTMENT OF MECHANICAL AND MANUFACTURING ENGINEERING
WINNIPEG, MANITOBA
2008

An Experimental and Theoretical Study of Transient Liquid Phase Bonding of Nickel Based Materials

BY

Mohamed Abdelfattah

A Thesis/Practicum submitted to the Faculty of Graduate Studies of The University of Manitoba in partial fulfillment of the requirement of the degree

Of

MASTER OF SCIENCE

Acknowledgements

I would like to acknowledge my supervisor Dr. O. A. Ojo whose help and counselling has been paramount in my understanding, and whose advice and support have guided me through this journey. His patience and guidance will forever be appreciated. I would like to thank Dr. M.C. Chaturvedi for allowing me to use his laboratory facility. I would also like to thank Dr. N.L. Richards, Dr. J. R. Cahoon, Dr. R. Sidhu, and all the members of the metallurgical lab at the University of Manitoba.

I acknowledge the financial support for this research provided by the University of Manitoba. I would like to also thank John Van Dorp and Don Mardis for their technical assistance.

Abstract

This thesis reports theoretical and experimental investigations carried out to better understand the effects of process parameters on the microstructure of transient liquid phase (TLP) joint, particularly, to study the cause of a previously reported anomalous increase in processing time with increase in temperature. The theoretical investigations were carried out using analytical and numerical models to simulate base metal dissolution and isothermal solidification stages of the TLP bonding process. The experimental investigation was carried out by using standard metallographic technique to study the microstructure of bonded materials using optical and scanning electron microscopes.

Deviation from parabolic relationship between solid/liquid interface migration and holding time during TLP bonding is suggested as a new alternate phenomenon responsible for the anomalous increase in processing time required to produce eutectic-free joint with increase in bonding temperature. The results of TLP joining of commercial pure nickel using a Ni-P filler alloy showed that an increase in bonding temperature would be beneficial provided that sufficient holding time is allowed for complete isothermal solidification of liquated insert. Otherwise, an increase in bonding temperature may result in formation of thicker deleterious eutectic along the TLP joint. Furthermore, it was observed that the joint centerline eutectic product and interface second phase particles that form during TLP bonding of Inconel 738 using a Ni-P filler alloy can be significantly reduced by post bond heat treatment. The effectiveness of this approach, however, requires proper selection of heat treatment temperature above Ni-P binary eutectic temperature.

Table of Contents

Chapter 4: Results and Discussion

Part I: Extension of Isothermal Solidification Completion Time with Increase in Bonding Temperature

Part II: Influence of Process Parameters on Microstructure of TLP Bonded Joint Using Phosphorous Bearing Filler Alloy

List of Figures

List of Tables

Chapter 1: Introduction

Aircraft and land-based power generation turbine engines are designed to perform effectively at severe operating conditions, which require proper selection of materials for producing the engine components. Increased demand for higher efficiency, which requires the engines to operate at higher temperatures has led to rapid degradation of engine parts due to creep, fatigue and oxidation among others. Nickel-based superalloys are used extensively in the manufacture of turbine engines due to their excellent elevated temperature strength and corrosion resistance [1]. They, however, degrade during service due to harsh operating condition. As a result, significant effort has been made to develop repair techniques for damaged components made of these alloys including conventional methods such as fusion welding. Nickel-based superalloys containing a significant amount of titanium and aluminum, however, have been found difficult to weld due to their high susceptibility to hot cracking during welding and post-weld heat treatment [2]. As a result, Duval et. al. [3] have developed the transient liquid phase (TLP) bonding process, also known as diffusion brazing, which combines the beneficial features of liquid phase joining and diffusion bonding technique for joining difficult-to-weld supersalloys. The process has evolved into an attractive joining technique due to its technological and economical advantages such as significant reduction of pressure required during bonding compared to solid-state diffusion bonding.

In TLP bonding process, an interlayer alloy containing a melting point depressant element such as boron, silicon or phosphorous, melts between two base metals that are to be joined. Subsequent to melting of the filler alloy, base metal dissolution occurs

resulting in rapid displacement of the liquid-solid interface. The liquid phase rapidly attains equilibrium with the solid base metal and inter-diffusion of alloying elements between the base metal and the liquid occurs resulting in increase in the melting point of the interlayer liquid that results in isothermal solidification of the liquid. As isothermal solidification progresses, the liquid present at the joint decreases and the liquid-solid interface recedes to the center of the joint. If sufficient holding time is provided, complete isothermal solidification of the liquid and homogenization of the joint with the base metal could occur. Insufficient holding time for complete isothermal solidification will result in residual liquid interlayer transformed into eutectic-type microconstituents at the joint centerline. These microconstituents are brittle in nature and have been found to reduce mechanical properties of bonded materials [4].

Holding time required to achieve complete isothermal solidification depends on certain process parameters such as bonding temperature, initial gap size, and type of filler alloy. Proper selection of process parameters is, therefore, paramount in optimizing the bonding process and achieving reliable TLP bonded joints. In addition to the bonded part having optimum mechanical properties, an efficient and economical bonding process is desired. Proper process parameter selection and minimization of bonding times will reduce component repair duration and labor time which could translate into significant cost reduction. In some instances where it becomes practically impossible to obtain eutectic free joint in realistic holding time, the use of post-bond heat treatments to modify the joint's microstructure has been suggested [5].

Despite the significant potential benefits of the TLP process, its commercial applications are rather limited. This is due to insufficient understanding of various process parameters on the microstructure of TLP joint. Therefore, the objective of the present research was to perform theoretical and experimental study of TLP bonding of nickel based materials to advance the understanding of influence of process parameters on microstructure of TLP bonded materials.

The first part of this work reports the results of theoretical and experimental investigations carried out to better understand the causes of a previously reported anomalous behaviour of prolonged isothermal solidification completion time with increase in temperature during transient liquid phase (TLP) bonding. The study was carried out using Inconel 738 superalloy as the base metal and MBF80 (Ni-Cr-B) as the filler alloy. Contrary to conventional TLP bonding analytical models, which assume a parabolic relationship between solid/liquid interface migration and holding time, deviation from this law was observed experimentally and by numerical simulation. This deviation is suggested as a new alternate phenomenon for the anomalous extension of holding time required to produce eutectic free joint with increase in bonding temperature. Increased extent of this deviation was found to be related to decrease in the rate of change of the solute concentration gradient in the base metal beyond a critical value. The study showed that decreasing certain process parameters such as initial filler alloy thickness, initial concentration of the MPD solute in the filler, and the use of a filler alloy having a MPD element with high solubility in the base metal could reduce the extent of deviation and, as a result, increase the critical bonding temperature above which increase in isothermal solidification completion time occurs.

The second part of this thesis is focused on the effect of process parameters, such as filler alloy thickness, bonding temperature and time, on the microstructure of TLP joint using a phosphorous-containing filler alloy. Using commercially pure nickel as the base metal, insufficient time for complete isothermal solidification resulted in formation of centerline eutectic along the joint. SEM EDS and X-ray line scans across the eutectic showed significant segregation of phosphorous into the centerline microconstituent. An increase in average width of the eutectic constituent from 17 μm to 27 μm was observed with an increase in initial thickness of the filler alloy from 38 μm to 76 μm. Two different effects of bonding temperature on the centerline eutectic product were observed. At short holding time of 1 h, an increase in temperature from 1100 °C to 1180 °C resulted in increased eutectic thickness from 22 μm to 32 μm due to increased base metal dissolution while longer holding time of 24 hrs at 1180 °C produced reduction in eutectic width compared to 1100 °C owing to higher diffusivity effect.

The third part of the thesis is focused on the effects of post-bond heat treatment temperature and holding time on the microstructure of TLP bonded Inconel 738 superalloy with Ni-P filler alloy. No significant change in the average size of eutectic microconstituent and interface second phase particles that formed in the alloy during TLP bonding was observed at post-bond heat treatment temperature below the Ni-P eutectic temperature of 870 °C. While an increase in holding time and temperature resulted in reduced centerline eutectic, noticeable decrease in the number density of the interface precipitates was only observed by an increase in temperature. The difference in the responses of the eutectic and interface precipitates to post-bond heat treatment parameters can be related to their mode of formation during TLP bonding.

Chapter 2: Literature Review

The physical metallurgy of nickel-based superalloys is both complex and sophisticated, and the development of these superalloys came out of a need to produce elevated temperature materials with remarkable tensile strength, creep rupture strength, corrosion and oxidation resistance as required in gas turbine engine applications [1]. Components made from these materials, however, often suffer degradation over time due to their use in stringent environments. Repair processes such as conventional welding has proved ineffective for precipitation hardened nickel-base superalloys due to their high susceptibility to heat affected zone (HAZ) cracking [2]. Transient Liquid Phase (TLP) bonding has evolved as potential alternative joining technique for these materials. This chapter reviews the literature on physical metallurgy of the nickel-based super alloy used in this work, Inconel 738 (IN738), and reviews the techniques used to join heat resistant alloys.

2.1 Overview of the Base Materials

2.1.1 Microstructure of as-cast Inconel 738

Inconel 738 (IN738) is a nickel based superalloy developed to provide gas turbine engine components with excellent creep strength at high temperatures and it is capable of withstanding hot corrosion in aircraft turbine engine environment [6]. The alloy is vacuum melted and cast to prevent the formation of voids which can be initiated by the introduction of gases. It is usually available in either low or high carbon versions and the low carbon version contains some amount of Zr that increases castability of larger sections [7].

The microstructure in IN738 is complex due to the large amount of alloying elements in it and the process by which it is normally produced; that is investment casting. The microstructure consists of precipitation of γ' in a γ matrix, carbides, and possible topologically close packed (TCP) phases such as σ in long-term service exposed materials. [7].

The high strength of IN738 is derived primarily by the precipitation of ordered Ll_2 intermetallic $Ni_3(Al, Ti)$ – type γ' phase in austenitic γ solid-solution matrix and also by carbides at the grain boundaries. Alloying elements play a major role in its properties where concentrations of Mo, Ta, W, Cr, Co and Re add solid solution strengthening to the superalloy. Its relatively high Co content increases the ability of the alloy to form γ' phase which is obtained by the addition of Al and Ti [6]. Table 2.1 lists the nominal composition of Inconel 738.

2.1.1.1 Gamma matrix (γ)

The matrix of IN738 is an FCC solid solution γ phase and it acts as a medium for the dispersion of ordered $Ni_3(Al, Ti)$-type γ' precipitates as well as carbides and other phases [7]. The common solid solution elements in the γ phase include cobalt, iron, chromium, molybdenum, tungsten, titanium and aluminum [8].

The γ matrix gains some of its strength by solid solution strengthening which can be related to the increase in resistance to dislocation motion due to induced lattice distortion caused by the difference in atomic size between nickel and the alloying solute atoms,

Table 2.1: Nominal composition of IN738 [6]

Element	Nominal Composition (wt%)
Ni	Bal.
Cr	15.84
Co	8.5
Mo	1.88
W	2.48
Nb	0.92
Al	3.46
Ti	3.47
Fe	0.07
Ta	1.69
C	0.11
B	0.012
Zr	0.04
S	0.001

aluminum, tungsten, molybdenum, and chromium contribute strongly in solid solution strengthening whereas iron, titanium, cobalt and vanadium serve only as weak solid solution strengtheners. At temperatures of about 0.6 of the melting temperature (T_m), the strengthening of the γ phase becomes diffusion dependent and the slow diffusing elements molybdenum and tungsten constitute the most contributing hardeners [7].

2.1.1.2 Gamma prime phases (γ')

The major contributor to the high strength of IN738 are ordered FCC Ll_2-type $Ni_3(Al, Ti)$ γ' phase particles that have a lattice parameter that is very close to that of the γ matrix. Similar unit cell dimensions allow the γ' precipitates to be coherent with the γ matrix. Hagel and Beattie [9] observed that γ' exhibits spherical shapes at 0 – 0.2% lattice mismatch, becomes cubes at mismatches around 0.5 – 1% and then becomes plates at mismatches above 1.25 %.

Increased strength due to the presence of γ' precipitates can also be attributed partly to their ordered structure. It is known that ordered precipitates have an energy called Antiphase Domain Boundary energy (APB) which represents the extra energy associated with ordered atom positions versus normal disordered or random positions [10]. Increasing the APB energy associated with the precipitates results in an increase in the force required for dislocations to shear them.

Upon thermal exposure above $0.6T_m$, γ' particles increase in size at a significant rate that facilitate dislocation by-pass. Minimizing the size increase is required to achieve long-term creep resistance. The coarsening of γ' is retarded significantly by combined addition

of cobalt, molybdenum, or a combined addition of molybdenum and tungsten. Increasing molybdenum from 2 to 5% was found to markedly reduce the coarsening rate despite an increase in coherency strains [7].

2.1.1.3 Carbides

Carbides form in IN738 when carbon combines with other refractory elements such as titanium, molybdenum, tantalum and tungsten to form MC carbides as shown in Figure 2.1. They usually form during ingot solidification of the alloy and typically with coarse random cubic or script morphology [7].

The mechanical properties of nickel-base superalloys can be strongly affected by the morphology and distribution of carbides. Script-type MC carbides along the grain boundaries can lower creep ductility by acting as a crack initiation site and crack propagation path if their distribution is continuous [11]. Discrete and disconnected grain boundary secondary $M_{23}C_6$ carbides can strengthen grain boundary regions by inhibiting intergranular sliding at elevated temperatures [10].

During heat treatment and service exposure MC carbides slowly decompose to yield carbon which permeates the alloy and triggers a number of important reactions such as: $MC + \gamma \rightarrow M_{23}C_6 + \gamma'$. A similar reaction where MC carbides transform to M_6C carbides has also been reported. Likewise, $M_{23}C_6$ can transform to M_6C depending on the composition of the superalloy and heat treatment [12].

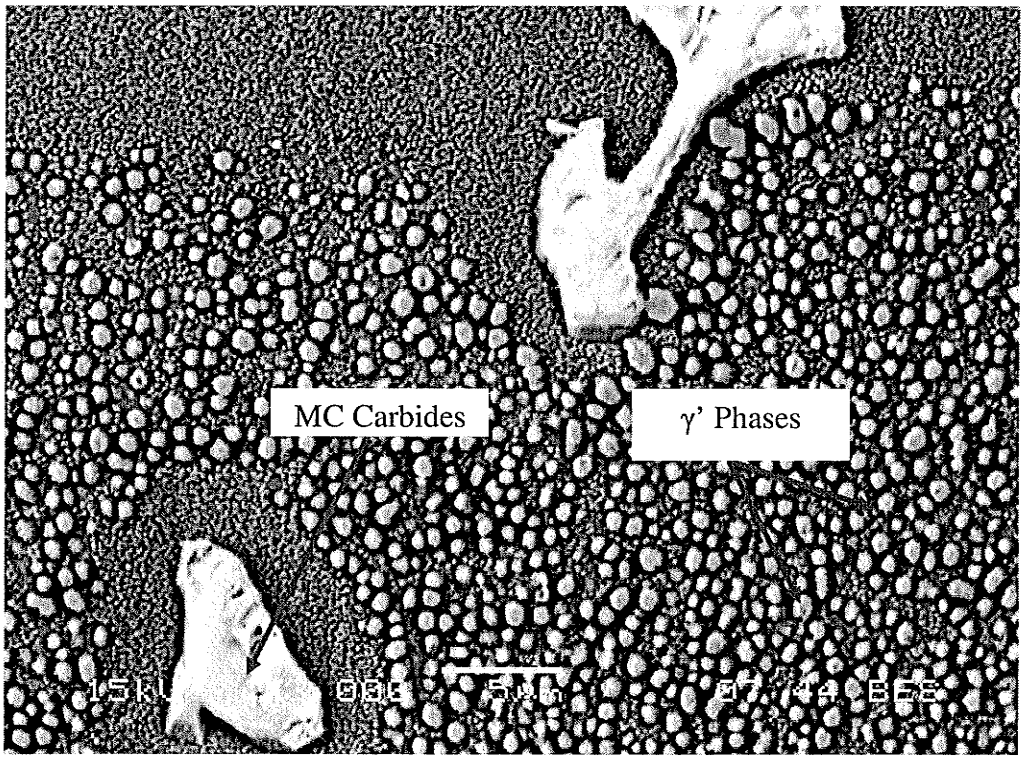

Figure 2.1: MC Carbides and γ' phases in IN738 as obtained by Scanning Electron Microscopy (X3000)

2.1.2 Pure nickel 270

Commercial pure nickel 270 has 99.98 % nickel and the rest are trace elements present in very low concentrations as listed in Table 2.2. This metal has excellent thermal conductivity and high ductility which allows for heavy cold deformations without annealing. Pure nickel is used in cathode shanks, hydrogen thyraton components, heat exchangers and heat shields. Compared to nickel alloys, commercial pure nickel has higher electrical conductivity and a high curie temperature. Nickel, like gold, silver and copper, has a relatively low work hardening rate [13].

2.2 Joining and Repair Techniques for Nickel-Based Superalloy Components

Repair of damaged gas turbine nickel-based superalloy components due to the severe working conditions is usually more economical than total replacement of affected engine parts. As a result, a lot of research on joining and repair of nickel-base super alloys has been undertaken. The common joining methods for repair of nickel-base superalloys are fusion welding and diffusion brazing that is also known as transient liquid phase bonding.

Table 2.2: Composition of commercially pure nickel 270 [13]

Element	Nominal Composition (wt %)
Ni	99.98
C	0.01
Mn	<0.001
Fe	0.003
Si	<0.001
Mg	<0.001
Cu	<0.001
Co	<0.001

2.2.1 Fusion welding

Fusion welding involves joining two mating surfaces by controlled melting through localized heating and subsequent cooling of the liquid metal. Welding is usually done such that the base material is at or near the room temperature which results in significant temperature gradients between the weld pool and the base material [14].

2.2.1.1 Welding processes

The three major types of fusion welding are as follows:

1. Gas Welding:
   - Oxyacetylene welding
2. Arc Welding
   - Shielded metal arc welding
   - Plasma arc welding
   - Gas-tungsten arc welding
   - Gas-metal arc welding
   - Flux cored arc welding
   - Submerged arc welding
   - Electro-slag welding
3. High-energy beam welding
   - Electron beam welding
   - Laser beam welding

The heat sources for gas, arc, and high-energy beam welding processes are gas flame, electric arc, and high energy beam, respectively. Gas welding produces the highest heat

input in a work piece and the lowest power density compared to arc welding and high energy beam welding techniques, such as electron beam and laser beam welding. High heat input increases damage to the work piece while high energy beam welding, with the lowest heat input, increases penetration and general quality of welds. Joints that require multiple-pass arc welding can be welded in a single pass by electron beam welding at high speeds which results in a very narrow heat-affected zone and little distortion [14]. The equipment required for electron beam welding, however, is very expensive and the associated x-ray shielding can be inconvenient and time consuming.

2.2.1.2 Limitations of fusion welding

Fusion welding is generally used to join some superalloy materials but its application to nickel-based superalloys that contain significant amount of titanium and aluminum is, however, limited. This is due to the high susceptibility of these materials to heat affected zone (HAZ) cracking during welding and subsequent heat treatments. Additionally, distortion of components can exist in the HAZ due to thermal gradient developed through the use of a concentrated heat source in the process [2]. The mechanical properties, such as fatigue resistance of welded joints are usually inferior to those of the base alloy. Fusion welding of complex geometries is sometimes not very effective as surfaces may not be easily accessible to heat sources. Also, the process can not be used in joining metals to non-metals [14].

2.2.2 Brazing

Brazing is used extensively in the aerospace industry due to its ability to join difficult-to-weld nickel-based superalloys. Conventional brazing is a joining technique that involves joining of two metal surfaces by the use of a filler metal and heating to temperatures above 425 °C. The filler metal melts at the brazing temperature and the resultant liquid is held within the joint by surface tension. Metallurgical reactions between the liquid and the substrate results in the joint formed upon cooling. Due to the short holding time associated with conventional brazing, limited extent of solid state diffusion of solute elements is possible [14]. Some brazing processes such as diffusion brazing involve much longer holding times so that significant diffusion of elements can take place.

2.2.2.1 Brazing techniques

Effective capillary joining during brazing requires efficient transfer of heat from the heat source into the joint. The size of individual assemblies, the numbers required, and the rate of production influence the selection of the heating method used. Consideration of the rate of heating, thermal gradients and cooling rate is also important when choosing a heating method since these factors vary tremendously with different heating methods.

The most common methods of heating are as follows [15]:

- Torch brazing
- Furnace brazing
- Induction brazing
- Dip brazing

- Resistance brazing
- Wide-gap brazing

Manual torch brazing is most frequently used for repairs with short production runs as an alternative to fusion welding. Heating of the assembly is achieved by using a gas (oxyfuel) as the heat source and a flux material is usually used to promote wetting of the filler metal [15].

Furnace brazing is a high volume production process for self-fixured assemblies with pre-placed filler metal. The furnace is usually purged with a gaseous atmosphere or evacuated of air and heated to a temperature above the liquidus of the filler metal but less than the melting point of the base metal. Pre-placed filler metal can be in the form of wire, foil, powder, paste, slugs or preformed shapes [15].

Induction brazing employs material's resistance to the flow of electricity induced by coils around a work piece to provide the heat required for brazing. The process relies on high-frequency alternating current flowing through the induction coils to create electromagnetic fields around the work piece. The opposing currents that are induced into the work piece generate the heat required for brazing. Some advantages of the process include selective heating of the work piece and quick attainment to brazing temperature. Induction brazing is also well suited for high-volume production applications that can be controlled remotely. High-strength components can be induction brazed with little loss of strength because of the precise heating capabilities of the process [15].

In dip brazing, the assembly is immersed in a heated bath of either molten metal or a flux bath of molten salt. The dipping technique is used for manufacturing of electronics and similar very small components. The parts being joined are held together and immersed in a bath of molten metal that flows into the joints for brazing [15].

Resistance brazing is most applicable to relatively simple joints in metals that have high electrical conductivity. In resistance brazing, the work piece with the filler pre-placed, is part of an electric circuit. Brazing heat comes from either placing carbon electrodes in contact with the brazement to conduct heat into the work or by relying on resistance of the brazement to generate heat [15].

Wide-gap brazing is usually employed to fill large defects and wide gap cracks and to rebuild large worn surface areas of airfoils. It uses a filler which is often a mixture of a filler metal and a high-temperature-melting powder. During brazing, the gap-filler powder particles remain largely un-melted and provide the necessary capillary forces to retain the molten filler metal and avoid excessive fluidity within the gap of the faying surfaces. The mixture, therefore, behaves like slurry with sufficient bridging power to fill the large crack [15].

2.2.2.2 Advantages of brazing

Brazing has many distinct advantages including the following [15]:

- Economical fabrication of complex and multi-component assemblies
- Simple method to obtain extensive joint area or joint length
- Excellent stress distribution and heat transfer properties.

- Ability to preserve protective metal coating and cladding.
- Ability to join non-metals to metals.
- Ability to join metal thicknesses that vary widely in size.
- Ability to fabricate large assemblies.
- Ability to preserve special metallurgical characteristics of metals.

Additionally, strong, uniform and leak proof joints can be made rapidly and inexpensively. Complicated assemblies comprising thick and thin sections, odd shapes, and differing wrought and cast alloys can be successfully brazed. Closer tolerances can be met using brazing than with fusion welding due to the much lower amount of base metal melting [16].

2.2.2.3 Limitations of brazing

Brazing, however, has the limitation of producing a joint with physical and mechanical properties that are inferior to the base metal due to the presence of intermetallic phases at the brazed joint. Brazements of several materials with different characteristics of deformation resistance can cause non-uniform stress distribution under externally applied loads. In addition, brazing foils in the form of paste has organic binders which burn during the brazing cycle causing voids and carbonaceous residues that weaken the joint [15].

2.2.2.4 Brazing atmosphere

It is necessary for brazing to be conducted under a protective atmosphere, including vacuumed environments to prevent the joint from volatile contaminants and the formation of oxides. Brazing in chemically inert gas atmospheres such as nitrogen, argon

or helium exclude oxygen and other gaseous elements that might react with the components to form surface films and inhibit flowing and wetting of the liquated interlayer [16]. Hydrogen-type atmosphere has been used in the past due to its ability to dissociate oxides developed at high temperatures during bonding. Its effectiveness is, however, reduced if employed on titanium and aluminum containing alloys such as Ni-base superalloys. Controlled gas atmospheres require a confining vessel which enables the incorporation of a heating furnace. This can reduce post-processing operations such as cleaning and removal of flux residues.

Brazing conducted in a high vacuum atmosphere can control the formation of oxide layers on the filler mating surfaces. Some advantages of using a vacuum atmosphere include reduction in formation of certain oxides, prevention of vacuum chamber hot corrosion, oxidation and elimination of volatile gases and impurities. Inert atmospheres such as argon and helium may also be employed by performing multiple inert gas purging prior to furnace brazing [16].

Some potential disadvantages of using a gaseous joining atmosphere include the high capital costs of the equipment, including the associated gas atmosphere handling or vacuum system and the recurring costs due to consumption of gas atmospheres used for processing and maintenance of vacuum pumps. Additionally, certain metals may not be compatible with standard atmospheres. Hydrogen atmospheres can cause hydrogen embrittlement of some metals including titanium, zirconium and tantalum. Likewise, nitrogen atmospheres cannot be used when the parent materials and filler metals contain elements susceptible to nitriding such as molybdenum, titanium and zirconium [15].

2.2.2.5 Surface preparation

Surface preparation is of paramount importance for the production of good quality joints. Any residual oxide films, grease or oils may inhibit the initiation of spreading and wetting of liquid filler after melting. The influence of low surface energy non-wettable interlayer oxides on liquid surface energies is practically important. Oxides entrapped at the liquid/solid interface may also act as a diffusion barrier. A good brazing surface requires sufficient surface roughness and good wetability by the filler alloy. Low viscosity and good flow are also important qualities that help improve the quality of brazement [16].

Mechanical cleaning involving grit blasting, grinding and brushing, which slightly roughens the surface, is sometimes necessary and is usually used when there are large amount of surface oxides. Traces of oil or grease may be removed by chemical cleaning methods which involve the use of degreasing solutions. Spraying, soaking, and suspension in hot vapor are some of the general techniques used during chemical cleaning. Chemically cleaned components can subsequently be cleaned ultrasonically in alcohol to ensure complete removal of all traces of degreasing solutions. Fluoride cleaning is another method of surface cleaning employed to effectively remove oxide layers on thermal fatigue cracks and other narrow hard-to-reach cracks. Cleaning is done by exposure to fluoride ions in a reducing atmosphere but proper control of the process is important to ensure adequate cleaning of deep narrow cracks and to avoid excessive surface depletion [15].

2.2.2.6 Fluxes

The primary purpose of brazing fluxes is to promote wetting of the base material by the liquid filler metal. Flux must be capable of dissolving any oxide remaining on the base metal after it had been cleaned and oxide films on the filler metal. In some instances, fluxes may serve to suppress the volatization of high-vapor-pressure constituents in a filler metal [15]. Fluxes need to be applied as an even coating and must completely cover and protect the surfaces until the brazing temperature is reached. Viscosity and interfacial energy between the flux and mating surfaces are important for good wetting and it is recommended that fluxes should be used in their proper temperature ranges and on the materials for which they are designed for.

Many chemical compounds are used in the preparation of fluxes. The most common ingredients of chemical fluxes are [15]:

- Borates (sodium, potassium, lithium, etc.)
- Fused borax
- Elemental boron
- Fluoborates (potassium, sodium, etc.)
- Fluorides (sodium, potassium. etc.)
- Chlorides
- Alkalis (potassium hydroxide, sodium hydroxide)
- Wetting agents
- Water

Certain filler metals contain alloy additions of deoxidizers, such as phosphorous, lithium, and other elements that have strong affinities for oxygen. In some instances, these additions make the filler metal self-fluxing without the application of prepared fluxes or controlled atmospheres. Such fillers are self-fluxing only in the molten state and will oxidize during heating cycle [15]. Therefore, the use of protective atmospheres or fluxes in conjunction with these fillers is usually preferred.

2.2.2.7 Filler alloys

Brazing filler alloys usually contain melting point depressant (MPD) elements such as boron, silicon, or phosphorous, which are added to depress their melting temperature. Other elements such as carbon, titanium and aluminum are deliberately excluded from filler alloys due to their tendency to form undesirable stable phases during bonding that can embrittle the joint. Suitability of a filler alloy for use in TLP bonding depends on some criteria that must be met. The liquidus temperature of the alloy must be less than the solidus temperature of the base material. Proper fluidity of the liquid filler at the brazing temperature is necessary to ensure wetting and flow over base material surfaces [16].

Filler alloys are available in various forms such as amorphous foil, tape, powder/paste, and rapidly solidified sheet. Brazing foils are usually made by rapid solidification during melt spinning operations, while powdered forms are usually produced by gas atomization. The powders may be mixed with plasticizers or organic cements to facilitate their positioning on the base metal surface. Tape forms are usually made up of powders that are uniformly applied to a flexible organic backing strip. In some instances organic

binders tend to burn during brazing causing voids at the joint. Cored fillers are another type of fillers where a base material such as pure nickel is surrounded by a surface rich in melting point depressant element produced by diffusion treatment. Some elements such as chromium are often added to Ni-base filler alloys to increase the oxidation and corrosion resistance of the resulting joint [16].

2.2.2.8 Base material characteristics

Certain characteristics of the base metal must be met to achieve an optimum joint. Firstly the base metal must be able to sufficiently accommodate the MPD solute. The base material should have sufficient strength and thermodynamic stability at the bonding temperature. Base metals which do not form second phases are well suited for brazing. The solidus temperature of the base alloy should be significantly higher than the liquidus temperature of the filler alloy. Another important factor to consider is that base materials that have an initial concentration of the MPD element may behave differently compared to base metals with no initial concentration of MPD elements [16].

2.2.3 Transient liquid phase (TLP) bonding

Transient Liquid Phase (TLP) bonding evolved from brazing as a high temperature fluxless process that combines the beneficial features of liquid phase joining and solid-state diffusion bonding. It has been used to produce high strength joints in difficult-to-weld heat resistant alloys. Fundamentally, the process involves no plastic deformation of the components being joined, although some pressure may be needed to ensure that mating surfaces are in intimate contact [15].

The process involves the use of an interlayer material (filler alloy) that contains a melting point depressant (MPD) element(s) such as boron, silicon and phosphorous. At the joining temperature below the solidus temperature of the base metal, the interlayer melts and interdiffusion of alloying elements occurs between the substrate and the liquated interlayer. This results in changes in the composition of the solid and the liquid phases until equilibrium is established at the joint's interface. Further diffusion of the MPD into the base metal raises the melting point of the liquid resulting in its isothermal solidification. Complete isothermal solidification can be achieved if sufficient holding time at the joining temperature is provided before cooling to the ambient temperature. Longer holding time, after achieving complete isothermal solidification, may also be necessary to homogenize both the microstructure and the composition of bonded materials.

In contrast to brazing, TLP bonding is more suited for joining components intended for demanding elevated temperature service. The microstructure and mechanical properties of the TLP bonded joint can closely approach those of the base material. Dissimilar base alloys with complex shapes and varying thicknesses can also be joined by TLP bonding and mass production can be employed which can significantly reduce production costs [17]. Due to the solid state diffusion that must occur during TLP bonding, long holding time may be required to achieve complete isothermal solidification; which somewhat limits the use of the process commercially. An incomplete isothermal solidification results in the formation of eutectic-type microconstituents at the joint, which are brittle and provide easy path for crack initiation and propagation. Precipitation of second phase particles within the joint-

substrate interface due to the diffusion of the MPD into the base material may also have detrimental effect on mechanical properties of bonded materials. Improper or inadequate surface preparation or poor bonding atmosphere can also result in a poorly joined part or filler spillage upon melting.

2.3 Mechanisms of TLP Bonding

Various models have been developed to further the understanding of the TLP bonding process. In these models, it is generally assumed that after the formation of a liquid phase, the solid and liquid phases rapidly equilibrate to their respective solidus and liquidus compositions at the bonding temperature. Solid-state diffusion of the MPD in the base alloy follows the equilibration and results in gradual isothermal solidification of the liquated filler. Duvall et. al. [18] defined three stages of TLP bonding as: i) base metal dissolution; ii) isothermal solidification of liquid filler; and, iii) homogenization of the solid bond region. Tuah-Poku et. al. [19] defined a fourth stage, namely, homogenization of the liquid after base metal dissolution. An initial stage prior to base metal dissolution (stage 0) was added by MacDonald and Eager [20] to account for the heating time from room temperature to just before the onset of liquation of the filler. This is due to possible loss of solute during heating of the joint, which was also reported by Niemann and Garrett [21]. They noticed that at slow heating rates insufficient liquid forms at the interface due to premature diffusion of MPD solute into the base material. Zhou et. al. [22] re-classified TLP bonding into four stages: i) Heating stage, ii) dissolution and widening which is subdivided into two stages, ii(a) heating from melting point to bonding temperature and ii(b) isothermal dissolution at the bonding temperature, iii) Isothermal solidification and iv) homogenization.

2.3.1 Initial bonding condition

A binary eutectic diagram shown in Figure 2.2, with A being the base material and B the MPD solute, can be used to explain the bonding process where the B composition of the MPD solute in the filler alloy is usually slightly higher than the liquidus composition of the base alloy at the bonding temperature. As illustrated in Figure 2.3, the filler alloy has an initial thickness of W_o and initial MPD (B atoms) composition of C_F. In practice, the base material may or may not have an initial MPD solute present.

2.3.2 Heating and melting of filler alloy

During the heating stage, the TLP bonding assembly is heated up from room temperature to a temperature above the melting point of the filler. The filler may melt over a range of temperatures but the alloy is normally assumed to have compositions close the eutectic composition. During heating to the melting temperature of the filler, some solid-state diffusion between the filler alloy and the base metal may occur. The extent of diffusion will depend on several factors including the eutectic temperature, heating rate and diffusivity of the MPD element. Very slow heating rates may result in severe depletion of solute concentration in the filler causing its concentration to be lower than the solidus composition at the bonding temperature. As a result, no liquid will form upon reaching the joining temperature heating. This problem becomes most severe with very thin filler alloys and low solute concentrations [21]. Upon melting, the filler wets the solid substrate and flows throughout the joint. Wetability depends on the surface energy of both the liquid and the solid as well as on the viscosity of the liquid.

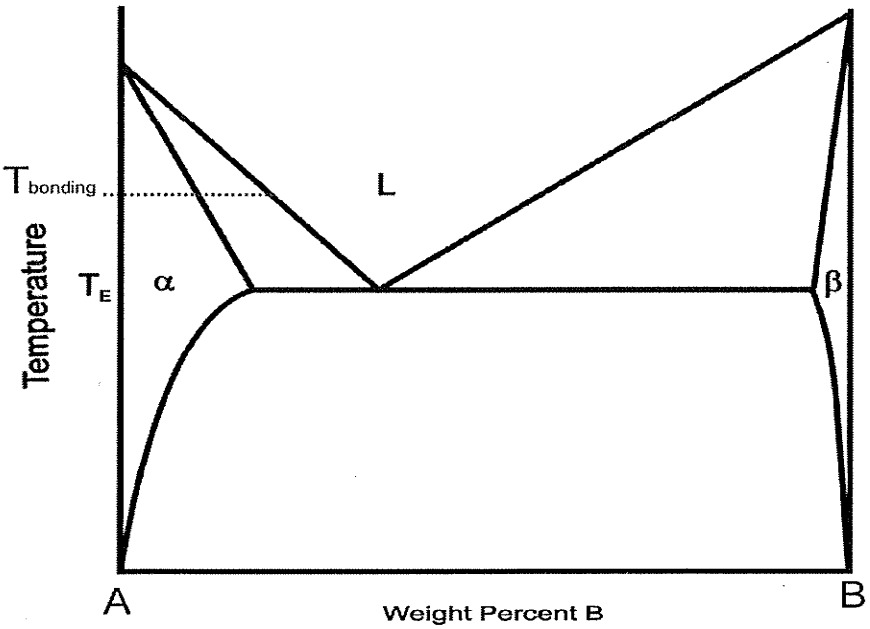

Figure 2.2: Binary eutectic phase diagram [23]

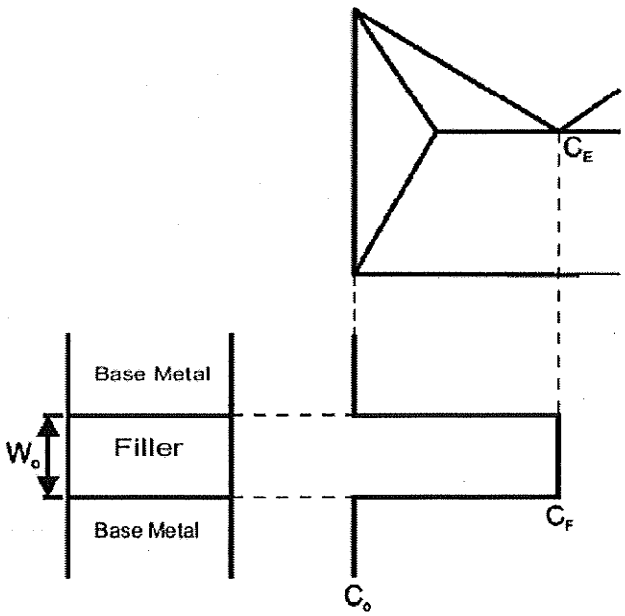

Figure 2.3: Initial conditions of TLP bonding assembly [23]

2.3.3 Base metal dissolution

Base metal dissolution occurs after liquation of filler alloy and progresses during heating from filler melting temperature to the bonding temperature. The amount of solute at the liquated joint is generally higher than the solidus and liquidus compositions required to achieve equilibrium to the bonding temperature. Therefore, to attain equilibrium at the solid-liquid interface, the base alloy melts-back into the liquid, which results in increase in the volume of the interlayer liquid phase.

The interfacial reactions are rapid and are controlled by liquid diffusion. The maximum width of the liquid represents the maximum dissolution width W_{max} which is reached some time after reaching the bonding temperature $T_{Bonding}$ and the solute concentrations in the solid and liquid at the interface equals to the equilibrium solidus and liquidus concentrations $C_{\alpha L}$ and $C_{L\alpha}$, respectively, as illustrated in Figure 2.4.

The dissolution stage becomes very important in aerospace applications such as thin honeycomb structures, rocket fins and thin foil structures where large base metal dissolution can lower the load bearing capability of thin sections. The extent of base metal dissolution depends on many factors including the initial concentration of MPD solute in the filler C_F, initial filler thickness and solubility of the MPD solute in the base material.

Several authors have suggested various analytical models to represent the dissolution stage. Nakao et. al. [24] analyzed base metal dissolution based on the Nernst-Brunner theory and formulated the equation shown below:

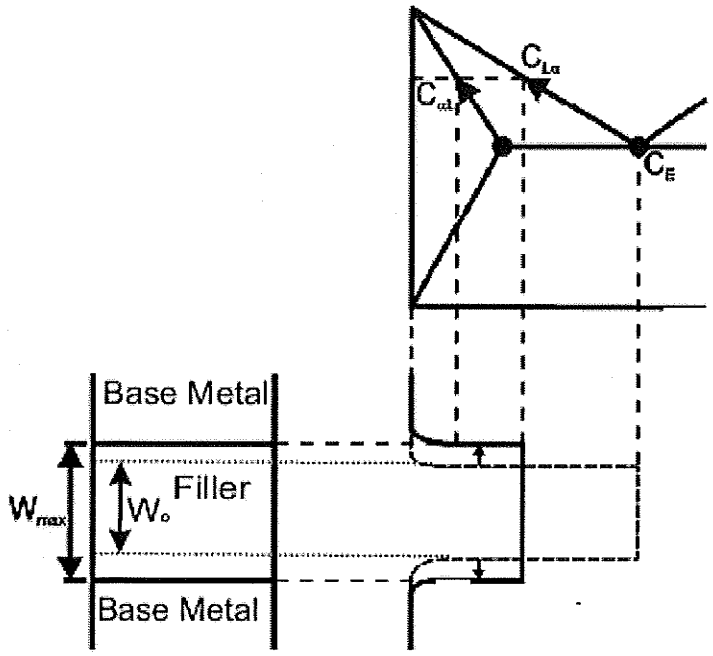

Figure 2.4: Base metal dissolution and widening during TLP bonding [23]

$$\frac{dC}{dt} = K(\frac{A}{V})*(C_s - C_t) \qquad (2.1)$$

where C_s is the solute concentration at the saturated state; C_t is the solute concentration at spontaneous time t; K is the dissolution rate constant. A is the surface area of the solid and V is the volume of the liquid. C_s and C_t can be calculated as shown in the following equations 2.2 and 2.3:

$$C_l = \left[\frac{ph}{x+ph}\right]C_i \qquad (2.2) \qquad C_s = \left[\frac{ph}{x_s+ph}\right]C_i \qquad (2.3)$$

where C_i is the initial concentration of the MPD in the liquid filler; p is the ratio ρ_l/ρ_s where ρ_l is the density of the liquid filler and ρ_s is the density of the base metal; h is half the initial thickness of the filler; x is the instantaneous dissolution width and x_s is the maximum dissolution width at the saturated state. A dissolution parameter P was then be expressed as follows:

$$P = Kt = h\left\{\ln\frac{x_s(x+ph)}{ph(x_s-x)}\right\} \qquad (2.4)$$

Nakao et. al. [25] reported that there was a linear relationship between the dissolution parameter P and the holding time. Dissolution time was found to be in the order of seconds or few minutes and did not play a significant role in the total time required for TLP bonding which is usually in hours. Nakao et. al.'s model [24] assumes that the liquid and adjacent solid have compositions fixed by respective liquidus and solidus values before and after equilibration. In order to improve the analysis, Gale and Wallach [26] used equation 2.5 where the concentration of the melting point depressant in the base alloy can be obtained as a function of the holding time. They assumed that the MPD solute diffuses out of a finite liquid interlayer into a semi-infinite solid substrate. They

also assumed that the diffusivity of the solute is that observed in the solid substrate and ignored its greater diffusivity in the liquid. This results in flattening of the concentration profile in the liquid, which influences the diffusion in the solid substrate.

$$C(x,t) = 0.5C_o\left[\frac{erf(h-x)}{2\sqrt{D.t}}\right] + \frac{erf(h-x)}{2\sqrt{D.t}} \qquad (2.5)$$

where C(x,t) is the concentration of the solute as a function of distance from the center of the interlayer (x) and time (t); 2h is the width of the interlayer; D is the diffusivity of the solute in the substrate and C_o is the initial solute concentration in the filler.

2.3.4 Isothermal solidification stage

Isothermal solidification is normally assumed to commence after the dissolution stage and proceeds at a constant bonding temperature during which the MPD solute diffuses into the base material across the liquid-solid interface. Local equilibrium is maintained at the solid-liquid interface throughout the isothermal solidification process and the compositions of the liquid and the adjacent solid remain fixed at $C_{\alpha l}$ and $C_{l\alpha}$. A decrease in the amount of liquid that can be maintained at constant temperature due to the loss of the MPD solute causes isothermal solidification to occur by migration of the liquid-solid interface towards the centerline of the joint as illustrated in Figure 2.5. If the holding time is sufficient, the liquid can be removed entirely resulting in complete isothermal solidification.

The isothermal solidification stage is much slower than the dissolution stage since it is controlled by solid-state diffusion of the MPD solute in the base metal. The time required

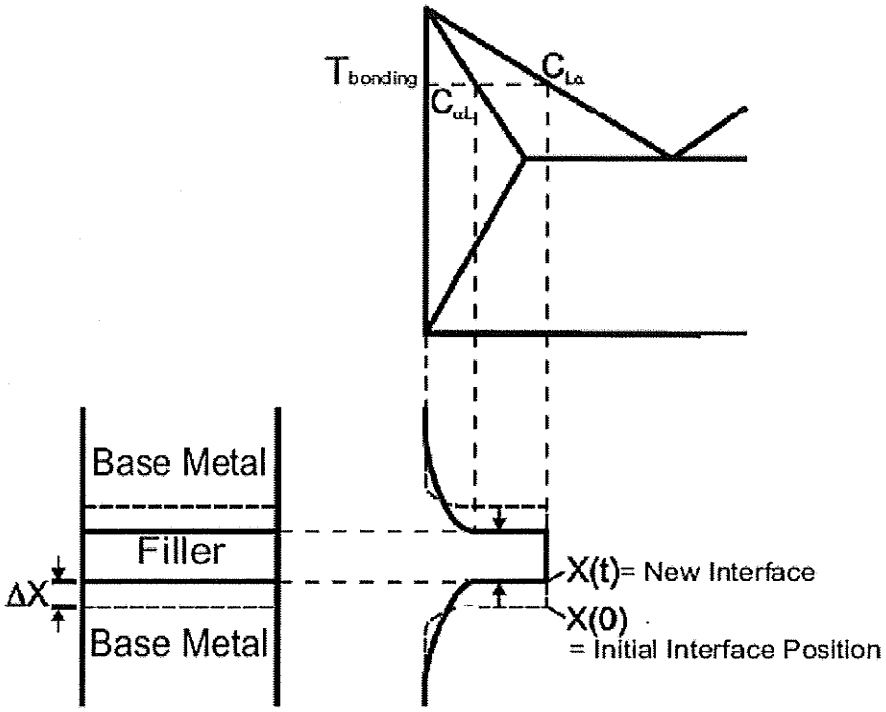

Figure 2.5: Isothermal solidification stage during TLP bonding [23]

to complete the isothermal solidification process is system specific because it depends on the diffusion flux of the solute in the base metal and on the amount of solute that must be diffused. These depend on many factors including diffusion coefficient of the solute in the base metal, initial filler thickness, solubility of the MPD element and its concentration gradient in the base material.

Modeling of the isothermal solidification stage has been done by various authors in an effort to understand the controlling mechanism of the isothermal solidification process. In these models, local equilibrium is assumed to exist at the solid-liquid interface at the bonding temperature and the effect of convection in the liquid is assumed to be negligible due to the small thickness of the liquid interlayer and its assumed uniform composition. The interdiffusion coefficients in the liquid and the solid are assumed to be independent of composition and the base metal is generally taken to be semi-infinitely long medium.

Analytical modeling approach is used extensively in practice and a close examination of its basic concepts indicates that it can be classified into two categories, single phase solution and two-phase solution. The single phase solution treats the system as a single semi-infinite phase, the base metal, having a constant solute concentration ($C_{\alpha l}$) at the surface of the base metal. This eliminates the trouble of dealing with the liquid phase and the migrating solid-liquid interface [27]. The two-phase analytical solution treats the system as two semi-infinite phases with a coupled diffusion-controlled moving solid-liquid interface. This is more accurate than the single-phase solution since it approximates real situations better and allows the interface to advance toward the centerline as the liquid is consumed.

Tuah-Poku et. al. [28] proposed a single phase analytical solution using a mass balance approach as represented by equations 2.6 to 2.8 to predict the time for complete isothermal solidification by assuming a stationary interface. Solving the mass balance equation 2.7, he obtained an equation for the total time for isothermal solidification as seen in equation 2.8.

$$C_F.W_o = 2.M(t) \qquad (2.6)$$

where C_F is the MPD solute concentration of the filler metal; W_o is the initial filler thickness and M(t) is the total mass transferred during isothermal solidification.

$$M(t) = 2.(C_{\alpha L} - C_o).\sqrt{\frac{D.t}{\pi}} \qquad (2.7)$$

where $C_{\alpha l}$ is the solute concentration at the interface; C_o is the initial composition of the melting point depressant in the base metal; D is the solute diffusion coefficient and t stands for time.

$$t = \frac{\pi}{16.D}.\left(\frac{C_F.W_o}{C_{\alpha L} - C_o}\right)^2 \qquad (2.8)$$

Using a two-phase analytical approach, Lesoult [29] treated the solid-liquid interface as a moving boundary to derive an expression for the time for complete isothermal solidification. Taking X(t) as the moving interface and knowing that X(t) must be proportional to the root of time as seen in equation 2.9, he used a mass balance approach where K is the rate constant.

$$X(t) = -2.K.\sqrt{D.t} \qquad (2.9)$$

Increasing K results in faster solid-liquid interface motion and shorter duration for complete isothermal solidification. Lesoult [29] used numerical methods to calculate the rate constant K in equation 2.10 and used the value of K to compute the time required for complete isothermal solidification based on equation 2.11. Similar approach was also followed by Sokomoto et. al. [30] and Ramirez and Liu [31].

$$\frac{C_{\alpha L}-C_o}{C_{L\alpha}-C_{\alpha L}}=\sqrt{\pi}.\frac{K.(1+erf(K))}{\exp(-K^2)} \qquad (2.10)$$

$$t=\frac{W_{\max}^2}{16.K^2.D} \qquad (2.11)$$

Where W_{max} is the maximum width of liquated region obtained during dissolution calculated using equation 2.12.

$$W_{\max}=\frac{C_F.W_o}{C_{L\alpha}} \qquad (2.12)$$

The single phase solution obtained by Tuah-Poku et. al. [28] reported high estimates of the isothermal solidification time compared to experimental results but it has one advantage over the two-phase solution in that the latter requires a numerical solution to solve the rate constant K. As previously stated, in analytical models the base metal is assumed semi-infinite which may be valid for some engineering applications where the thickness of the pieces to be joined is often large relative to diffusion distances. In certain applications, however, such an assumption might not hold. For example in the microelectronics industry and honey-comb structures, the parts can be very small or very thin, and as such assuming a semi-infinite "sink" can be grossly inaccurate [32].

Numerical modeling approaches have to be used if a finite size is to be treated since the kinetics of solidification can be significantly affected. Numerical solution approach to model the isothermal solidification process generally assume a one dimensional planar geometry as shown in Figure 2.6 and a variable s(t) is introduced to describe the position of the solid-liquid interface. The moving boundary problem can be expressed by the diffusion equations 2.13 to 2.15 [33] where equation 2.13 describes the diffusion to the left of the interface in phase A which is liquid. Equation 2.14 describes the diffusion in the solid phase B. Equation 2.15 describes the moving boundary condition at the interface where c_A and c_B represent the equilibrium liquidus and solidus concentration respectively.

$$\frac{\partial c(x,t)}{\partial t} = \frac{\partial}{\partial x}\left(D_A(c(x,t)) \frac{\partial c(x,t)}{\partial x} \right) , \qquad 0 < x < s(t) \qquad (2.13)$$

$$\frac{\partial c(x,t)}{\partial t} = \frac{\partial}{\partial x}\left(D_B(c(x,t)) \frac{\partial c(x,t)}{\partial x} \right) , \qquad s(t) < x < L \qquad (2.14)$$

$$D_A(c(x,t)) \frac{\partial c(x,t)}{\partial x}\bigg|_{x=s-} - D_B(c(x,t)) \frac{\partial c(x,t)}{\partial x}\bigg|_{x=s+} = [c_B - c_A] \frac{ds(t)}{dt} , \qquad x = s(t) \qquad (2.15)$$

Nakagawa et. al. [34] and Cain et. al. [35] approach to solving these diffusion equations was by discretizing the distance between x = 0 to x = L, as seen in Figure 2.6, into fixed points and imposing the interface to be located at one of the discretization points. This means that only step-wise motion is permitted. Such a constraint on the interface position, however, may introduce significant errors due to inaccurate approximation of the interface position and, as a result, will affect estimates of the diffusion fluxes at the interface [32].

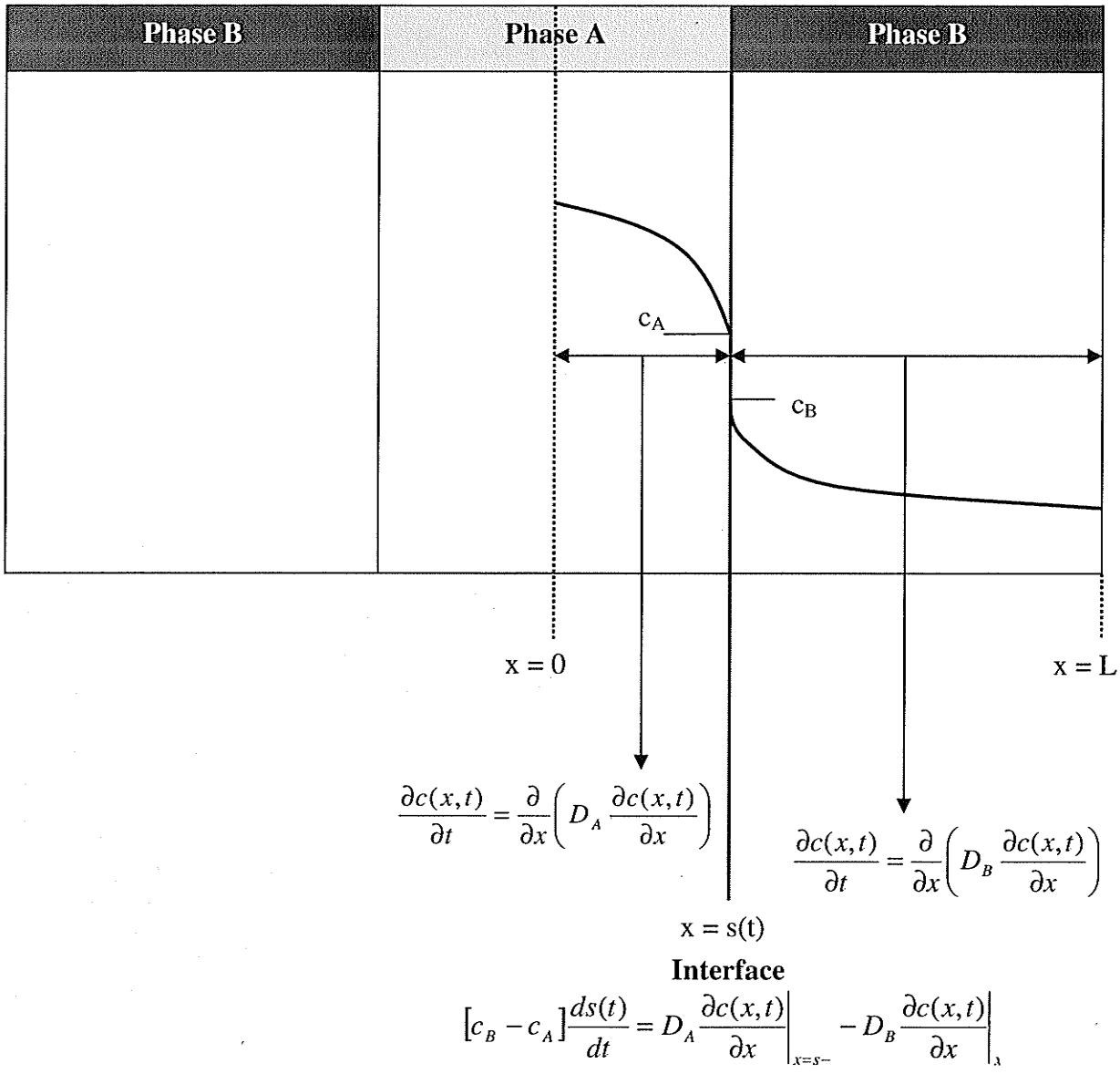

Figure 2.6: Illustration of system used in numerical analysis

Shinmura et. al. [34] produced a more refined model which explicitly account for interface position to predict its motion. They solved the three diffusion equations 2.13 to 2.15 explicitly but since the diffusion equations are interdependent, the model result was quite inaccurate owing to non-conservation of the diffusing solute.

Using Shinmura's *et. al.* [34] approach, Zhou and North [33] proposed using a quadratic expression for the concentration profile near the interface to better estimate the fluxes there and thereby improve the accuracy of the model. Their model, however, involved a semi-implicit scheme where only the diffusion equations 2.13 and 2.14 were solved implicitly while the diffusion equation for the interface was solved explicitly. This caused a limitation on the size of time step that can be used to generate a solution, since the interface motion is generally rapid at the early stages of TLP bonding. Calculations using large time steps, on the other hand will contain inaccuracies since solute is no longer conserved. Reducing the time steps, on the other hand, will increase computational effort required to solve the problem.

Using the approach by Tanzilli and Heckel [35], Illingworth et. al. [32] solved the problem of using fixed spatial discritization, which does conserve solute by using variable spatial discretization approach. A mesh which varies in a way that it takes account of the moving interface was used and the interface position was ensured to coincide with a discretization point without constraining its motion. Illingworth et. al. [32] further improved the algorithm by ensuring that all the diffusion equations were solved implicitly resulting in a greater accuracy. Using his model to simulate the interface motion during TLP bonding of Ni-P interlayer and pure Ni base metal, it was reported

that his predictions do not exceed the theoretical maximum liquid layer thickness W_{max}, which is consistent with the fact that his model does conserve solute.

Analytical and numerical solutions are both based on Fick's second law of diffusion and have been used to predict the time for complete isothermal solidification. Both approaches, however, use different methods in obtaining the solution, and as such, quantitative predictions often vary. Their solutions often provide means of studying certain TLP bonding phenomena by comparing theoretical predictions with experimental observations. Analytical and numerical solutions have some common assumptions such as assuming local equilibrium at the migrating interface and that the liquid phase exhibit complete wetting of the base metal and exclude the quality of the mating surfaces such as the presence of oxides, all of which may not be exact in practice.

Quantitative results derived from theoretical predictions based on binary phase diagram data may not be very accurate if a complex multi-component system is used. This is due to the role of secondary alloying elements in TLP bonding mechanisms, many of which are still unknown. Deficiencies in the availability of reliable data for diffusion coefficients and solubilities also make it even more difficult to obtain reliable quantitative predictions. One solution to the unavailability of reliable phase diagrams of multi-component alloys has been the use of calculated diagrams. This approach was used by Campell and Boettinger [36] to study TLP bonding in the Ni-Al-B system. The presence of more than one MPD solute in the filler also makes the analysis more complicated. It has been suggested [37, 38] that in such cases two regimes could exist where the faster

diffusing MPD solute controls the first regime while the second MPD solute controls the other regime.

Due to the microstructural complexity in real systems deviation from conventional expectations can be observed. For example, development of significant amount of solute concentrations immediately adjacent to the liquid-solid interface may lead to the precipitation of second phases which is not predicted by conventional models. The effect of these phases on the accuracy of quantitative predictions can be somewhat important. Despite all the limitations, modeling tools prove are attractive qualitative methods of understanding TLP bonding behavior due their speed and ability to investigate qualitative influence of various process parameters that can be manipulated individually and in combination.

2.3.5 Homogenization stage

The homogenization stage is usually assumed to follow the isothermal solidification stage. Figure 2.8 illustrates the initial stage of the homogenization process right after complete solidification had occurred. During homogenization, concentration of the MPD solute at the joint decreases whiles other elements from the base alloy diffuse into the joint [33]. The homogenization stage is complete when the microstructure and the chemistry of the joint are similar to that of the base alloy. There can be an acceptable amount of MPD solute remaining at the joint, which depends on the material and intended application of the repaired component. The solute concentration at the joint, however, needs to be below the concentration required to form second phases that are considered deleterious to the mechanical properties of the material.

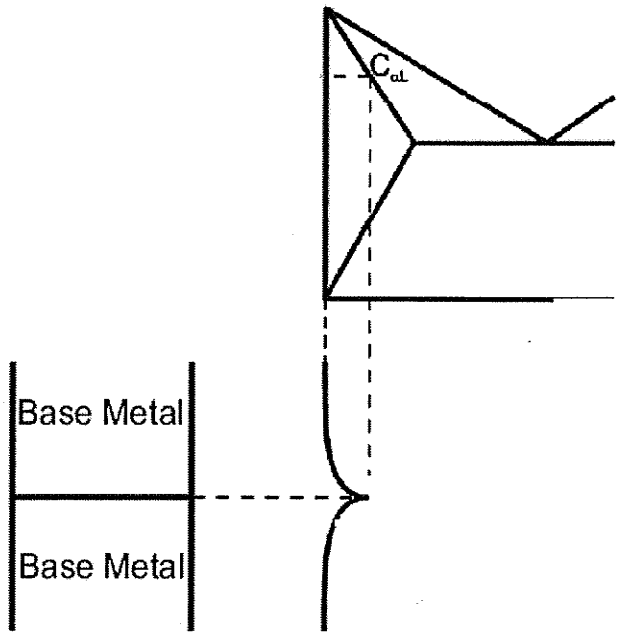

Figure 2.7: Initial condition of the homogenization stage right after complete solidification [23]

2.3.6 Grain boundary effects

The presence of grain boundaries can affect both the kinetics of TLP bonding and the microstructure of bonded materials. Faster grain boundary diffusion has been used to explain shorter than expected isothermal solidification completion times in some materials [35]. During TLP bonding, solid-liquid interface microstructure evolves from a relatively flat surface with small grooves at the grain boundaries to a rough surface with large spherical protrusions. The spherical protrusions are due to the action of grain boundary grooving caused by surface tension coupled with the migration of the liquid-solid interface. Macdonald and Eager [20] has observed that the rate of isothermal solidification for fine grained structures was almost twice that of coarse-grained structures.

Kokawa et. al. [40] also reported that grain boundary energy has an effect on the deviation of the liquid-solid interface migration kinetics from planar predictions. He reported that liquid penetration of the grain boundaries is a function of grain misorientation where high angle grain boundaries show deeper penetration due to higher grain boundary energy and higher diffusion rates. It was found that fine grained nickel contains larger fraction of grain boundary sites and as a result the overall liquid-solid interfacial area was increased and the time to complete isothermal solidification reduced. Nakagawa et. al. [41] noted that the formation of a non-planar liquid-solid interface due to grain boundary penetration increased the effective liquid-solid interfacial area and accelerated the solute diffusion into the base metal.

Tuah-Poku et. al. [28] noted that liquid penetration at the grain boundaries and the accompanying departure from a planar solid/liquid interface made measurement of the liquid width difficult. In some instances complete isothermal solidification at the joint was achieved but some liquid remained where grain boundary penetration had occurred. Rameriz and Liu [31] suggested that liquid penetration increases the solidification rate as a result of increased surface area of the liquid-solid interface which would increase solute transport. Ikeuchi et. al. [39] has shown that liquid penetration depth is dependent on the ratio of grain boundary energy to liquid-solid interfacial energy. Based on their model, enhanced diffusivity at grain boundaries suggested displacement of the liquid-solid interface in a direction opposite of that observed in actual brazing situation.

Saida et. al. [41] studied the influence of base metal grain size on isothermal solidification rates. Faster interface kinetics along with notable grain growth was found in fine grained samples. Longer isothermal solidification completion times were observed in single crystal and coarse-grained alloys. They deduced that increased surface area for diffusion and a greater number of enhanced diffusion paths resulted in reduced solidification time. Base metal dissolution was also found to be related to grain size where increased dissolution was observed in fine-grained samples.

2.4 Scope of Present Work

As indicated in previous sections, TLP bonding is an evolving process for effective joining of difficult-to-weld engineering structural alloys. Lack of adequate understanding of the effect of various process parameters on microstructure of joints produced by bonding techniques has limited its wide commercial usage. The primary objective of this

work, therefore, is to better understand the effect of process parameters on the microstructural changes during TLP bonding of nickel-based materials.

The first part of this work was aimed at studying the cause of a reported anomalous behavior where increased holding time is required to prevent the formation of deleterious eutectic-type microconstituents in TLP joint when temperature is increased.

A large extent of work has been done in studying TLP bonding using fillers containing boron as a MPD [17, 18, 24, 30]. . This is due to boron's fast diffusivity in nickel based alloys that produce shorter processing times. In certain engineering applications, however, such as the repair of nuclear power plant parts by TLP bonding, boron containing fillers can not be used. This is due to the very large neutron absorption cross-section when materials containing boron are used, which results in reduced nuclear reactor performance. Additionally, boron can transmute to helium due to radiation induced porosity, risk of material swelling and, as a result, may cause brittleness of structural materials [42]. In such circumstances, fillers containing alternative MPD such as phosphorous or silicon need to be used. There are few reports on the influence of process parameters on the microstructure of TLP joints produced by using fillers containing these MPD elements. Thus, the second part of this work is focused on studying the effect of process parameters on the microstructure of TLP bonded joints in nickel using a Ni-P filler alloy.

Furthermore, the time required to prevent the formation of the eutectic-type microconstitiunt by complete isothermal solidification of liquated filler may be

prohibitively long for some TLP bonding applications involving the use of fillers containing MPD with limited solubility in the base metal such as phosphorous in nickel. In such cases, it has been suggested that post-braze heat treatment can be done to modify the joint's microstructure and eliminate/reduce the detrimental eutectic-type microconstituents. The final part of this thesis focuses on the study of the effects of post-braze heat treatment parameters on the microstructure of TLP joint in IN738 superalloy using a Ni-P filler alloy.

Chapter 3: Experimental Techniques

3.1 Materials

3.1.1 Base materials

The nickel base superalloy used in the experimental investigation of this research was IN738 superalloy supplied by Hitchiner Manufacturing Co. Inc. in the form of 16 X 8 X 0.6 cm cast plates. The alloy was used in the as-cast condition and its chemical composition is listed in Table 3.1. In addition, a commercially available pure nickel supplied in the form of 16 X 8 X 0.6 cm plates was also used in the study.

3.1.2 Filler alloys

MBF80(Ni-Cr-B) and MBF60(Ni-P) foils supplied by Metglass as 38 μm thick foils were used as the primary filler alloys. Additionally, Nicrobraze150(Ni-Cr-B), Nicrobraze30(Ni-Cr-Si) and Nicrobraze50(Ni-Cr-P) supplied as 200 μm thick tapes were also used to investigate the effect of MPD solute on isothermal solidification rate. Nominal chemical composition of the filler alloys are presented in Table 3.1.

3.2 Sample Preparation and TLP Bonding

As-received base material plates were sectioned using numerically controlled Electro-discharge Machining (EDM). Machined surfaces were ground using 600 grade silicon carbide papers to remove oxide layers and the ground specimens were subsequently cleaned in an ultrasonic bath of acetone solution for 15 minutes. Ceramic paste was applied on the edges of the specimens to prevent spillage of liquated filler during bonding.

Table 3.1: Nominal compositions of filler alloys and base materials [6, 13]

Base Material	**Nominal Chemical Composition wt%**
Inconel 738LC	2.48W, 1.88Mo, 0.07Fe, 0.92Nb, 3.46Al 3.47Ti, 1.69Ta, 0.001S, 0.04 Zr, 0.012B, Bal. Ni
Pure Ni 270	0.01C, 0.003 Fe, <0.001 Mn, <0.001Si <0.001 Mg, <0.001 Cu, <0.001 Co, Bal. Ni
Filler Alloy	**Nominal Chemical Composition wt%**
MBF60(Ni-P)	0.10C, 11.0P, Bal. Ni
MBF80(Ni-Cr-B)	15.2Cr, 0.06C, 4B, Bal. Ni
Nicrobraz150(Ni-Cr-B)	15Cr, 0.06C, 3.5B, Bal. Ni
Nicrobraz50(Ni-Cr-P)	10P, 14Cr, 0.06C. Bal. Ni
Nicrobraz30(Ni-Cr-Si)	10.2Si, 19Cr, 0.06Cr, Bal. Ni

Filler alloy was placed between the cleaned mating surfaces and the assembly was tack-welded using a stainless steel foil to ensure firmness during joining. TLP bonding process was carried out using a temperature-time cycle shown schematically in Figure 3.1 in a vacuum furnace operated at a vacuum of approximately 5 X 10^{-5} torr.

3.3 Microscopic Examination

Bonded specimens were sectioned by electro discharge machining (EDM) due to the brittle nature of eutectic microconstituent within the TLP joints. Sectioned specimens were polished and etched using Kallings solution containing 30 ml CuCl + 90 ml HCL + 90 ml H_2O. Electrolytic etching was done on some specimens using 12ml H_3PO_4 + 40ml HNO_3 + 48 ml H_2SO_4 solution at 6V for 5 seconds. Microstructure of the bonded specimens was examined using an inverted optical microscope and a JEOL 5900 scanning electron microscope equipped with an ultra thin window Oxford energy dispersive x-ray spectrometer (EDS). On average, 20 measurements were taken across the joint on each sample to determine the width of the centerline eutectic product. Chemical compositional analysis of phases formed in the joint was carried out by EDS equipped with INCA analytical software.

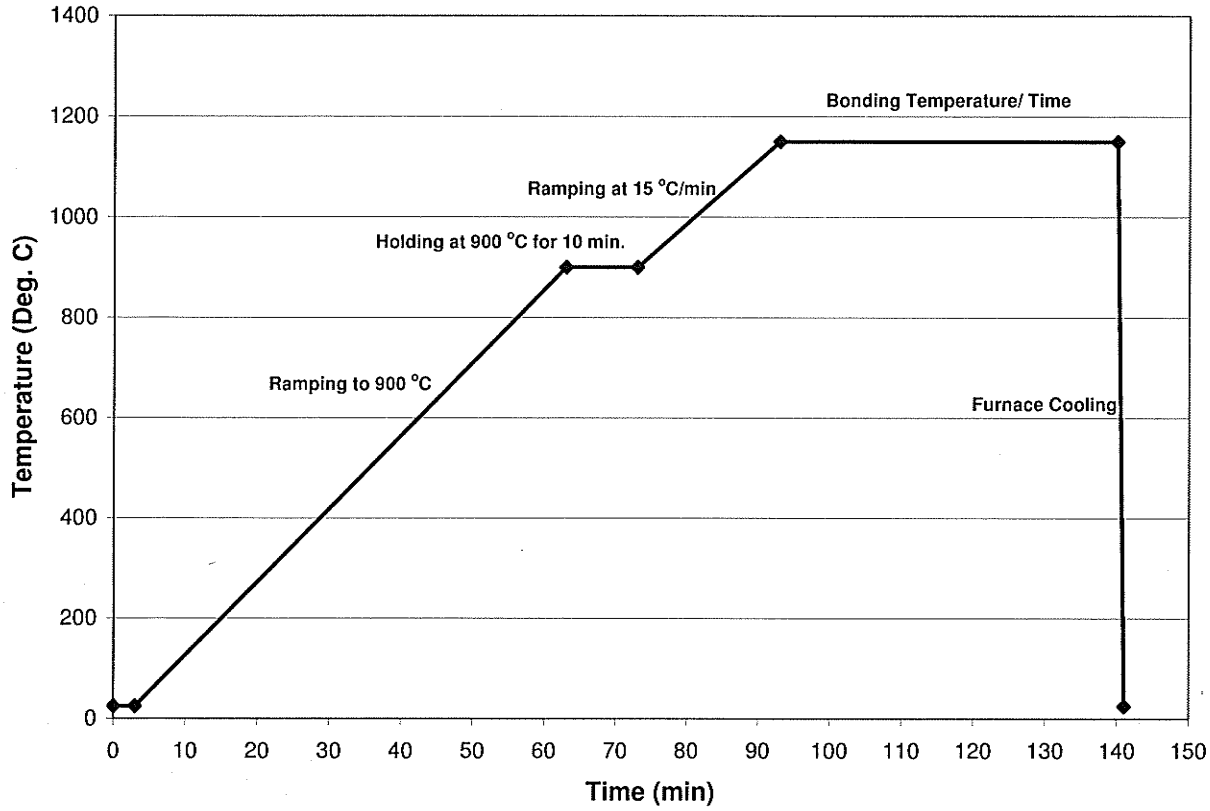

Figure 3.1: Heating cycle used during vacuum brazing

3.4 Analytical Modeling of TLP Bonding

Theoretical calculations of the time t_f required to achieve complete isothermal solidification and the maximum dissolution width W_{max} in binary systems were obtained by writing and using an executable program in VisualBasic using Microsoft Visual Studio.

The program solves the analytical equation 3.1 numerically using Newton-Raphson method to solve for K efficiently. It then uses the result obtained from equation 3.1 to solve for t_f and W_{max} based on equations 3.2 and 3.3. Analytical predictions of the process parameters were also performed using the program. Appendix B provides the details of the program and the method of implementation.

$$\frac{C_{\alpha L}-C_o}{C_{L\alpha}-C_{\alpha L}}=\sqrt{\pi}.\frac{K.(1+erf(K))}{\exp(-K^2)} \qquad (3.1)$$

$$t=\frac{W_{\max}^2}{16.K^2.D} \qquad (3.2)$$

$$W_{\max}=\frac{C_F.W_o}{C_{L\alpha}} \qquad (3.3)$$

Input parameters include initial filler thickness W_o, initial concentration of MPD solute in the filler C_F and in the base metal C_m, solidus and liquidus concentrations of the MPD solute in base metal, $C_{\alpha l}$ and $C_{l\alpha}$ respectively, and diffusivity of the MPD solute, D, in the base metal. Normally, C_F is obtained from charts which list the nominal concentration of the MPD solute in the commercially available filler alloy. In the absence of such charts, the eutectic concentration of the MPD solute in base metal was taken as C_F. Liquidus and solidus concentrations $C_{\alpha l}$ and $C_{l\alpha}$ were obtained using binary phase diagrams for Ni-B,

Ni-P, and Ni-Si systems shown in Appendix A. Binary systems such as Ni-B and Ni-P exhibit very small solidus concentrations which prevent reading $C_{\alpha l}$ directly from the phase diagram. Therefore, linear approximation of the solidus line was assumed and $C_{\alpha l}$ at the bonding temperature was obtained by linear interpolation. Diffusivity of the MPD solute in the base material was calculated using Arrhenius equation 3.4 where R is the gas constant and T is the absolute bonding temperature. The activation energy for diffusion, Q, and the frequency factor, D_o, were obtained from published data in the literature. A list of the activation energies and frequency factors used for the three binary systems used in the course of this study are listed in Table 3.2.

$$D = D_o \exp(-Q / RT) \qquad (3.4)$$

3.5 Numerical Simulation of TLP Bonding

Numerical simulation of TLP bonding was carried out by writing and using a program in MatLAB language that solves an algorithm for solving Fick's diffusion equation developed by Illingworth et. al. [32], which implicitly tracks the liquid-solid interface motion during TLP bonding in binary systems. Details of the algorithm are discussed further in the next chapter and the mathematical implementation is discussed in detail in Appendix C.

Assuming symmetry in the base metal-filler couple, the program was used for simulating the effects of varying process parameters on the time, t_f, required to achieve complete isothermal solidification. Similar to the analytical modeling program, user defined inputs such as half-thickness of filler alloy, C_F, C_m, $C_{\alpha l}$ and $C_{l\alpha}$ are needed to obtain a solution.

The time step and total number of time steps must also be specified in addition to the MPD solute's diffusivity in liquid and solid base metal, D_l and D_s respectively, and D_l was assumed to be relatively constant at $5x10^{-6}$ m^2/sec. After running a simulation, the program automatically plots three graphs, namely: square root of bonding time vs. half-width of liquated region, log of bonding time vs. half-width of liquated region, and percentage of base metal thickness vs. solute concentration. Appendix C provides details of the mathematical implementation and a user's guide for using the program.

Table 3.2: Frequency factors and activation energies used to calculate MPD solute's diffusivity in base metal

Binary System	**Frequency Factor D_o (m^2/sec)**	**Activation Energy (kJ/mol)**	**Reference**
Ni-B	0.14	226	[43]
Ni-P	0.49	284	[43]
Ni-Si	0.00106	271	[44]

Chapter 4: Results and Discussion

Part I: Extension of Isothermal Solidification Completion Time with Increase in Bonding Temperature

4.1 Introduction

An important process parameter in the consideration of TLP bonding for commercial applications is the holding time, t_f, required to achieve complete isothermal solidification and prevents the formation of deleterious eutectic product at the joint. It is generally reported that the time required to achieve complete isothermal solidification decreases with increasing bonding temperature. This is premised on increased isothermal solidification rate caused by higher diffusivity with increased temperature. However, recent studies [19, 30, 38, 45, 46, 47] have shown that there exists an anomalous behavior where isothermal solidification time, t_f, actually increases when the bonding temperature is raised above a certain critical value, T_c. Several causes for this phenomenon have been suggested in the literature, namely:

- Presence of second phase particles within the base alloy at the joint-substrate interface can slow down the solidification process resulting in elongation of the time required to prevent the formation of eutectic-type microconstituents at the joint [30].
- Presence of a second MPD solute in liquated filler can cause a slower diffusing MPD solute to be the controlling factor in the solidification process and, as a result, prolongs isothermal solidification completion time [38].

- Increased base metal dissolution with increase in bonding temperature can produce large liquated volume of insert that requires longer holding time for complete solidification [45].
- Decrease in the solubility of MPD solute in the base metal as bonding temperature is raised causing reduction in the rate of isothermal solidification [19].

Regarding the first suggestion, actual experimental observations [31] have shown that precipitation of the second phase particles reduces considerably and becomes less prominent with increase in temperature. Additionally, precipitation of second phase particles does not explain the anomalous behavior in systems that do not form interfacial precipitates. Therefore, the formation of second phase particles is unlikely to be the main cause of reduction in isothermal solidification rate with increase in temperature.

Likewise, the second suggestion based on the presence of a second MPD solute can not explain the occurrence of the anomalous behavior in systems where only one MPD solute is involved. Reported decrease in the rate of isothermal solidification at higher temperatures in binary systems where there were essentially no secondary solutes [31] suggests that èvents fundamentally related to diffusion process, instead of second MPD solute effect may be responsible for the phenomenon.

Limited information is available about the effect of increased base metal dissolution and decreased solute solubility on the time required to complete isothermal solidification during TLP bonding at high joining temperatures. Therefore, the effects of base metal

dissolution and solute solubility on increase in isothermal solidification completion time with increase in temperature were studied and compared in this section of the thesis. The study led to identification of a significant cause of the anomalous behavior which has not been reported in the literature prior to the present work. This phenomenon is also reported and discussed in this section.

4.2 Effect of Bonding Temperature on Base Metal Dissolution

Using a 76 μm thick MBF80(Ni-Cr-B) filler, IN738 was bonded at three different temperatures, 1100, 1140 and 1180 °C for 7 hrs . Micrographs of the joints are shown in Figures 4.1 to 4.3. Average dissolution widths obtained from the micrographs were plotted against bonding temperatures as presented in Figure 4.4, which showed an increase in dissolution width with increase in temperature.

An analytical TLP model by Tuah-Poku et. al. [28] and Ramirez and Liu [31] was also used to simulate the effect of temperature on dissolution width using 80 μm Ni-B filler and pure nickel base material and the result is shown in Figure 4.5. Similar to the experimental result, a linear relationship between dissolution width and temperature was predicted. The increased base metal dissolution width with temperature can be understood from the nature of the Ni-B phase diagram. Based on this diagram, liquidus concentration reduces with temperature increase, which implies that for an initial filler alloy composition close to the eutectic value, more base material will be required to melt-back into the liquated filler in order to dilute the liquid to attain equilibrium composition.

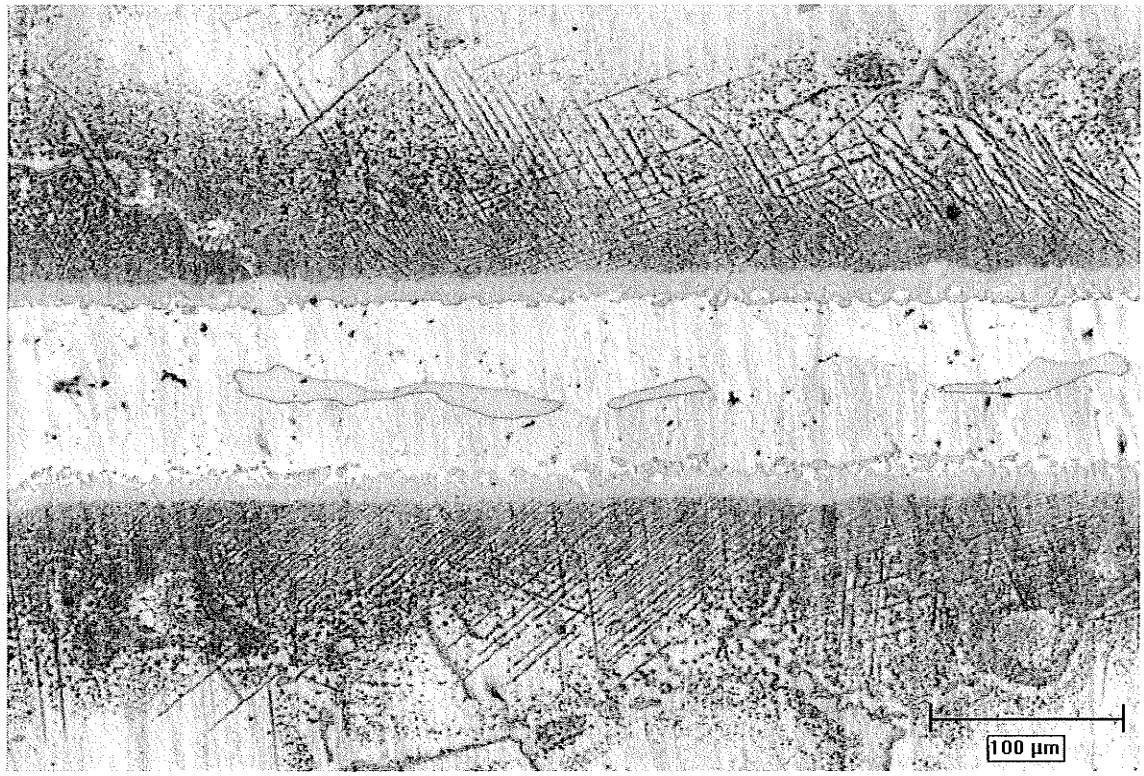

Figure 4.1: Micrograph of IN738 bonded with 76 µm MBF80 filler at 1100 °C for 7 hrs (X200)

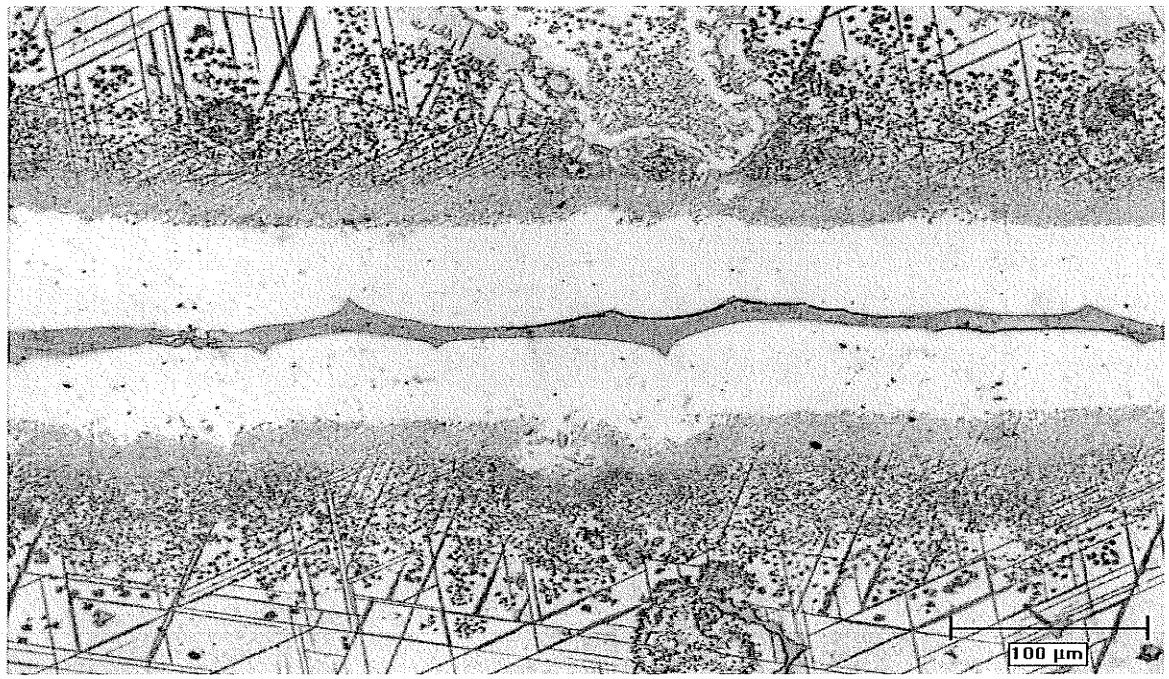

Figure 4.2: Micrograph of IN738 Bonded with 76 µm MBF80 filler at 1140 °C for 7 hrs (X200)

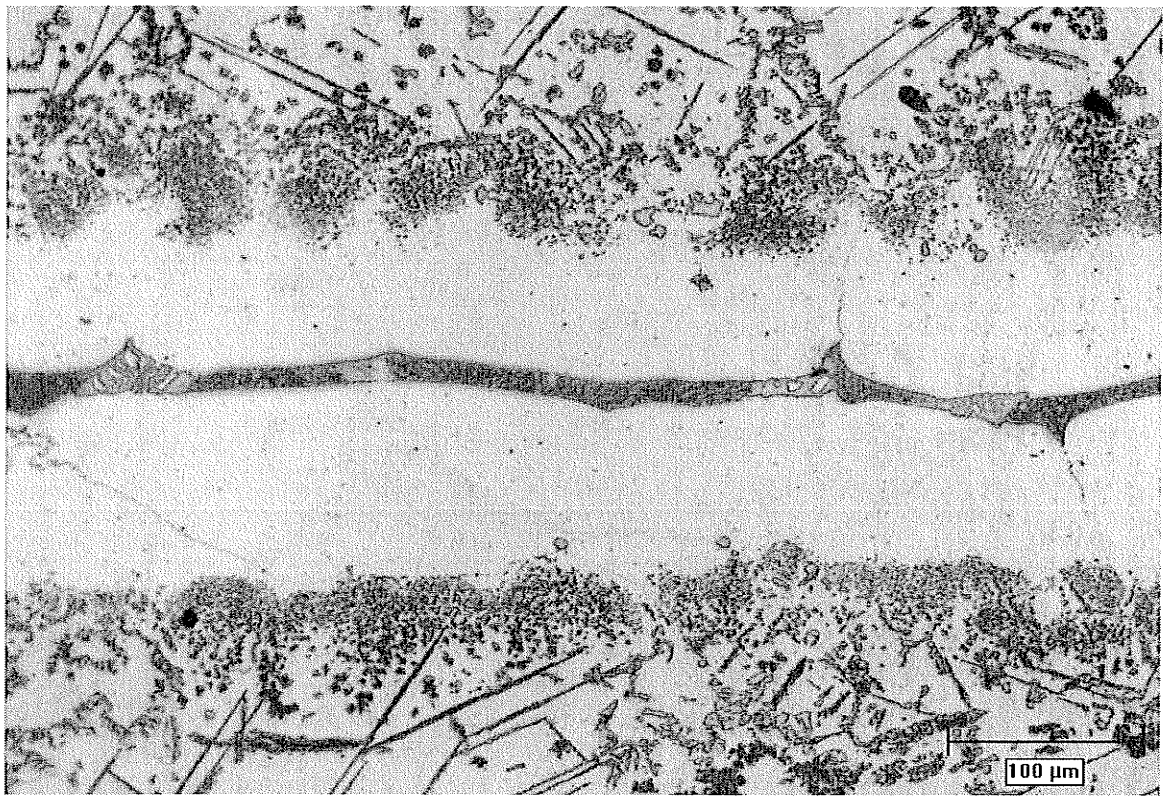

Figure 4.3: Micrograph of IN738 bonded with 76 µm MBF80 filler at 1180 °C for 7 hrs (X200)

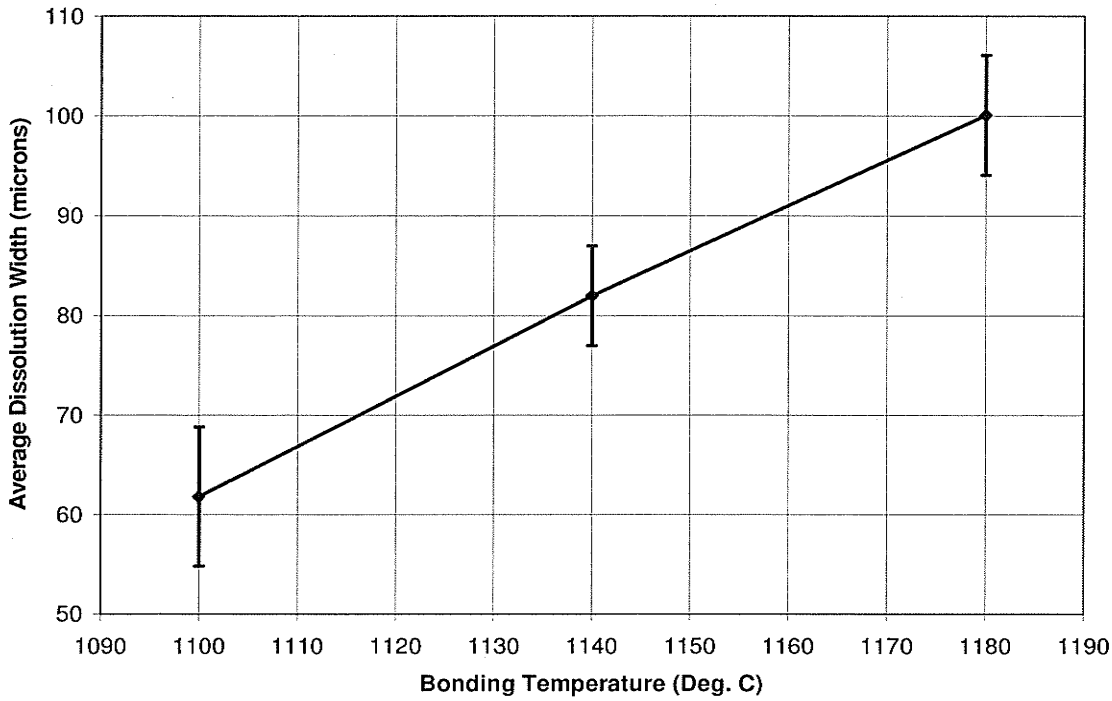

Figure 4.4: Effect of holding temperature on the average dissolution width during TLP bonding of IN738 using 76 μm MPF80 filler

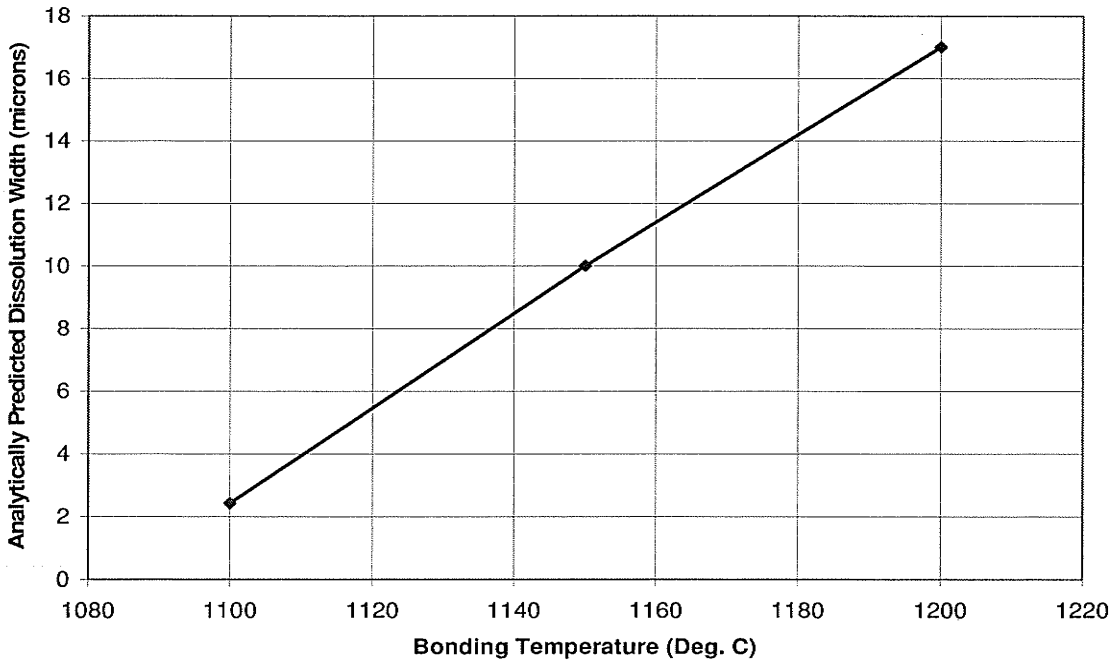

Figure 4.5: Analytical simulation of maximum dissolution width with bonding temperature during TLP bonding of pure Ni using 76 μm Ni-B filler

It was noted that the experimental dissolution width obtained for IN738 was larger than the calculated value for pure nickel using the analytical model. It is possible that the other alloying elements present in IN738 played a role in increasing the dissolution width compared to the case of pure nickel where only the effect of boron was considered.

The effect of other alloying elements on base metal dissolution has been previously suggested by Nakagawa et al. [40]. They reported that dissolution may increase with increase in base metal alloying element concentration and that the time for completion of the dissolution stage may also increase for complex commercial superalloys relative to binary systems due to the presence of elements other than the MPD solute in the base material. Since increase in temperature produces increased base alloy dissolution, it is, thus, apparent why increased temperature can be expected to cause increase in isothermal solidification completion time, t_f, as suggested by MacDonald and Eager [45]. Nevertheless, it is to be noted that reduction of solute solubility in the base metal with increase in temperature can also produce similar effect.

4.3 Comparison of the Effects of Increased Base Metal Dissolution and Reduced Solute Solubility on Extension of t_f

To study the relative effect of base metal dissolution and solute solubility on extension of t_f with increase in temperature, analytical modeling was used to simulate TLP bonding of pure nickel using Ni-P filler. This was performed by keeping the maximum liquid interlayer width W_{max} constant at varying temperatures where the solubility of the MPD solute in the base metal differs to examine the sole effect of solubility without any change in dissolution width.

The result presented in Figure 4.6 show that, at a constant W_{max}, t_f initially decreases with increasing bonding temperature up till a critical temperature T_c, above which increase in temperature increases t_f. According to Ni-P phase diagram, solubility of phosphorous reduces with increase in bonding temperature above the eutectic temperature. This, thus, indicates that increase in isothermal solidification completion time with increase in temperature can occur during TLP bonding due solely to the effect reduced solute solubility without contribution from increased base alloy dissolution.

Even though reduction in solute solubility with increased temperature can cause extended t_f at temperatures above T_c, analytically predicted T_c (1250 °C) for the Ni-B system, beyond which this would occur is excessively higher than what has been observed experimentally [46]. This suggests that besides the mere reduction in solute solubility, there is possibly another phenomenon contributing to the anomalous behavior of extension in t_f with increase in temperature. Moreover, an important assumption in the analytical model, on which the effect of solute solubility is based, appears unfeasible for some TLP bonding conditions. This issue, which resulted in identification of a new alternate cause of T_c in this study, deviation from parabolic law between average eutectic width and holding time, is reported and discussed next.

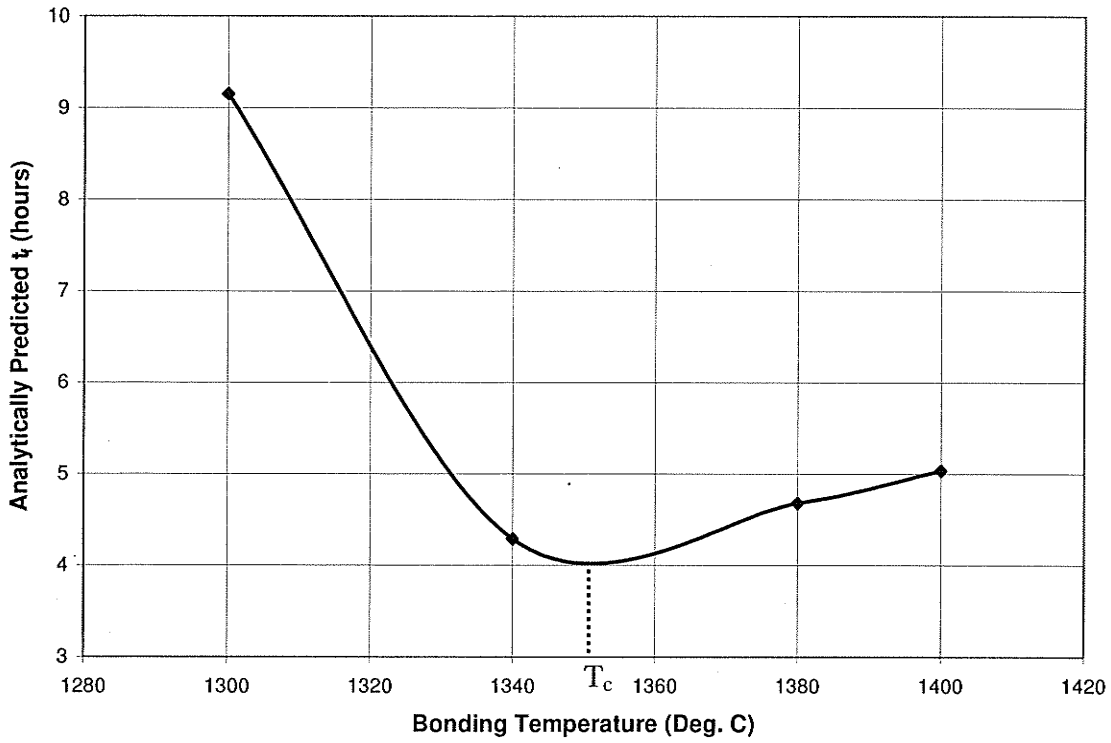

Figure 4.6: Analytical simulation of variation of isothermal completion times with bonding temperature using a constant W_{max} for Ni-P system

4.4 Deviation from Parabolic Behavior – A New Cause of T_c

As stated earlier, theoretical diffusion-based models have been developed to represent the underlying mechanism of isothermal solidification stage of TLP bonding and to predict the t_f necessary for producing a eutectic free joint. Standard analytical models generally rely on an assumption of a parabolic-type relationship between solid-liquid interface displacement and holding time to predict t_f. Predictions based on this approach have been previously found to correlate reasonably well with some experimentally determined t_f in different alloy systems including IN738 superalloy [46, 48]. Nevertheless, a more careful consideration of Fick's diffusion equation on which the standard analytical models are based, suggests that the parabolic behavior may not be a general rule applicable to all process conditions during TLP bonding. Proper understanding of influence of salient TLP bonding parameters on t_f is imperative to the calibration of existing models and fundamental to the development of more versatile, effective and reliable models for optimizing the joining technique for industrial applications. An objective of the present work was, therefore, to experimentally verify the supposed limitation of the parabolic behavior concept and to gain better understanding of the influence of process variables on preclusion of deleterious eutectic microconstituent during TLP bonding of IN738 superalloy.

To study the issue of parabolic behavior, IN738 specimens were TLP bonded at 1140°C and 1200°C for various holding time ranging from 10 – 720 mins. The microstructure of the joint prepared for 10 mins, as observed by SEM operated in back scatter mode, is shown in Figure 4.7.

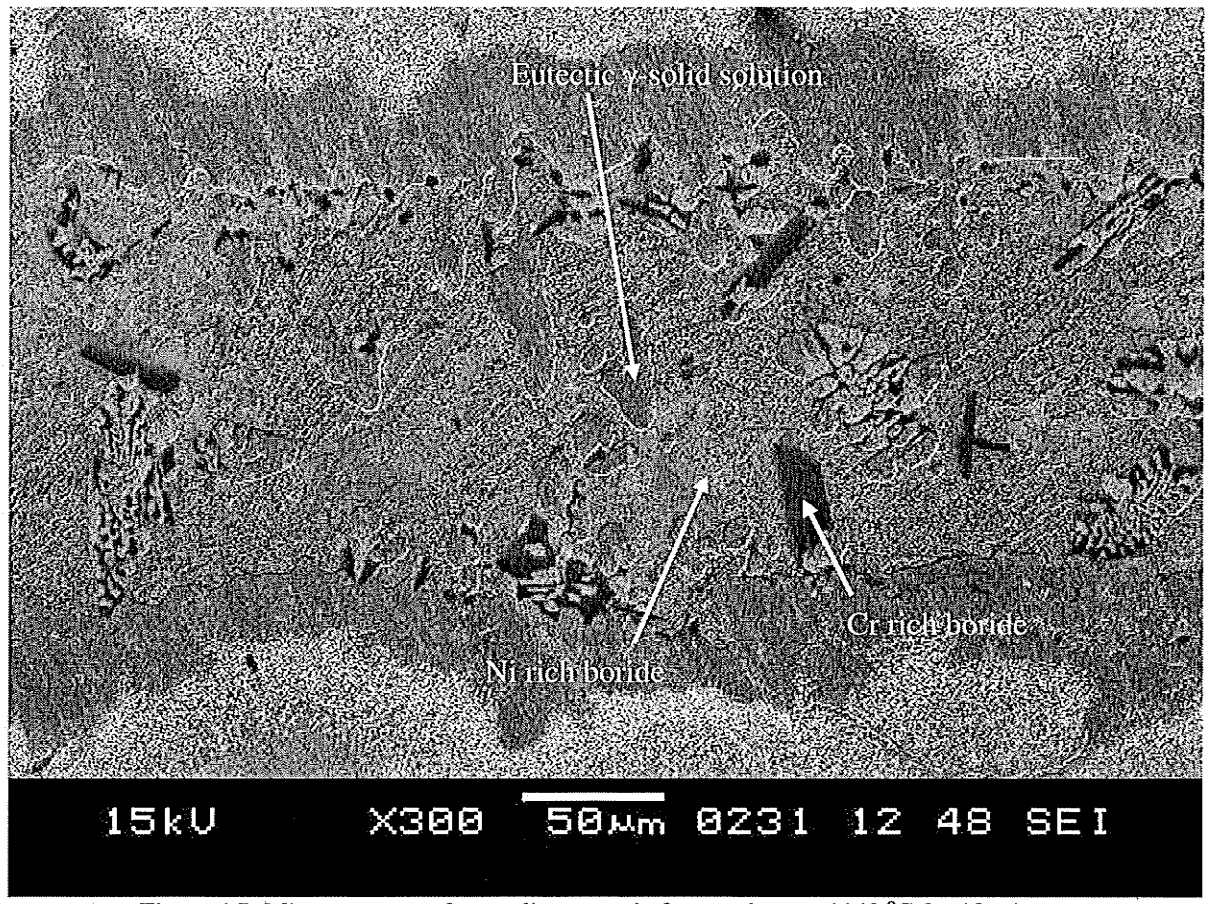

Figure 4.7: Microstructure of centerline eutectic for test done at 1140 °C for 10 min

The microstructure showed the existence of a continuous distribution of centerline eutectic microconstituent consisting of nickel base solid solution phase, nickel rich boride phase, and chromium rich boride phase. Similar eutectic product in the centerline of TLP bonded Ni alloys have been reported in the literature [46, 48-50]. The eutectic was formed from residual liquated insert during cooling from the bonding temperature due to insufficient diffusion of MPD solute, boron, away from the liquid to achieve complete isothermal solidification during holding. Increase in the holding time resulted in increased boron diffusion and isothermal solidification with corresponding decrease in the eutectic width. A plot of average eutectic width against square root of holding time is presented in Figure 4.8, which shows a linear relationship up to a holding time of 330 mins, beyond which significant deviation from linearity occurred.

Analytical TLP bonding models are based on solutions to Fick's second law of diffusion equation:

$$\frac{\partial C}{\partial t} = D\frac{\partial^2 C}{\partial x^2} \qquad (4.1)$$

where $\partial C/\partial t$ is the change in solute concentration with time at a given position in the base metal, D is the diffusion coefficient, and $\partial^2 C/\partial x^2$ is the rate of change of solute concentration gradient with respect to distance [19, 20, 22, 24]. In these standard mathematical models, it is generally assumed that during isothermal solidification stage, diffusion-induced migration of the solid/liquid interface, h, follows a parabolic law,

$$h = 2\varphi\,(t^{1/2}) \qquad (4.2)$$

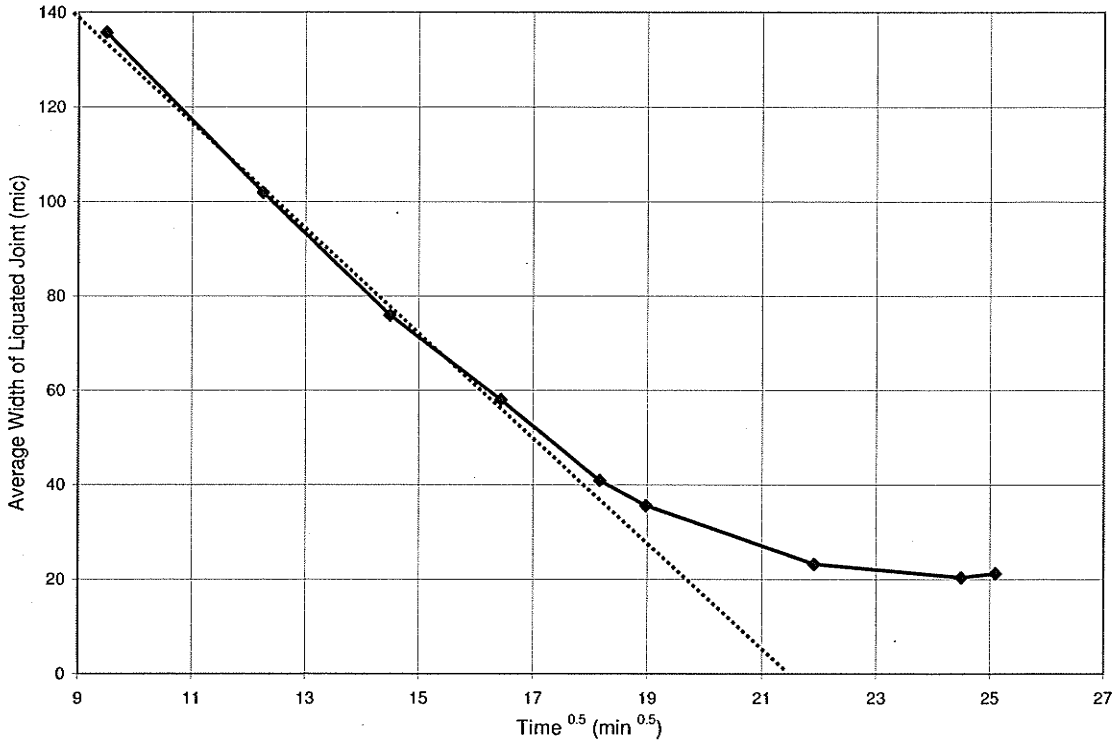

Figure 4.8: Plot of average eutectic width vs. square root of time

where t is the holding time and the parameter φ indicates the rate of interface migration. This implies a linear relationship between residual liquid thickness and square root of holding time. It is implicitly assumed in these models that the base material is of infinite or semi-infinite thickness, which permits the use of error function solutions of the Fick's diffusion equation to represent solute distribution in the solid substrate. This approach allows the solid-liquid interface displacement to maintain its parabolic behavior with time during continual diffusion of the MPD solute into the base material, even as its concentration gradient in the solid reduces persistently.

In most TLP bonding experiments, however, the base materials do have finite thickness and this could lead to consequential deviation of experimental observations from predictions based on the standard analytical models. This possibility and its consequences have not been generally reported in TLP bonding studies. An important possible case is that, for a finite base material thickness, reduction in the rate of change of solute concentration gradient with respect to distance below a critical value at any given location in the substrate can cause significant departure from the parabolic migration of the solid-liquid interface with time.

This plausible diffusion event, which is not captured or predicted by standard analytical TLP bonding models, can be duly elucidated by the application of implicit finite difference model to numerically solve the Fick's diffusion equation. The rate of change of solute concentration gradient with respect to distance at any location in the base material affected by solute diffusion is in turn dependent on the actual concentration gradient at such location.

Proper study of deviation from parabolic behavior can be done if a suitable simulation tool is chosen. In contrast to analytical models which depend on error function solutions, numerical models can solve the diffusion equation for a range of initial and boundary conditions, even though the analysis is complex due to the moving solid-liquid interface. The numerical approach does not assume a constant solidification rate and, as a result, deviation from the parabolic behavior between holding time and width of the remaining joint's microconstituents can be duly detected.

A mathematical algorithm for solving the standard Fick's equation 4.1 has been developed by Illingworth et. al. [32]. Their approach uses a variable spatial discretization and a transient finite difference method to solve the governing equations stated previously in equations 2.13 to 2.15 from which equations 4.3 to 4.5 are derived; where equation 4.5 is a discretization equation for the displacement of liquid-solid interface derived ensuring conservation of solute.

$$\left[p_i^{j+1}s^{j+1} - p_i^j s^j\right]\left[u_{i+1/2} - u_{i-1/2}\right] = \frac{\delta t}{s^{j+\sigma}}\left[(D_A)_{i+1/2}^{j+\sigma}\frac{p_{i+1}^{j+\sigma} - p_i^{j+\sigma}}{u_{i+1} - u_i} - (D_A)_{i-1/2}^{j+\sigma}\frac{p_i^{j+\sigma} - p_{i-1}^{j+\sigma}}{u_i - u_{i-1}}\right]$$
$$+ (s^{j+1} - s^j)\left[p_{i+1/2}^{j+\sigma}u_{i+1/2} - p_{i-1/2}^{j+\sigma}u_{i-1/2}\right] \tag{4.3}$$

$$\left[q_i^{j+1}(L - s^{j+1}) - q_i^j(L - s^j)\right](v_{i+1/2} - v_{1-1/2}) = \frac{\delta t}{L - s^{j+\sigma}}\left[(D_B)\frac{q_{i+1}^{j+\sigma} - q_i^{j+\sigma}}{v_{i+1} - v_i} - (D_B)\frac{q_i^{j+\sigma} - q_{i-1}^{j+\sigma}}{v_i - v_{i-1}}\right]$$
$$+ (s^{j+1} - s^j)\left[q_{i+1/2}^{j+\sigma}(1 - v_{i+1/2}) - q_{i-1/2}^{j+\sigma}(1 - v_{i-1/2})\right] \tag{4.4}$$

$$\frac{D_B \delta t}{L - s^{j+\sigma}}\left(\frac{q_1^{j+\sigma} - c_B}{v_1}\right) - \frac{D_A \delta t}{s^{j+\sigma}}\left(\frac{c_A - p_{N-2}^{j+\sigma}}{1 - u_{N-2}}\right)$$
$$= (s^{j+1} - s^j)\left[\frac{1+u_{N-2}}{2} p_{N-1-1/2}^{j+\sigma} + \frac{1-u_{N-2}}{2} c_A - (1 - \frac{v_1}{2}) q_{1/2}^{j+\sigma} - \frac{v_1}{2} c_B\right]$$

(4.5)

Where δt is the time step; s^j is the future interface position in time step j; p_i^j is the concentration in phase A in position i in time step j; q_i^j is the concentration in phase B in position i in time step j; L is the thickness of phase B plus half-thickness of phase A; u is the proportional position in phase A; v is the proportional position in phase B; M and N is the number of discretisation points; D_A is the diffusion coefficient in phase A; D_B is the diffusion coefficient in phase B; c_A is the equilibrium concentration of phase A in contact with B; c_B is the equilibrium concentration of phase B in contact with A; σ is a constant between 0 and 1.

In the present work, a program was written in MatLAB code which implicitly solves equations 4.3 to 4.5 using the algorithm outlined in appendix C. The program produces a converged numerical solution for the liquid-solid interface migration during TLP bonding. A detailed guide to the mathematical implementation of the program is provided in appendix C.

The above approach was used in the present work to simulate TLP bonding of 6 mm thick Ni base metal having initial boron concentration of 0.012 wt % with a filler alloy of varying thicknesses and containing 4 wt% of boron at 1140 °C. Figures 4.9 and 4.10

shows a plots of residual liquid half-layer thickness against square root of holding time and the corresponding distribution of boron concentration in the base metal after completion of isothermal solidification, respectively, for different initial gap sizes. As can be seen by the plots, a linear relationship exists between the liquid thickness and square root of time throughout the duration of holding time required to achieve complete isothermal solidification for initial gap sizes 60 and 80 μm. An increase of the gap size to 120 and 130 μm, however, resulted in a considerable deviation from the linear relationship toward the end of isothermal solidification, which can be related to the concomitant reduction of solute concentration gradient below a certain critical level, $(\partial C/\partial x)_c$. This, thus, theoretically shows that an increase in diffusion of MPD solute due to increased gap size during TLP bonding can lead to a situation where the parabolic relationship between solid-liquid interface displacement and holding time will cease to hold due to considerable reduction in solute concentration gradient.

The result of the present work, which showed deviation from the linear relationship in a 120 μm gap size specimen experimentally, supports this concept. A review of reported data in the literature also showed deviation from the parabolic rule under some experimental conditions [23, 30, 31] even though the occurrence was not related to $(\partial C/\partial x)_c$. In a recent study of a novel technique involving the use of differential scanning calorimetry (DSC) to accurately quantify the kinetics of solid/liquid interface migration during TLP bonding, it was observed that an increase in filler gap size resulted in notable deviation from the parabolic law [23]. Their observation could serve as further experimental support to the concept that increased diffusion of MPD due to larger gap size can result in breakdown of the parabolic behavior.

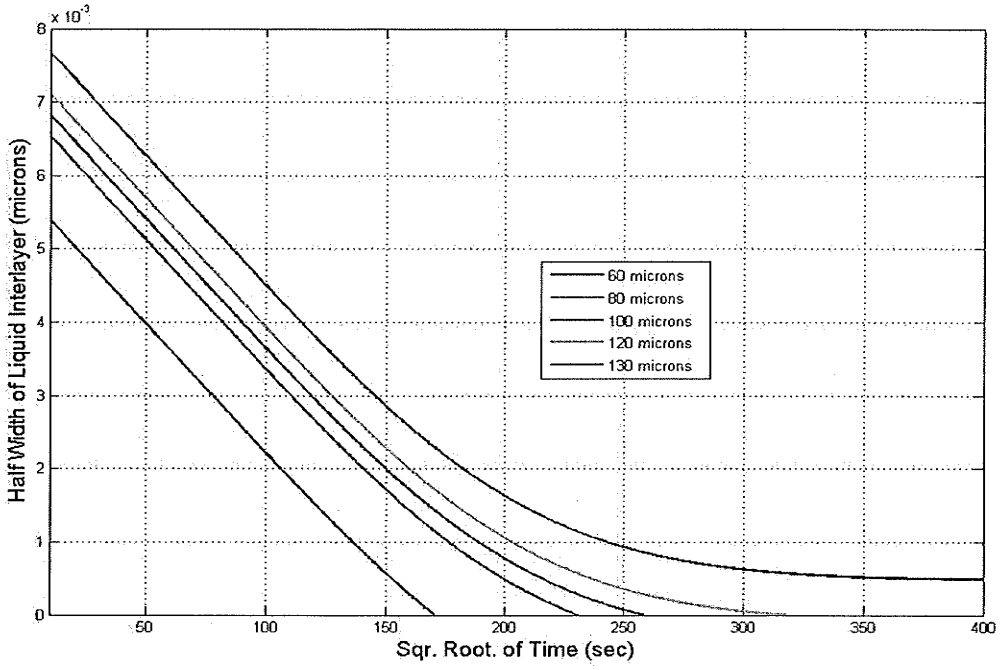

Figure 4.9: Numerically simulated variation of half-width of liquated interlayer with square root of time using different initial gap sizes

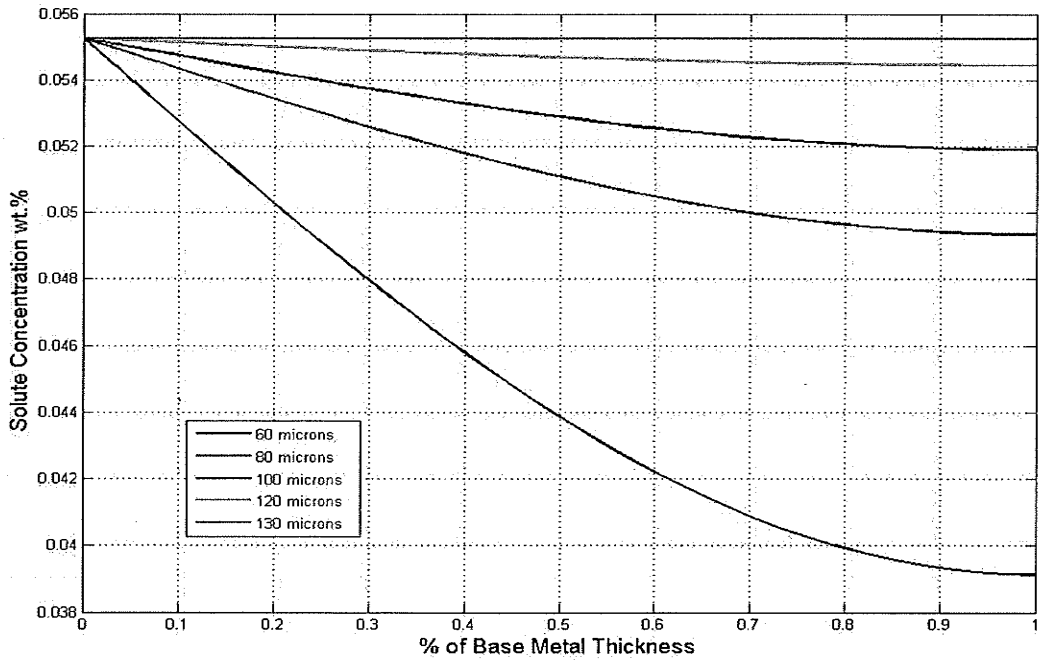

Figure 4.10: Numerically simulated variation of boron concentration in 6mm base metal thickness using different initial gap sizes

It has been previously suggested that deviation from parabolic behavior during TLP bonding is a consequence of presence of two MPD solutes with different solubilities and/or diffusivity in the liquated interlayer during joining [38]. Nevertheless, reported observation of this phenomenon in a binary system containing exclusively one MPD solute [31] provides experimental evidence that deviation from the parabolic law is possible under the influence of concentration gradient of a single diffusing solute without a necessary contribution from a second diffusing MPD solute, as explicated above.

Besides the mere occurrence of departure from parabolic behavior, the consequence of this deviation with regard to the influence of a crucial joining parameter, bonding temperature, on preclusion of deleterious eutectic microconstituent is vital. At the onset of deviation, the constant parameter φ in equation 4.2 becomes inadequate in representing isothermal solidification rate as the rate reduces continuously within the deviation zone. The rate of decrease of the isothermal solidification rate within the deviation zone and, thus, the size of the zone, which determines the time required for complete isothermal solidification, are dependent on the magnitude of $\partial C/\partial x$. The $\partial C/\partial x$ is influenced by the solubility of the diffusing solute in the base material at the particular bonding temperature. As illustrated in Figure 4.11, a decrease in boron solubility from 0.055 – 0.0051 wt% raised $(\partial C/\partial x)_c$, which caused wider deviation zone in the 60 μm joint. This can constitute a major practical significance in situations where the solubility of a MPD solute reduces with increase in temperature, for instance, above the eutectic temperature of Ni-B system. Above any temperature where deviation from parabolic behavior occurs, a higher $(\partial C/\partial x)_c$ due to decreased solute solubility will produce extended deviation zone with an attendant greater extent of isothermal solidification rate reduction. This may lead

to a situation where a longer holding time t_f will be required to produce eutectic-free joint by complete isothermal solidification at a higher bonding temperature compared to what is needed at a lower temperature. To verify this possibility, in the present work, IN738 specimens with 120 μm initial gap size were TLP bonded at 1140 and 1200 °C for 16 h. Microstructural examination of the joints showed that while complete isothermal solidification was achieved in the 1140 °C specimen after the 16 hrs of holding, centerline eutectic was formed in the 1200 °C joint due insufficient holding time for complete isothermal solidification as seen in Figures 4.12 to 4.14. This is in contrast to the general expectation that an increase in bonding temperature will reduce the time required to achieve complete isothermal solidification. A notable observation was made in the 1200°C joint in that the centerline eutectic was found to consist of boron rich particles, which were not present in the 1140 °C joint prepared for same holding time.

This indicates that the diffusion of boron in the base alloy away from the liquid interlayer was reduced at the 1200°C bonding temperature compared to 1140 °C, which can be related to higher degree of deviation from parabolic behavior at 1200 °C. Similar experimental observations in other base and filler alloy systems where increase in bonding temperature above a certain temperature, T_c, resulted in elongation of t_f, has been reported in the literature. However, this is the first time that this phenomenon will be related to the effect of deviation from parabolic behavior.

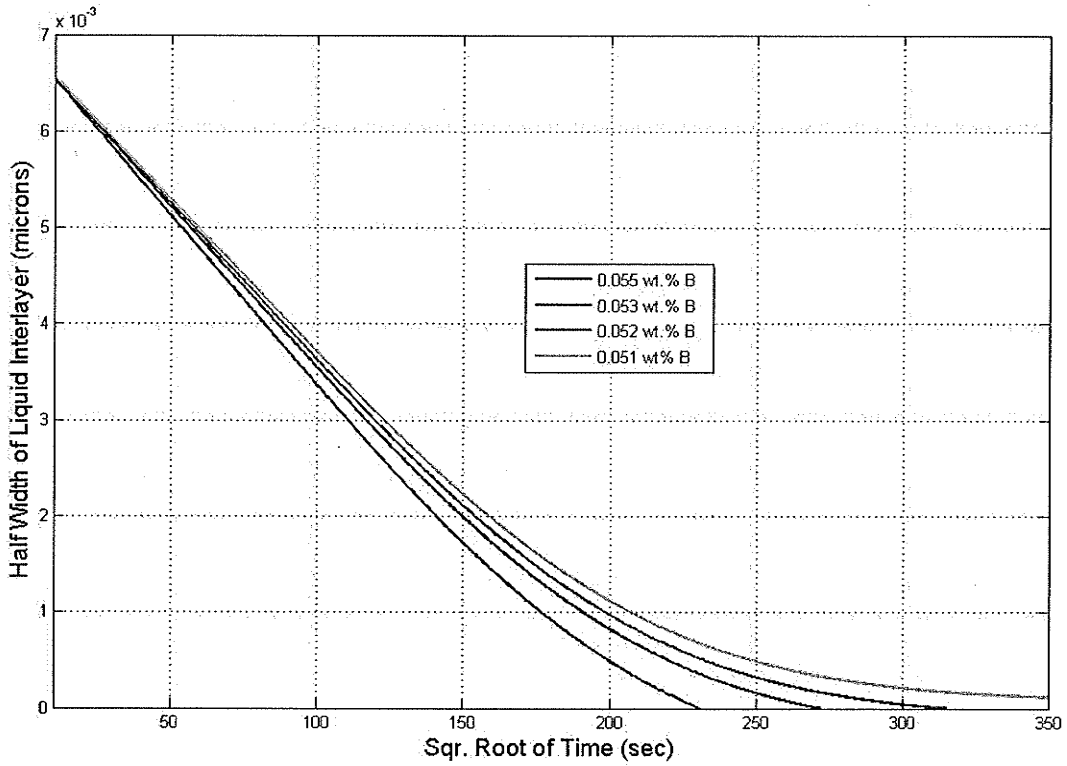

Figure 4.11: Numerically simulated variation of half-width of liquated interlayer with square root of time obtained by reducing boron solubility in base metal

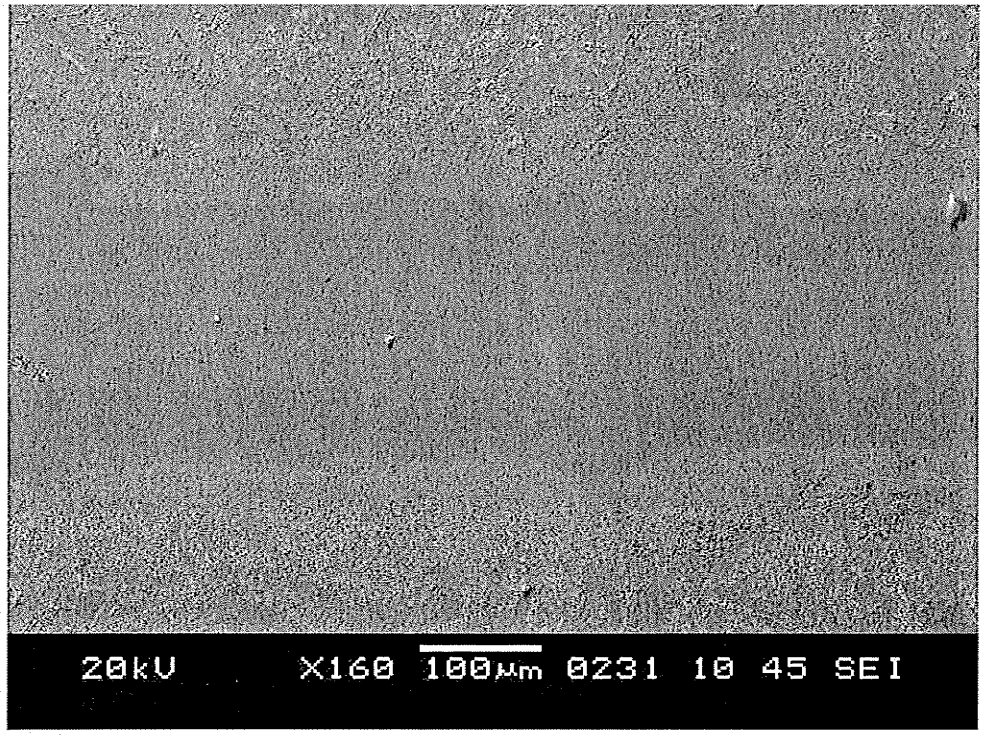

Figure 4.12: Complete isothermal solidification for test done at 1140 °C, 16 hrs

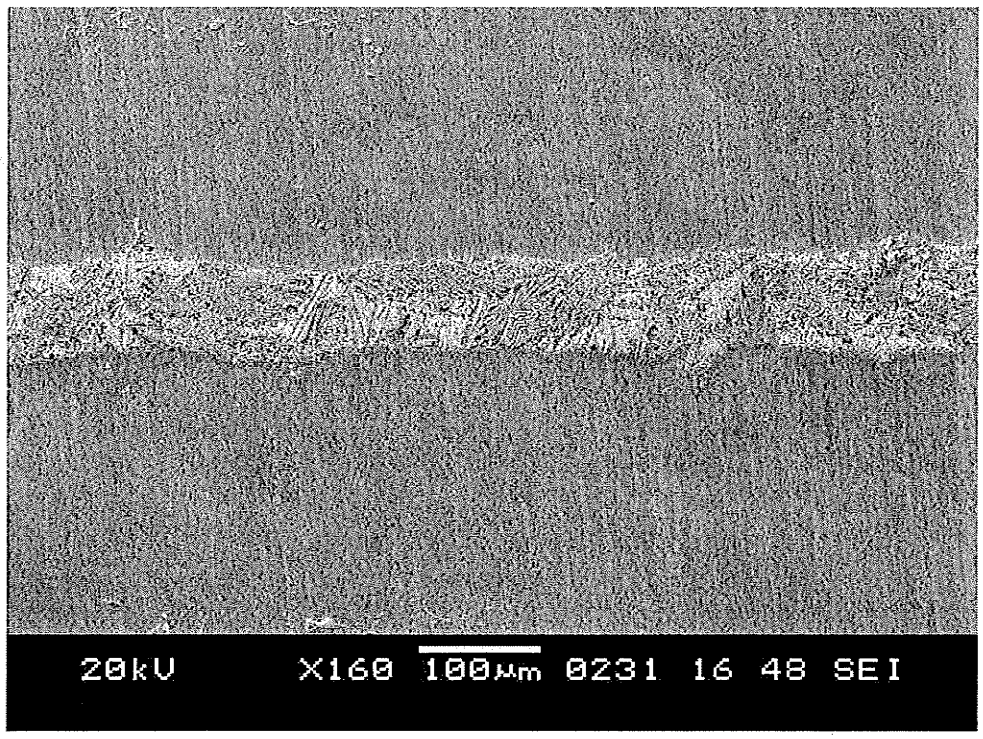

Figure 4.13: Centerline eutectic present for test done at 1200 °C, 16 hrs

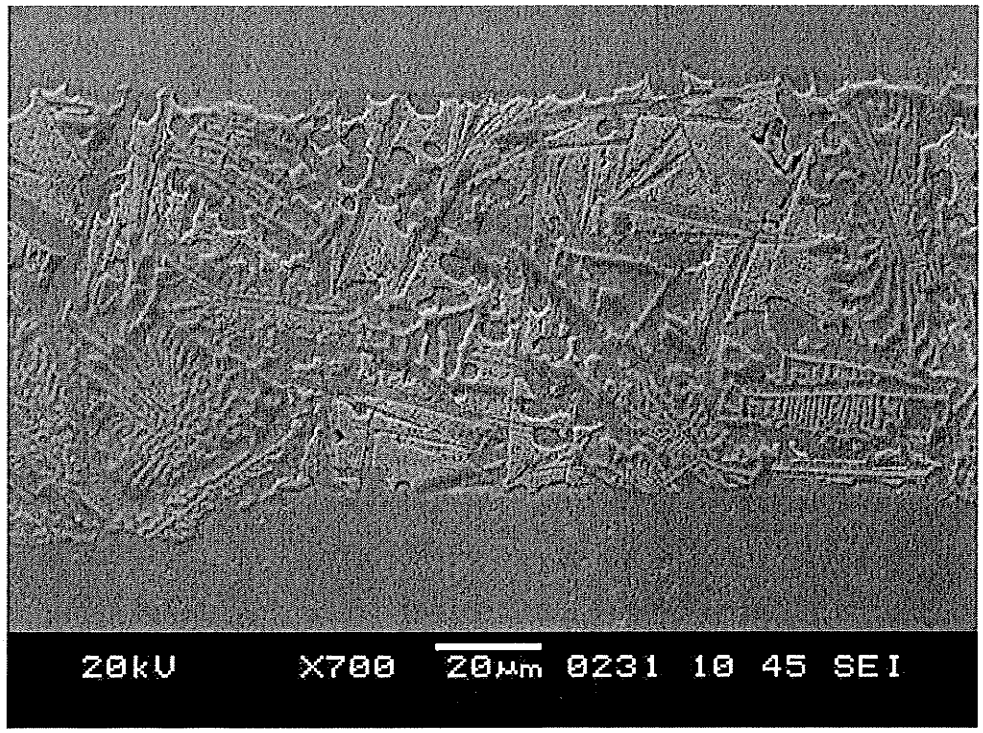

Figure 4.14: High magnification of centerline eutectic present for test done at 1200 °C, 16 hrs

It is needed to clarify here that the concept of increase in t_f with increase in temperature above T_c due to deviation from the parabolic behavior that is discussed in the present work is strategically different from another concept by which t_f can increase with increase in temperature due exclusively to decrease in solute solubility. In the case of the latter concept, in the absence of deviation from the parabolic relationship, based on Ficks diffusion equation, an increase in temperature can lead to a temperature where reduced $\partial C/\partial x$ at the onset of isothermal solidification due to lower solute solubility can override the increased diffusion coefficient and, thus, result in elongation of t_f. This concept is the only type that is captured and predicted by standard analytical TLP bonding models. According to standard analytical models, for a given filler-base alloys system, the temperature, T_c, is constant, typically very high and it is independent of initial gap size. On the contrary, however, based on the concept of deviation from parabolic behavior, for a given filler-base alloys system T_c is a variable that is dependent on gap size. An increase in gap size will reduce T_c below the constant value predicted by analytical TLP model. A tactical criterion that can be used to determine which of the two concepts is possibly operational in TLP bonding experiment where T_c occurs is suggested here. In the absence of deviation from parabolic behavior, the isothermal solidification rate will be lower at temperatures above T_c compared to some at temperatures below it, for all holding time as shown for an example in Figure 4.15. However, in situations where T_c is caused by deviation from parabolic behavior, at some temperatures initially higher relative to that at lower temperatures until after the considerable extent of solute diffusion to initiate deviation has occurred, subsequent to which the rate will decrease as shown in Figure 4.16.

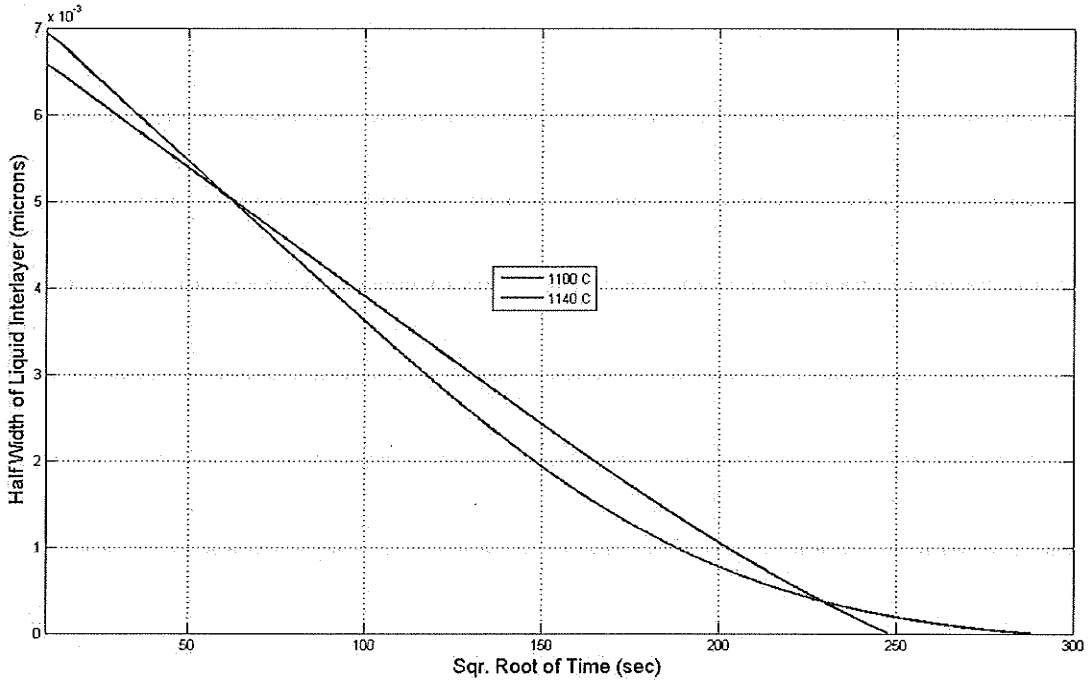

Figure 4.15: Numerically simulated variation of half-width of liquated interlayer with square root of time as temperature is increased beyond T_c

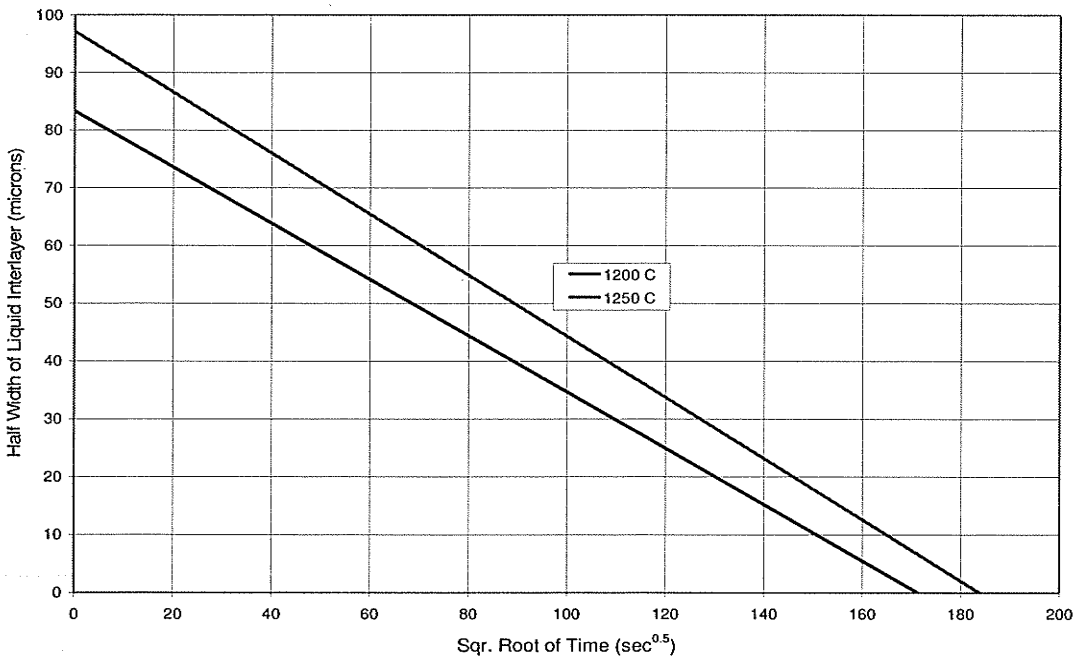

Figure 4.16: Analytically simulated variation of half-width of liquated interlayer with square root of time showing a constant solidification rate throughout the solidification process

Proper consideration of possible deviation from the parabolic rule, which is not envisaged by standard analytical models and its likely consequence on reliable prediction of t_f, is crucially important in the optimization of TLP bonding parameters to obtain joints free of deleterious eutectic microconstituents.

4.5 Influence of Process Parameters on T_c Based on the Concept of Deviation from Parabolic Behavior

4.5.1 Effect of solubility of MPD solute on T_c

Based on the concept that deviation from parabolic law occurs due to decrease in $\partial C/\partial x$ below a critical value, an increase in solute solubility in the base material can be expected to have an effect on the deviation and T_c.

In order to theoretically study the effect of solubility of the MPD solute on deviation from parabolic behavior, numerical simulation was performed by varying solubility of boron at 1200 °C and the result in presented in Figure 4.17. An increase in solubility would increase $\partial C/\partial x$ in the base material which in effect extend the region where solid-liquid interface migration maintains a parabolic relationship with holding time, thereby preclude the occurrence of deviation from parabolic behavior.

Boron and silicon are commonly used MPD solutes in filler alloys for joining nickel base superalloys. While boron exhibits higher diffusivity in nickel, its solubility in nickel alloys is significantly lower than that of silicon. Numerical simulation was performed to study the effect of the low boron solubility compared to that of silicon on the occurrence

of deviation from parabolic behavior and, thus, the occurrence of T_c during TLP bonding. Simulated variation of isothermal solidification time with bonding temperature using boron and silicon containing fillers is shown in Figure 4.18 and 4.19. As can be seen from the figures, deviation from the parabolic law occurred in the Ni-B system, while the parabolic law was obeyed for all bonding temperatures in the Ni-Si system.

The maintenance of parabolic relationship in Ni-Si system in contrast to Ni-B system can be related to the higher solubility of Si in nickel, which would result in higher concentration gradients and, thus, $(\partial C/\partial x)_c$. This can be significantly important, in that, even though Si exhibits lower diffusivity in Ni, the rate of isothermal solidification can be faster in Ni-Si system compared to Ni-B at bonding temperatures where deviation from parabolic occurs in Ni-B system. To experimentally investigate this possibility, TLP bonding of IN738 was performed at 1140 °C for 7 hours using 200 μm thick Nicrobraz150(Ni-Cr-B) and Nicrobraz30(Ni-Cr-Si) filler. Optical micrographs of the joints are shown in Figures 4.20 and 4.21. The average width of centerline eutectic was found to be 86 μm in the boron-containing filler 43 μm thick in the specimen bonded with silicon-containing filler. The thicker eutectic in the boron-containing joint due to deviation induced reduction in the rate of isothermal solidification is consistent with predicted behavior.

Accordingly, this suggests that the prohibitive extension of t_f due to deviation at higher bonding temperature can be avoided by the use of filler alloys that contain solutes with high solubility.

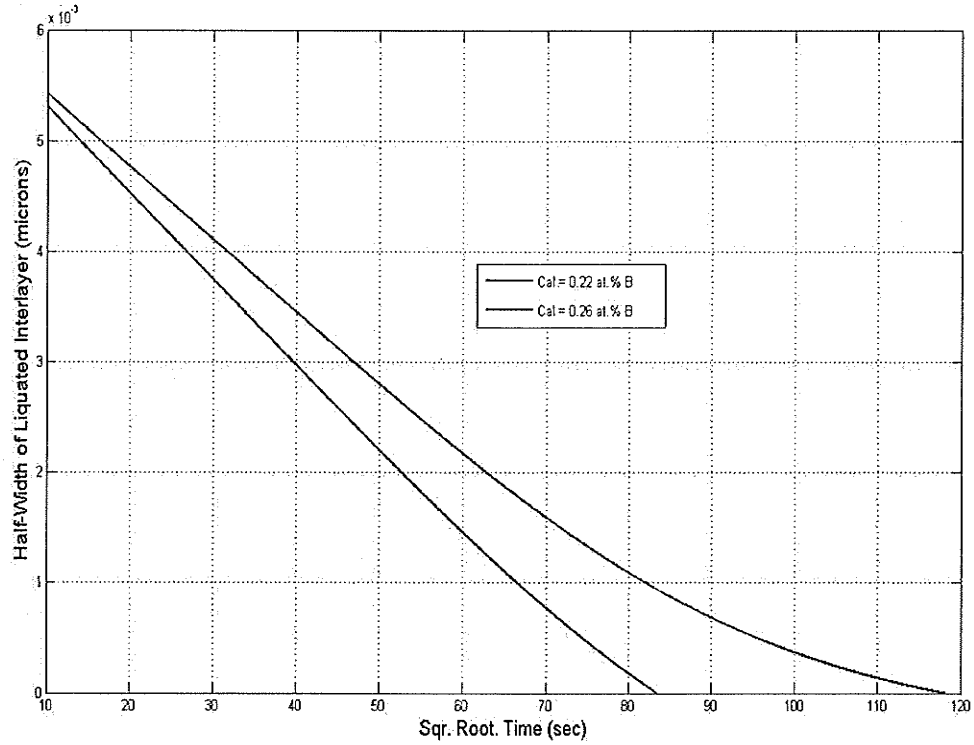

Figure 4.17: Numerically simulated variation of half-width of liquated interlayer with square root of time using increased solidus solubility of boron in nickel

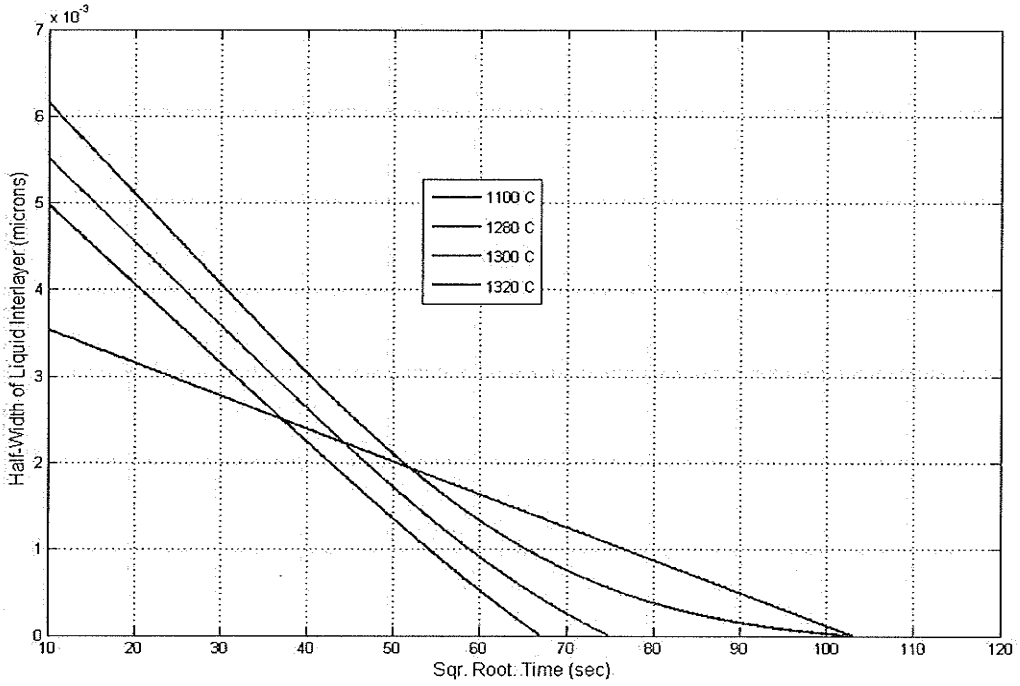

Figure 4.18: Numerically simulated variation of half-width of liquated interlayer with square root of time in Ni-B system

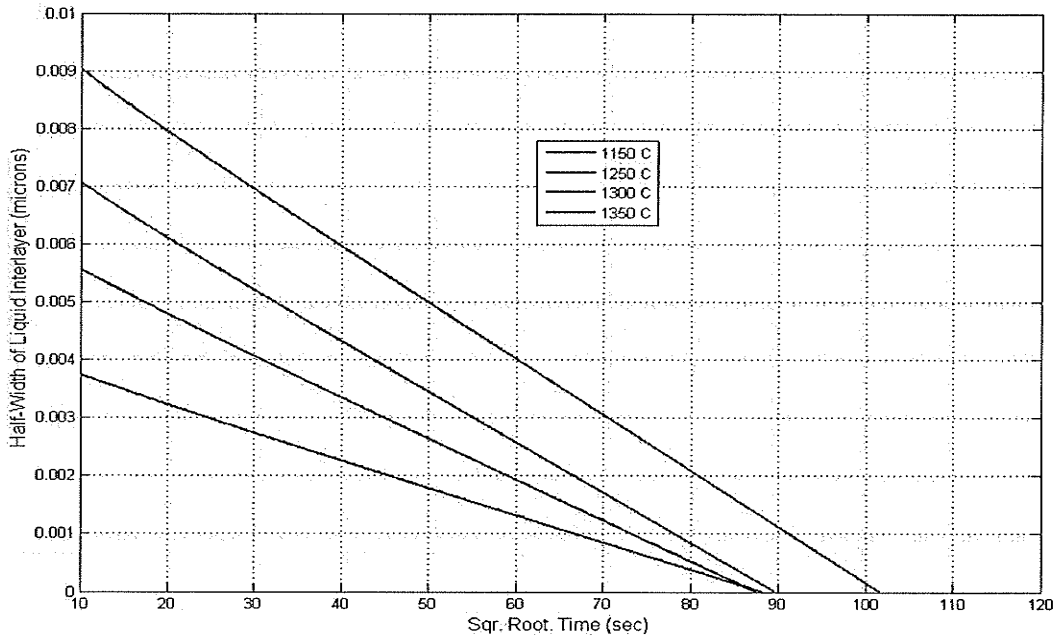

Figure 4.19: Numerically simulated variation of half-width of liquated interlayer with square root of time in Ni-Si system

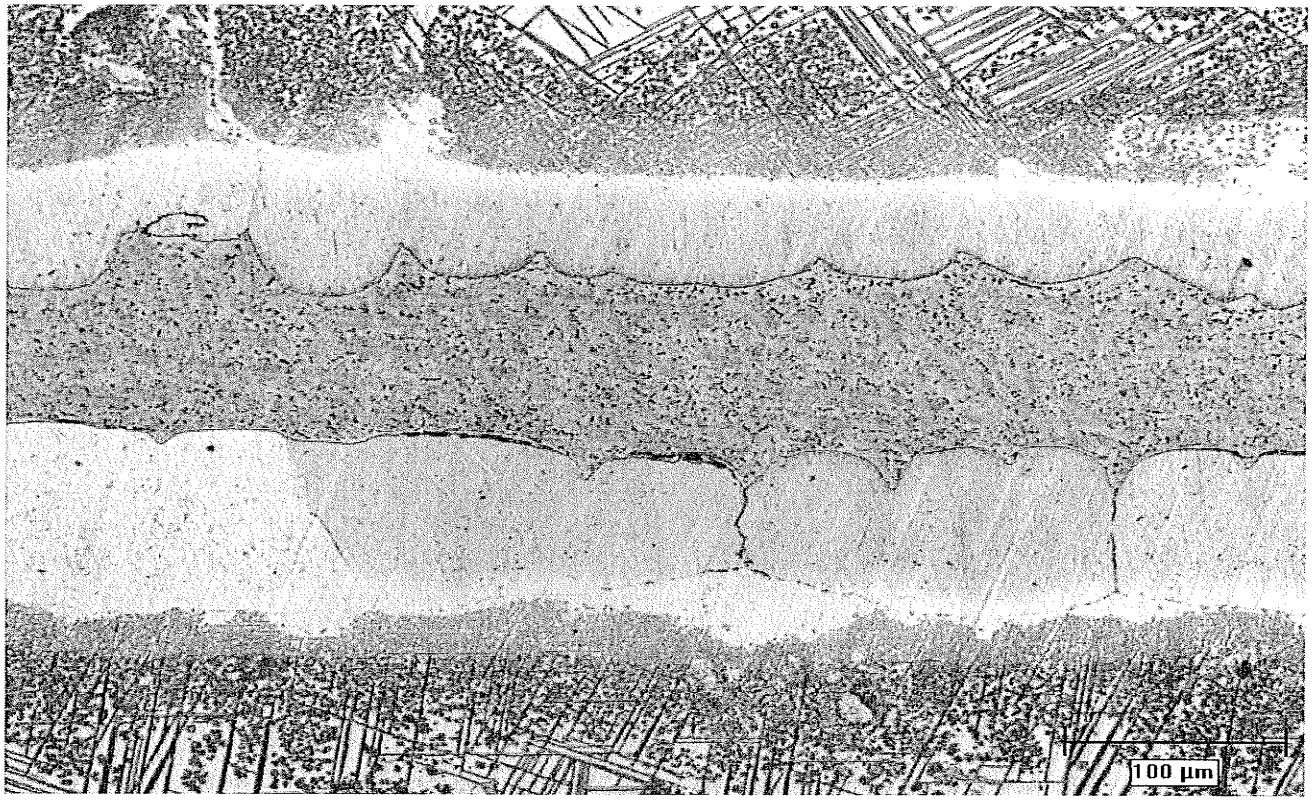

Figure 4.20: Micrograph of IN738 bonded with 200 µm Ni-B filler at 1140 °C for 5 hrs (X200)

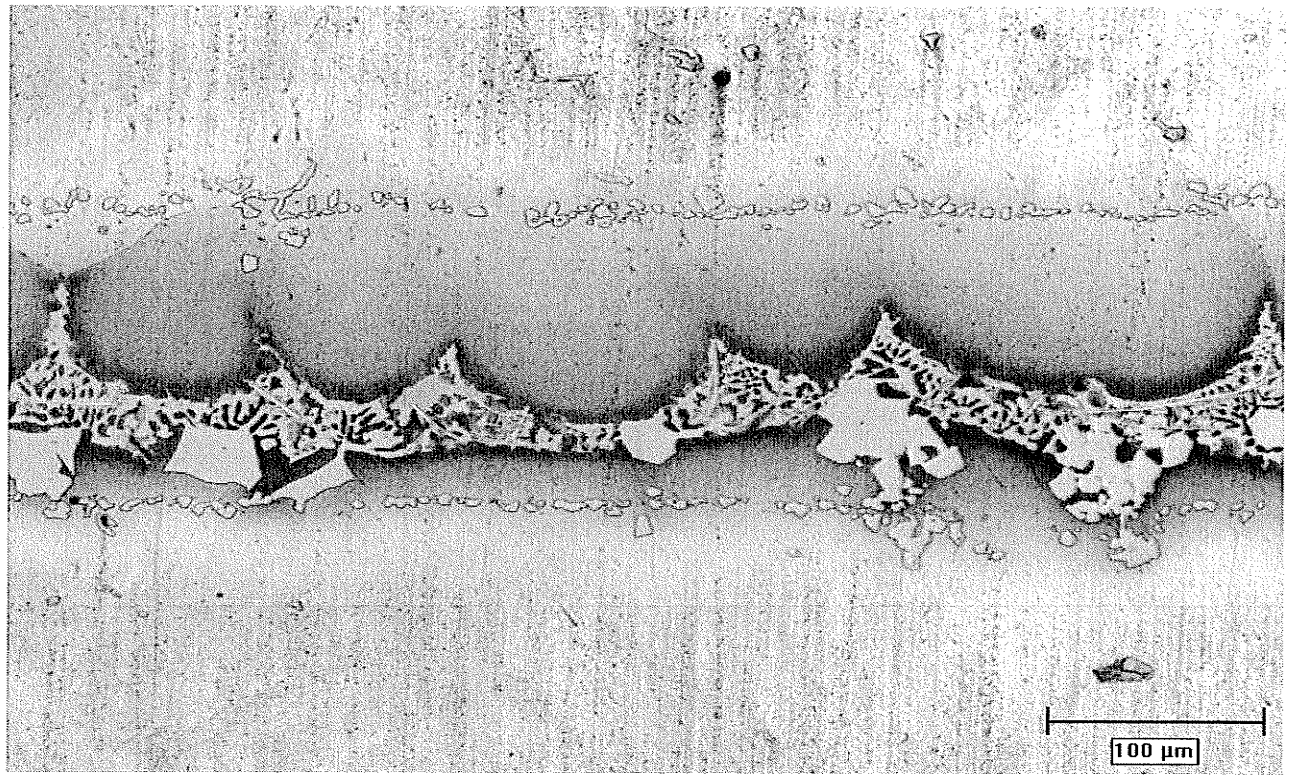

Figure 4.21: Micrograph of IN738 bonded with 200 µm Ni-Si filler at 1140 °C for 5 hrs (X200)

4.5.2 *Effect of initial concentration of MPD solute in filler on T_c*

Commercial filler alloys are usually available with varying concentration of MPD solutes, which may influence microstructural development in TLP joint depending on the process condition.

To study the effect of initial concentration of the MPD solute, C_f, on T_c, numerical simulations were carried out at by varying boron concentration in filler from 17 at.% - 33 at.% with a filler half-gap of 20 μm. Isothermal solidification completion time, t_f, was computed and plotted against bonding temperature as shown in Figure 4.22. As seen in the figure, a decrease in T_c was observed with increasing initial solute concentration.

An increase in the concentration of MPD solute in a filler alloy implies higher amount of solute to be diffused into the base material during joining. An increase in the amount of diffusing solute will reduce solute concentration gradient in the base alloy, which may decrease below the critical value $(\partial C/\partial x)_c$ that results in deviation from parabolic behavior. This is illustrated in Figures 4.23 and 4.24 where an increase in initial boron concentration in filler from 17 at.% to 33 at.% caused the solid-liquid interface displacement to deviate from parabolic relationship with holding time. Inducement of such deviation at a temperature where it would not normally occur, by an increase in C_f, would in effect reduce T_c, the temperature at which extension of TLP processing time with increase in temperature commences.

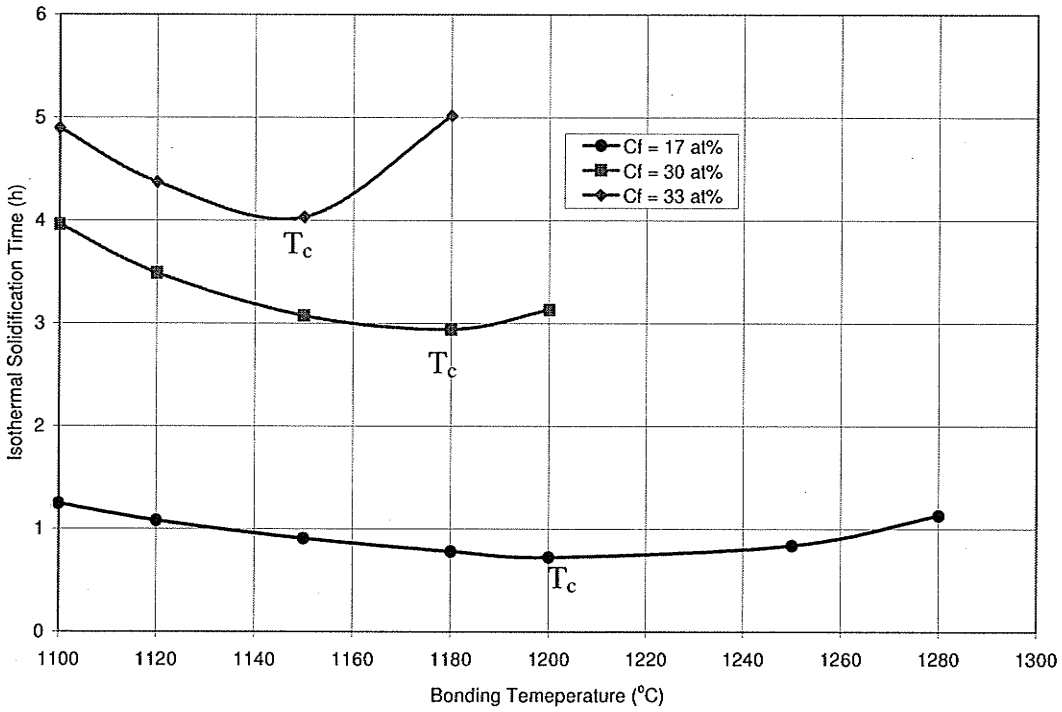

Figure 4.22: Numerically simulated variation of t_f with bonding temperature by varying initial MPD solute concentrations in filler alloy

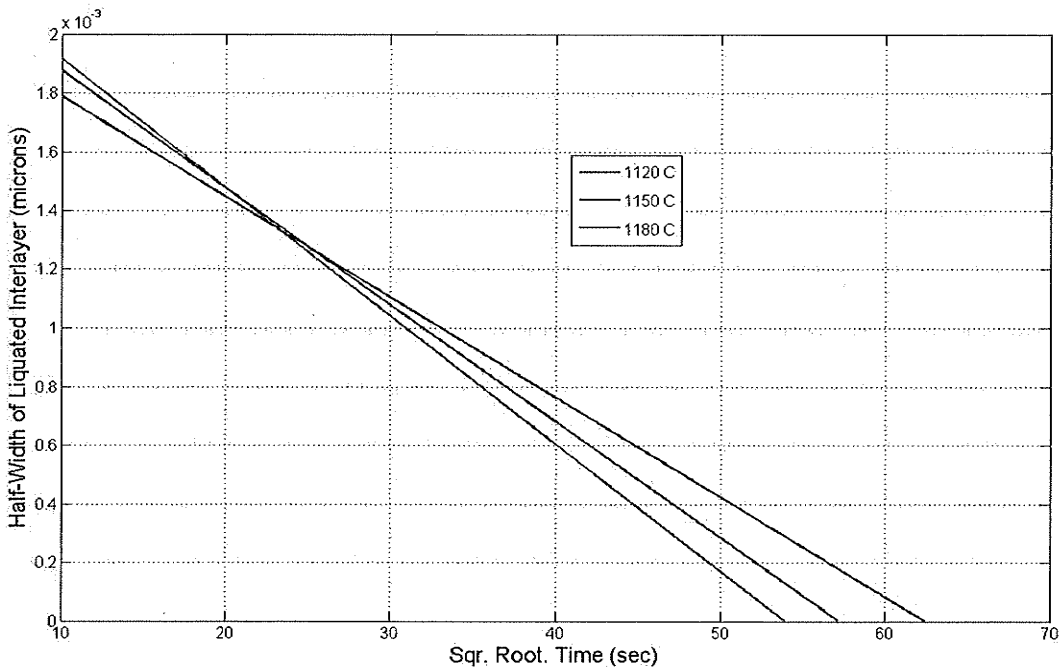

Figure 4.23: Numerically simulated variation of half-width of liquated interlayer with square root of time using C_f of 17 at%

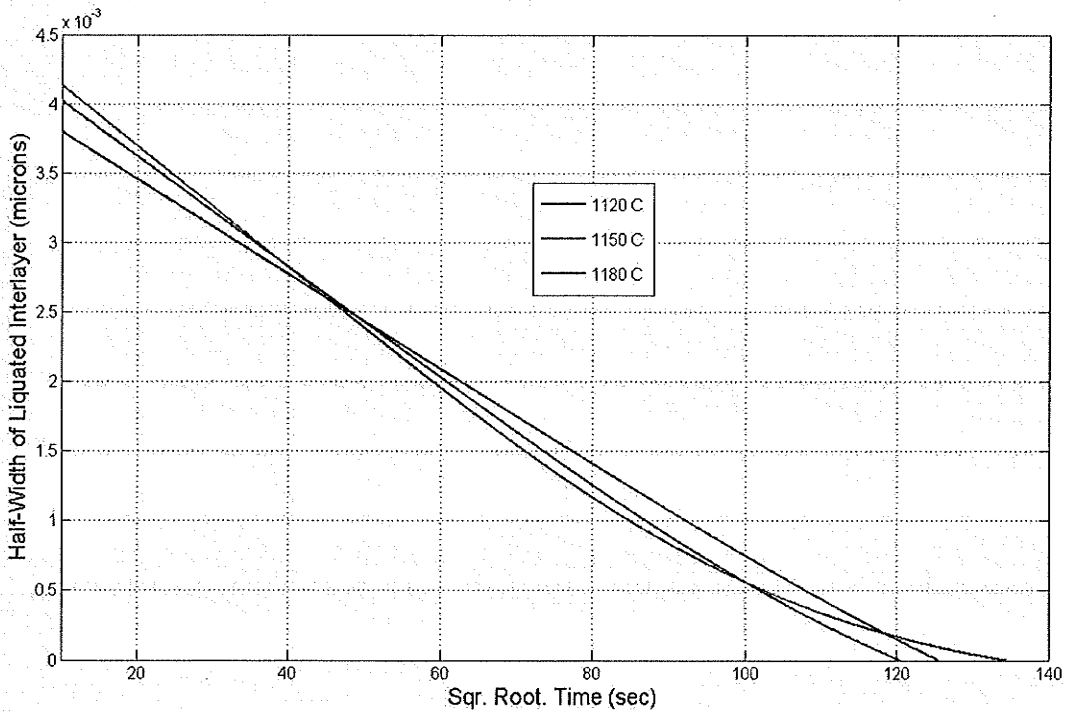

Figure 4.24: Numerically simulated variation of half-width of liquated interlayer with square root of time using C_f of 33 at%

Accordingly, this suggests that a possible approach of avoiding increase in processing time during high temperature TLP bonding is selecting filler alloy that contains reduced concentration of MPD solute.

4.5.4 Effect of initial concentration of MPD solute in base material on T_c

A very important issue that has not been generally considered during TLP bonding studies is that base materials can contain some level of MPD solute concentration prior to bonding, and the possible effect of this on the process kinetics has been largely neglected.

In the present work, to study the effect of initial MPD solute concentration in base material, C_m, on the temperature, T_c, above which isothermal solidification rate slows down, numerical simulation was performed by varying C_m from 0 at% to 0.09 at% B at various bonding temperatures. The simulation results in Figure 4.25 shows that increasing C_m from 0 to 0.08 at.% and then to 0.09 at.% resulted in a decrease in the temperature T_c. In the numerical simulation results shown in Figures 4.26 and 4.27, the parabolic law was obeyed for all temperatures between 1120 to 1180 °C at C_m of 0 at% and T_c was not observed within this temperature range. Increasing C_m to 0.09 at% resulted in notable deviation from the parabolic law at 1180 °C which caused the prolonged isothermal completion time and the existence of T_c within the temperature range between 1150 °C and 1180 °C.

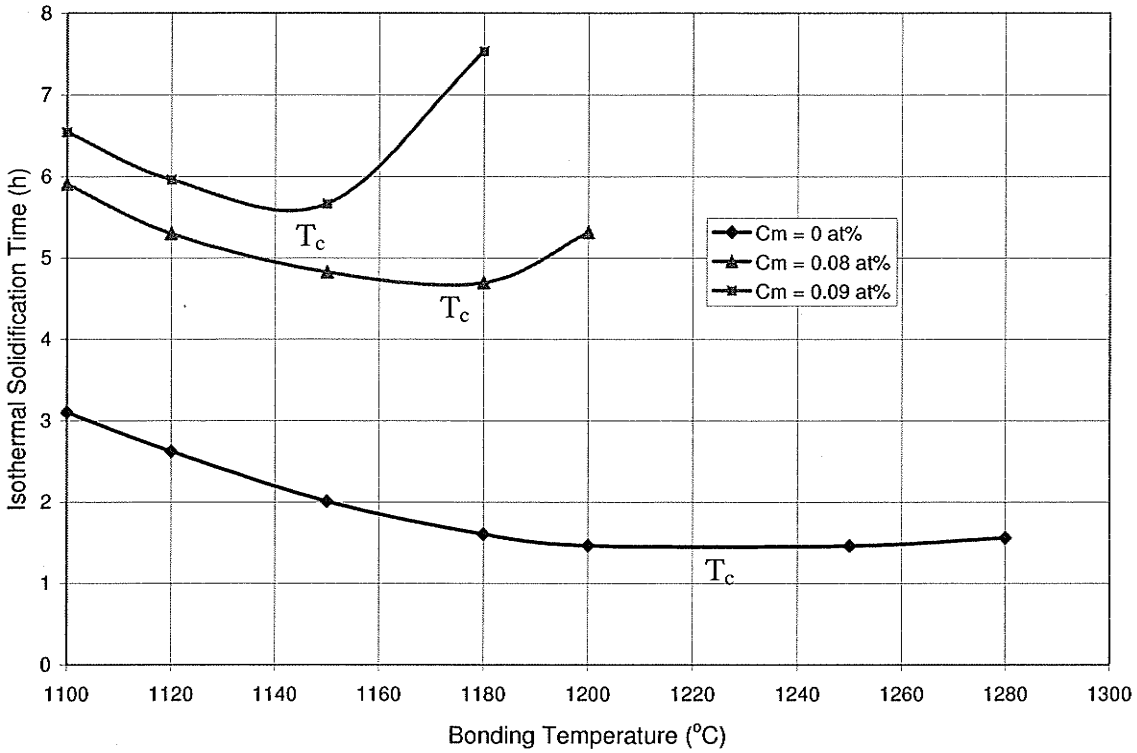

Figure 4.25: Numerically simulated variation of t_f with bonding temperature by varying initial concentration of MPD solute in the base metal

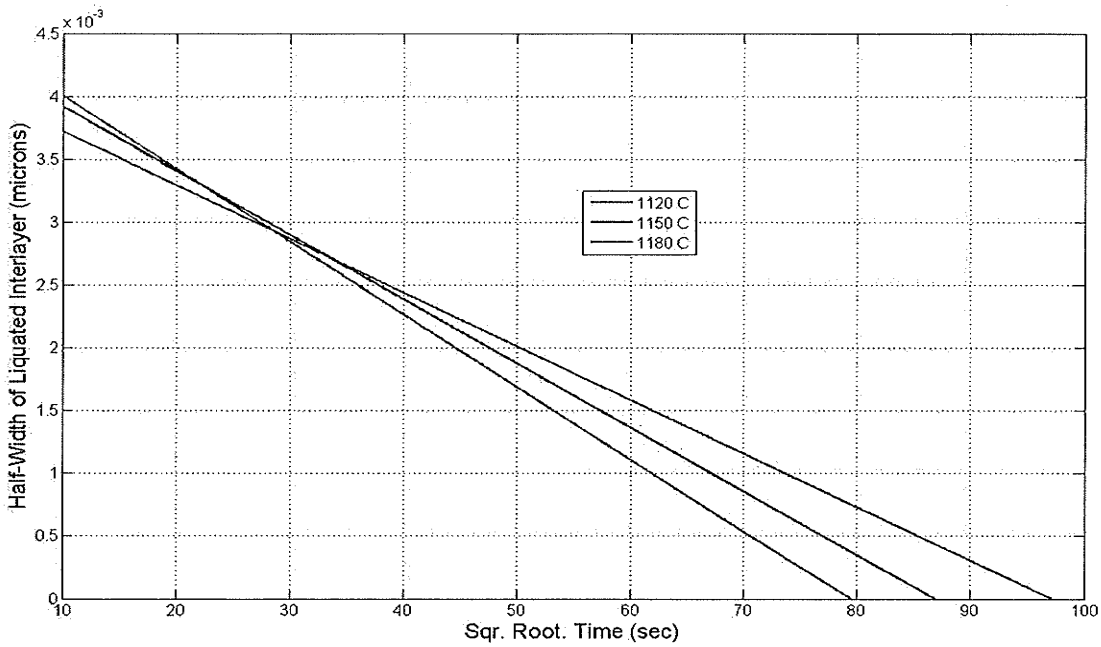

Figure 4.26: Numerically simulated variation of half-width of liquated interlayer with square root of time using C_m of 0 at%

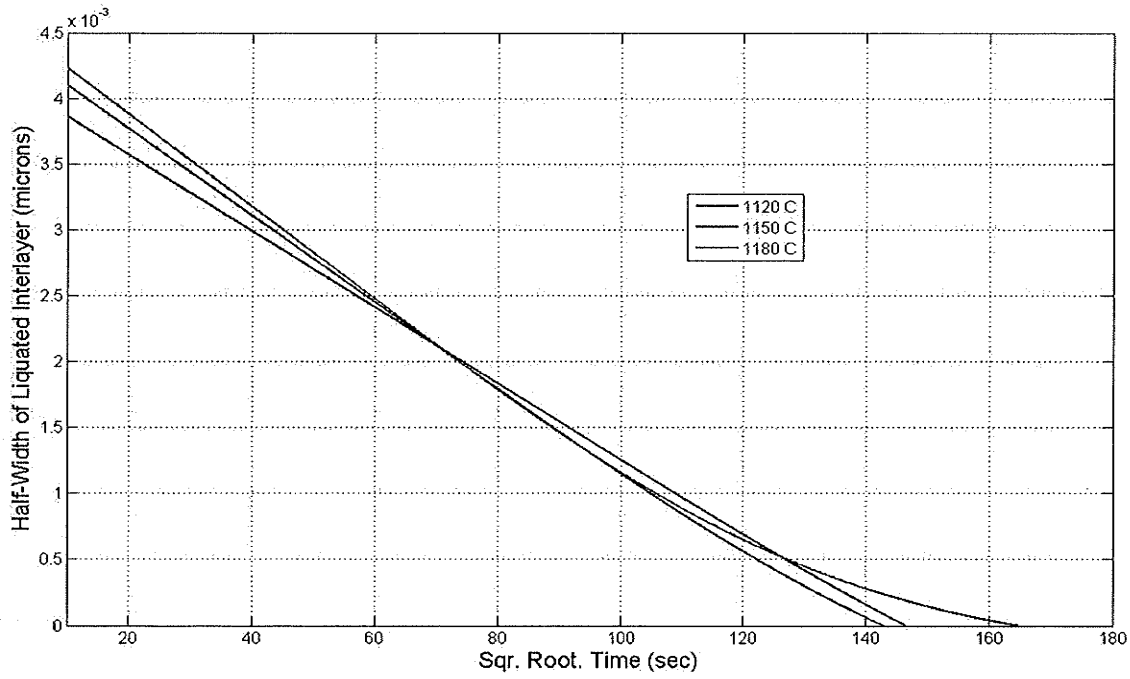

Figure 4.27: Numerically simulated variation of half-width of liquated interlayer with square root of time using C_m of 0.09 at%

Presence of MPD solute in a base material prior to bonding would lower the solute concentration gradient in the material during bonding. At any given temperature, the extent of such reduction in $\partial C/\partial x$ would increase with increasing initial solute concentration, which can lead to the occurrence of $(\partial C/\partial x)_c$ and, thus, deviation from the parabolic behavior. Lowering the temperature of commencement of deviation by an increase in C_m would in turn result in decrease in T_c as seen in Figure 4.25. Therefore, consideration of initial presence of MPD solute in base material and the mode of its existence either in solid solution form or in second phase particles is important in determining optimum process parameters for producing eutectic free TLP joint.

4.6 Effect of Base Metal Thickness on T_c

Analytical TLP bonding models generally treat base materials as semi-infinite or infinite diffusion mediums. However, as indicated in section 4.2, this can be grossly inaccurate assumption that neglects the possible departure from parabolic law. Numerical analysis has shown that decrease in solute concentration gradient below a critical value $(\partial C/\partial x)_c$ during TLP bonding can actually cause deviation from parabolic to occur in finite base materials. Based on the numerical approach concept, another very important factor of practical significance, that can influence $\partial C/\partial x$ and, thus, existence of the temperature, T_c, is the thickness of the base material. The larger the base metal thickness, the more available material for diffusion of MPD solute which can increase $\partial C/\partial x$ by alleviating solute build up. Hence, it is conceivable that increasing base metal thickness may eliminate deviation from parabolic behavior by increasing $\partial C/\partial x$ above the critical value $(\partial C/\partial x)_c$. To investigate this possibility, numerical simulation was performed by varying base metal thickness from 4 mm to 6 cm at 1150 °C with a half-gap size of 38 μm. The

result of the simulation including solute concentration profile in the substrate is presented in Figures 4.28 and 4.29, respectively. As can be seen from the figures, an increase in the base metal thickness 6mm raised the solute concentration gradient in the material and this resulted in removal of the deviation that existed in 4 mm base material. Further simulation, as presented in Figure 4.30, shows that such elimination of deviation can increase the temperature T_c, which suggests that reduction in isothermal solidification at higher temperatures during TLP bonding can be effectively avoided by increasing the thickness of base material.

Experimental investigation was carried out to verify this possibility by performing TLP bonding of IN738 superalloy with thicknesses of 6 mm, 21 mm and 30 mm at 1180 °C, a temperature where reduction in the rate of isothermal solidification was previously observed in the material. Microstructural examination of the joints produced in these specimens showed a notable variance with the theoretical predicted behavior. There was no apparent difference in the width of the eutectic product formed along the centerline of the joints. This implies that the rate of isothermal solidification was essentially the same in all the samples, regardless of the thickness of the base metal.

The cause of such unexpected departure from numerically predicted behavior generated a worthwhile interest. A subsequent closer examination of the numerical simulation result in Figure 4.31 showed that the predicted effect of base alloy thickness was premised on the assumption that the diffusing solute penetrates to the end of the substrate before the critical concentration gradient $(\partial C/\partial x)_c$ was attained. Under such condition, it is

reasonable to expect an increase in substrate thickness to raise $\partial C/\partial x$ above $(\partial C/\partial x)_c$ and thus increase the rate of isothermal solidification.

Experiment was then planned to examine the extent of solute penetration in the base material at temperatures where deviation from parabolic behavior was observed. The initial objective was to verify whether penetration of MPD solute to the end of a base material is a necessary condition for the occurrence of deviation from parabolic behavior as suggested by the numerical simulation result. A major initial challenge to the goal was with the quantification of boron concentration in the IN738 superalloy. The ultra-thin window energy dispersive spectrometer attached to the SEM used in the present work can detect boron but it can not quantify it with sufficient reliable accuracy. A rapidly growing technique for quantifying light trace elements like boron in nickel, laser ablation-inductively coupled plasma-mass spectrometry (LA-ICP-MS), was used for determining boron concentration profile in the base material of specimens bonded at 1180 °C, where deviation from parabolic behavior had occurred. The technique involves using a ultra-violet laser to ablate material in air-tight cell and form a stream of fine particles from the specimen surface. The ablated material is subsequently carried in a helium aerosol into an inductively coupled plasma mass-spectrometer (ICP-MS) where ionization occurs in argon-plasma at approximately 6000 K.

The result of the laser ablation experiment (Figure 4.32) shows that, in contrast to the aforementioned assumption, boron did not penetrate through to the end of the specimens despite the occurrence of deviation from parabolic behavior. This shows that practically, deviation from parabolic behavior can occur during TLP bonding without full solute

penetration to the end of the base material. In such situations, any increase in base metal thickness would have negligible, if any, effect in increasing isothermal solidification rate by eliminating the occurrence of deviation from parabolic behavior. This could explain why an increase in the base metal thickness from 6 mm to 30 mm did not produce any notable change in the thickness of centerline eutectic product observed in the joints as stated above.

Accordingly, the result indicates that the phenomenon of deviation from parabolic behavior and T_c may not be limited to thin sections or relatively small laboratory specimens, but it can also be operational large industrial components like gas turbine blades. This, therefore, underscore the need for careful consideration of the factors indicated in this study that can influence T_c, and thus, TLP processing time, in order to improve the commercial appeal of the bonding process.

4.7 Corollary

This study has identified a new alternate cause of increase in processing time at higher temperature during TLP bonding to be the departure from parabolic law due to decrease in concentration gradient of MPD solute below a critical value in the base metal. Salient factors that can potentially influence this phenomenon are initial concentrations of MPD solute in filler and base alloys, solubility of the MPD solute in base material and thickness of filler alloy. This can be partly illustrated by a 3D plot as shown in Figure 4.33.

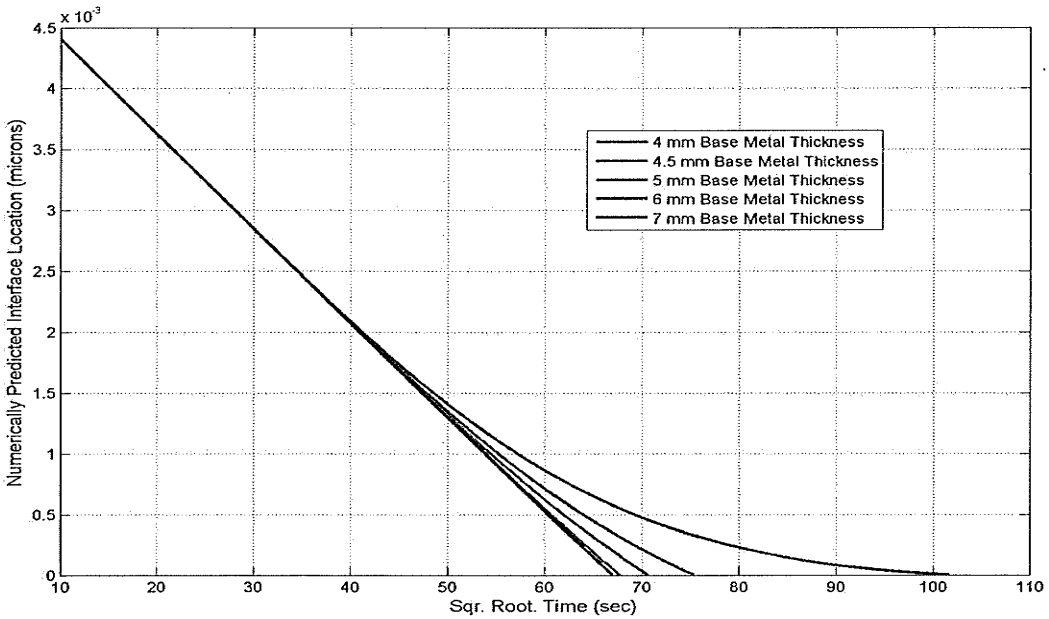

Figure 4.28: Numerically simulated variation of half-width of liquated interlayer with square root of time using varying base metal thicknesses

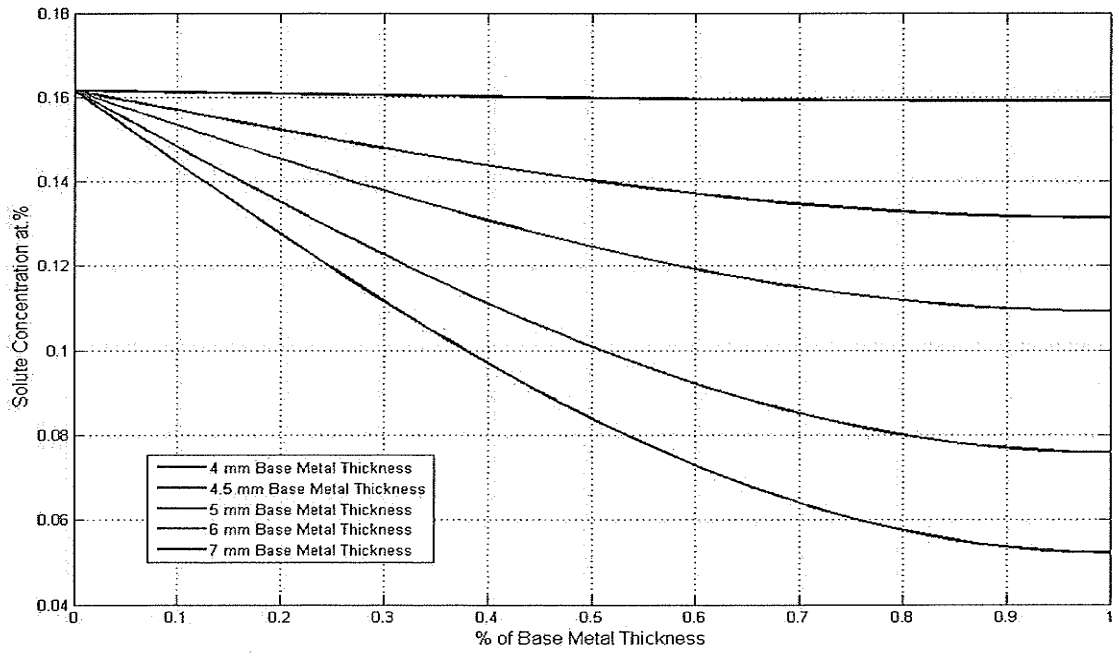

Figure 4.29: Numerically simulated variation of solute concentration with percentage of base metal thickness using various base metal thicknesses

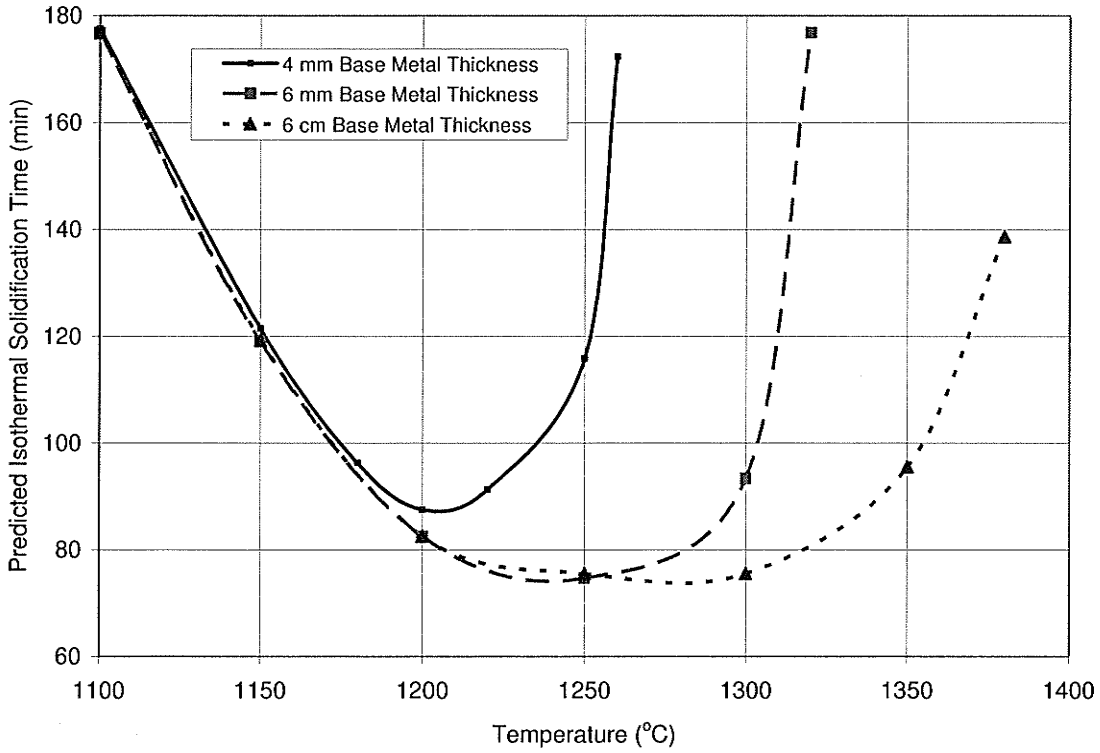

Figure 4.30: Numerically Simulated variation of t_f with bonding temperature for various base metal thicknesses

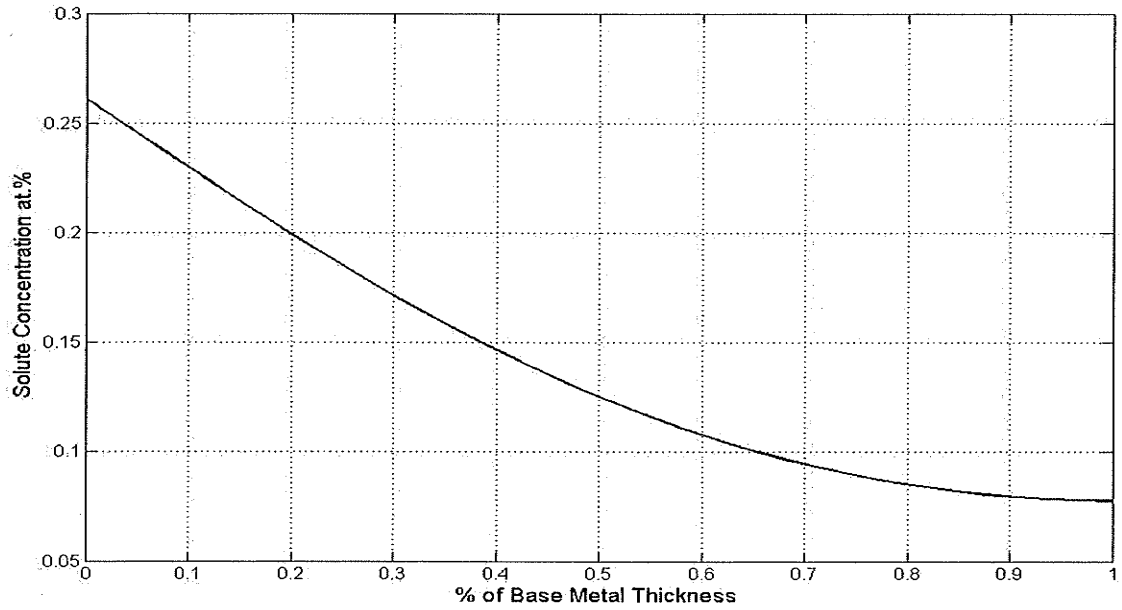

Figure 4.31: Numerical simulation of the extent of solute concentration with percentage of base metal thickness using an initial boron concentration in pure Ni of 0.012 wt%.

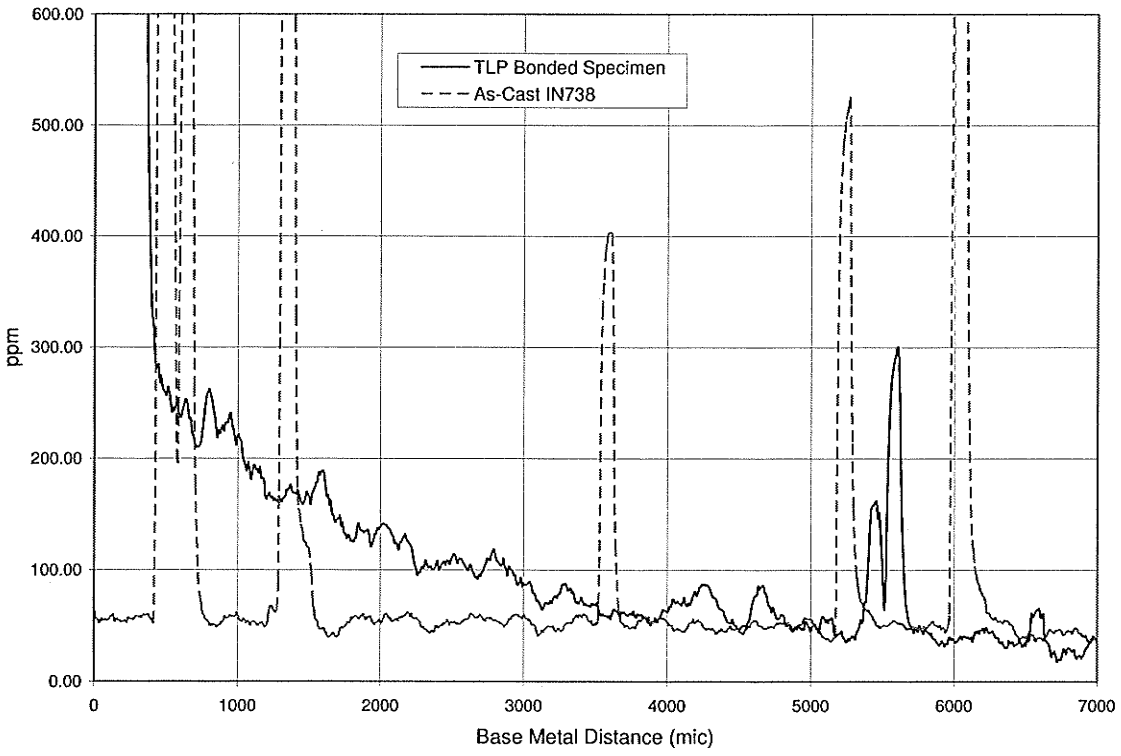

Figure 4.32: MPD solute in TLP bonded and as-cast IN738 performed by laser ablation analysis

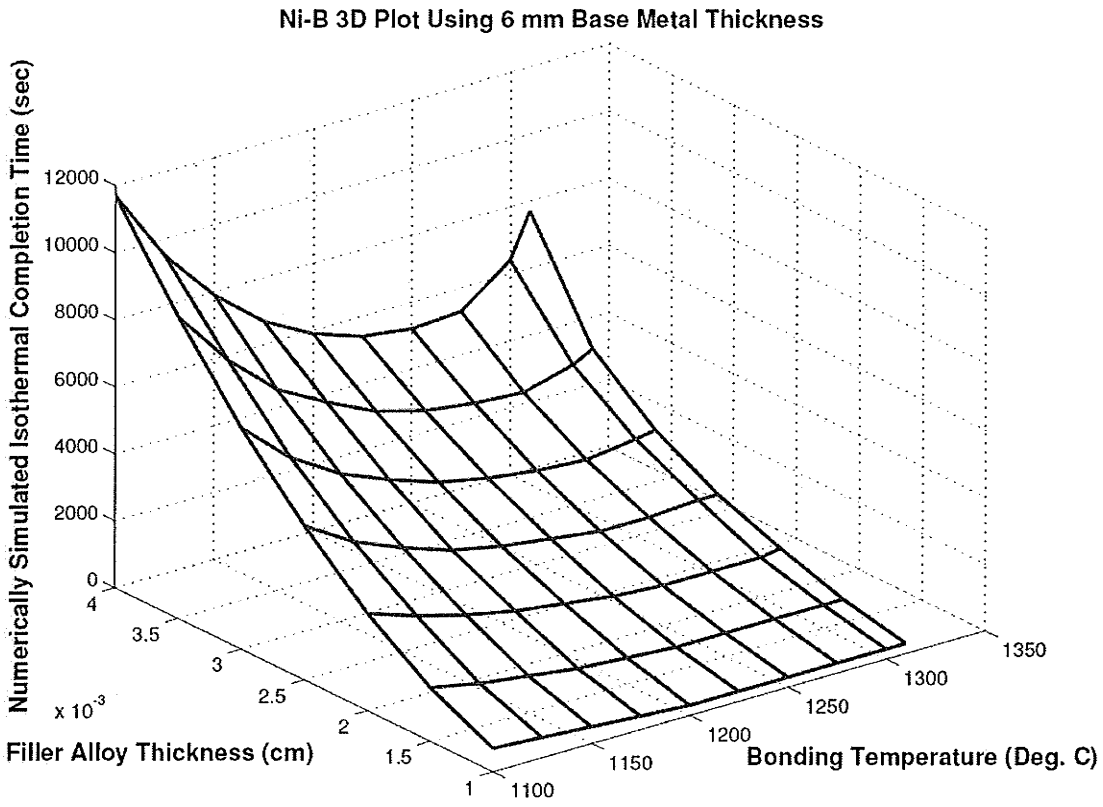

Figure 4.33: Numerical simulation of the effect of filler alloy thickness and bonding temperature on isothermal completion time

Part II: Influence of Process Parameters on Microstructure of TLP Bonded Joint Using Phosphorous Bearing Filler Alloy

4.8 Introduction

As previously stated, in certain applications such as the repair of nuclear power plant components, the use of materials containing boron can be harmful and can negatively impart performance in nuclear plants. For such applications, filler alloys containing phosphorous and silicon are preferred. However, there are limited published reports on the effects of process parameters on the microstructure of TLP bonded joints in nickel using phosphorous containing fillers.

In this section of the thesis, the effect of holding time, gap size and bonding temperature on microstructure of TLP bonded joint using a filler alloy containing phosphorous as the MPD solute. To preclude the complexity of base material alloying elements, TLP bonding of commercially pure nickel was used.

4.9 Effect of Holding Time on Microstructure of TLP Joint

The effect of holding time on microstructure of the joints was studied by performing TLP bonding of 38 μm gap specimens at 1100°C for 1, 4, and 24 hours. The microstructure of the joints after the respective holding times, as obtained by SEM operated in secondary electron imaging mode, is shown in Figures 4.34 to 4.36. All of the joint's microstructure consisted of a continuous centerline eutectic constituent. Eutectic morphology of the centerline microconstitiuent was further observed by atomic number based contrast of SEM backscatter electron imaging mode as shown in Figure 4.37. The

average width of the centerline eutectic decreased from 22.32 μm in 1 h specimen to 13 μm in 4 hrs specimen while 24 hrs of holding resulted in further reduction to a gap width less than 1 μm. Qualitative analysis using SEM EDS and X-ray line scan across the eutectic including that of the 24 hour specimen showed significant segregation of phosphorous into the centerline microconstituent as seen in Figures 4.38 to 4.40.

The Ni-P phase diagram [51] showed that phosphorus has very small solubility in the nickel and forms intermetallic phases Ni_3P, Ni_5P_2 and $Ni_{12}P_5$. According to the binary phase diagram, eutectic reaction between nickel solid solution and Ni_3P occurs at 880°C. The centerline eutectic observed in the present work, comprising of nickel solid solution and phosphorous rich phase is believed to be formed by solidification reaction during cooling due to an insufficient diffusion of phosphorous into the base metal to achieve complete isothermal solidification during holding at the bonding temperature. Formation of this non-equilibrium solidification microconstituent with continuously distributed morphology could be deleterious to mechanical properties of bonded materials, as it may provide a low resistance path for crack initiation and/or propagation and should therefore be avoided. An increase in the holding time during bonding would, however, permit increased diffusion of the melting point depressing element, phosphorus, into the base metal. Accordingly, this will result in increased isothermal solidification and concomitant reduction in the amount of residual liquid that transforms to centerline eutectic product during cooling. Phosphorous peaks were observed by SEM EDS in the isothermally solidified region of the joint, which supports diffusion of melting point depressant induced isothermal solidification (Figure 4.41).

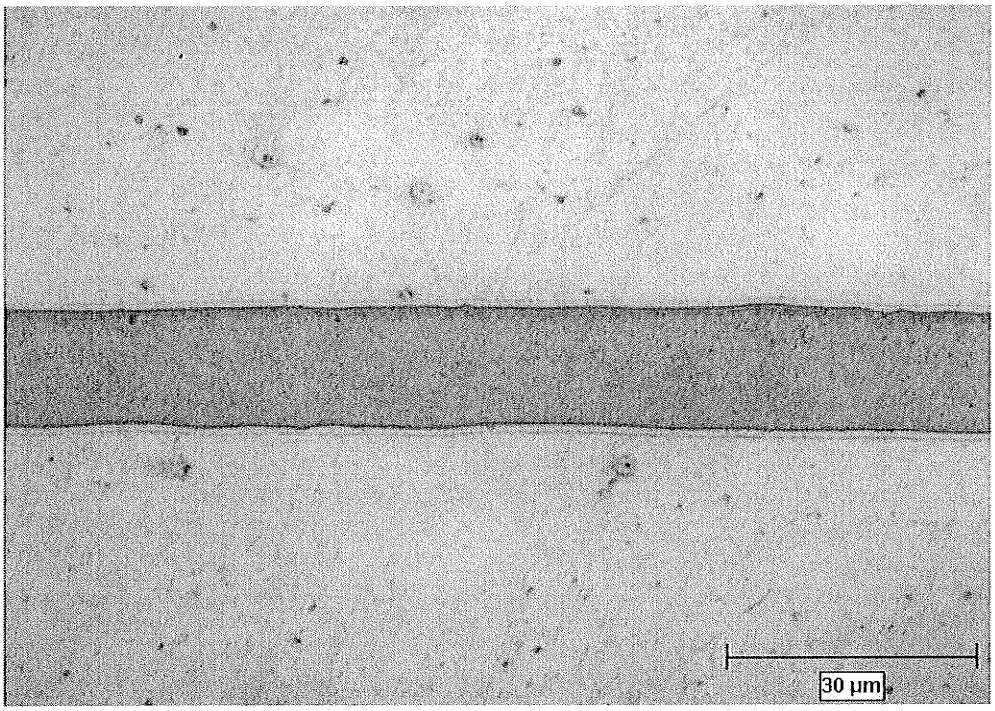

Figure 4.34: Microstructure of specimen using 38 µm Ni-P filler tested at 1100C for 1 h

(X 1000)

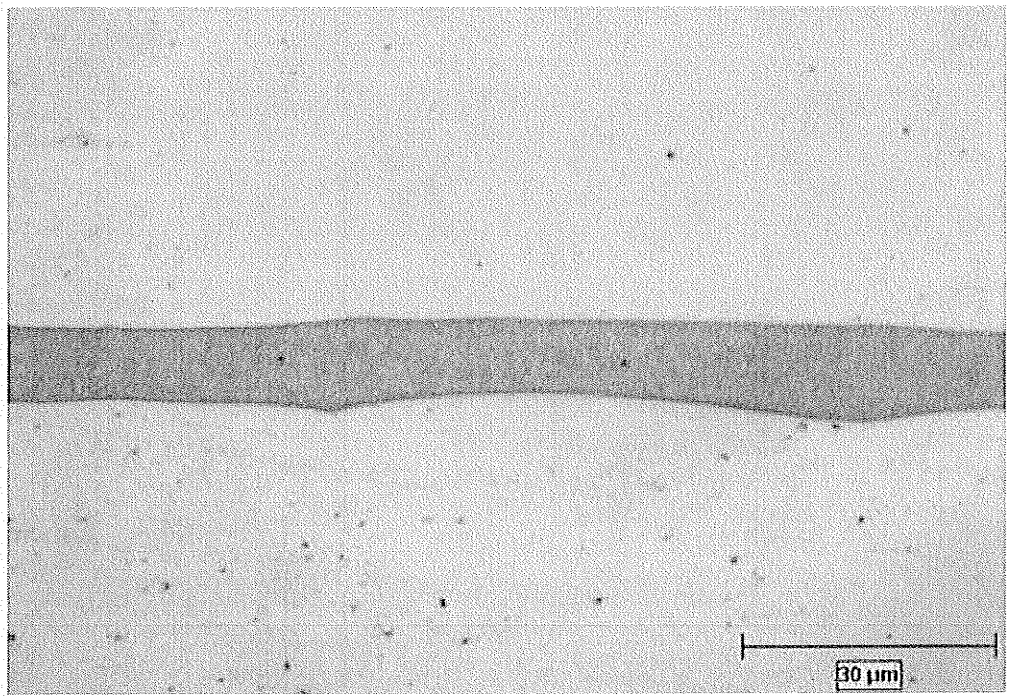

Figure 4.35: Microstructure of specimen using 38 µm Ni-P filler tested at 1100C for 4h

(X 1000)

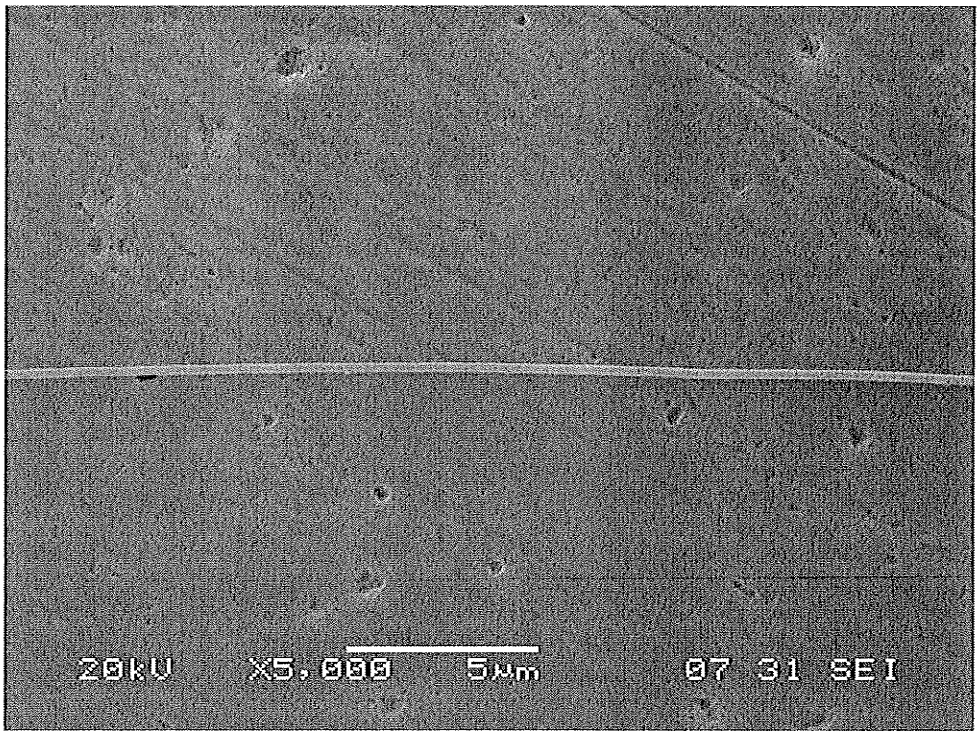

Figure 4.36: Microstructure of specimen using 38 µm Ni-P filler tested at 1100C for 24 hrs (X 5000)

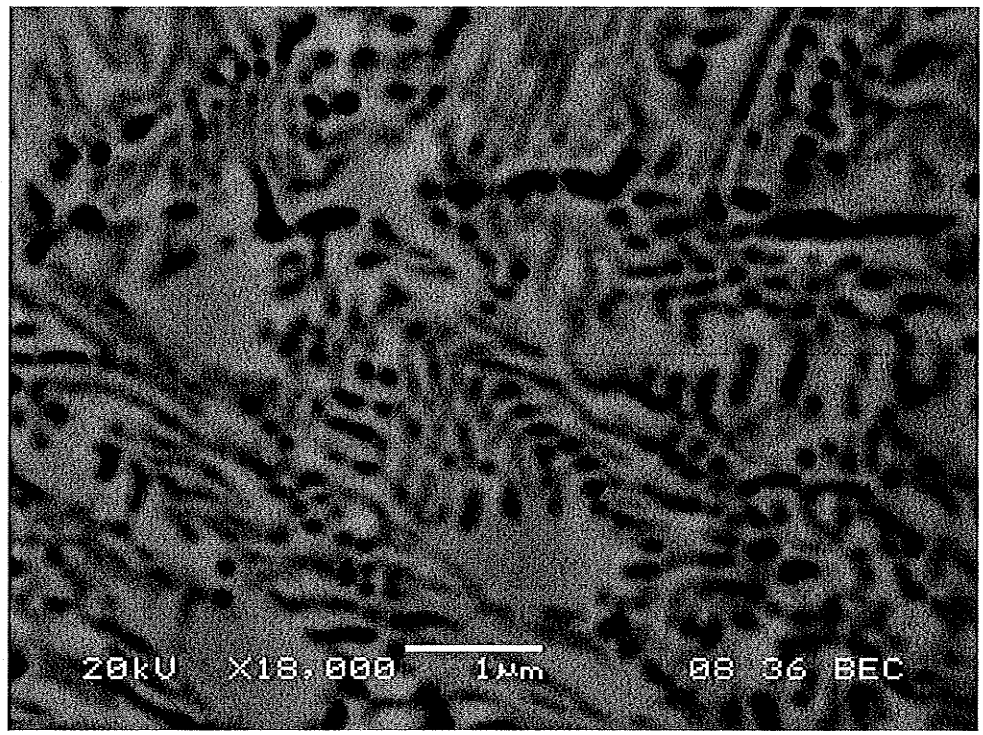

Figure 4.37: High magnification SEM backscatter electron image of centerline eutectic product

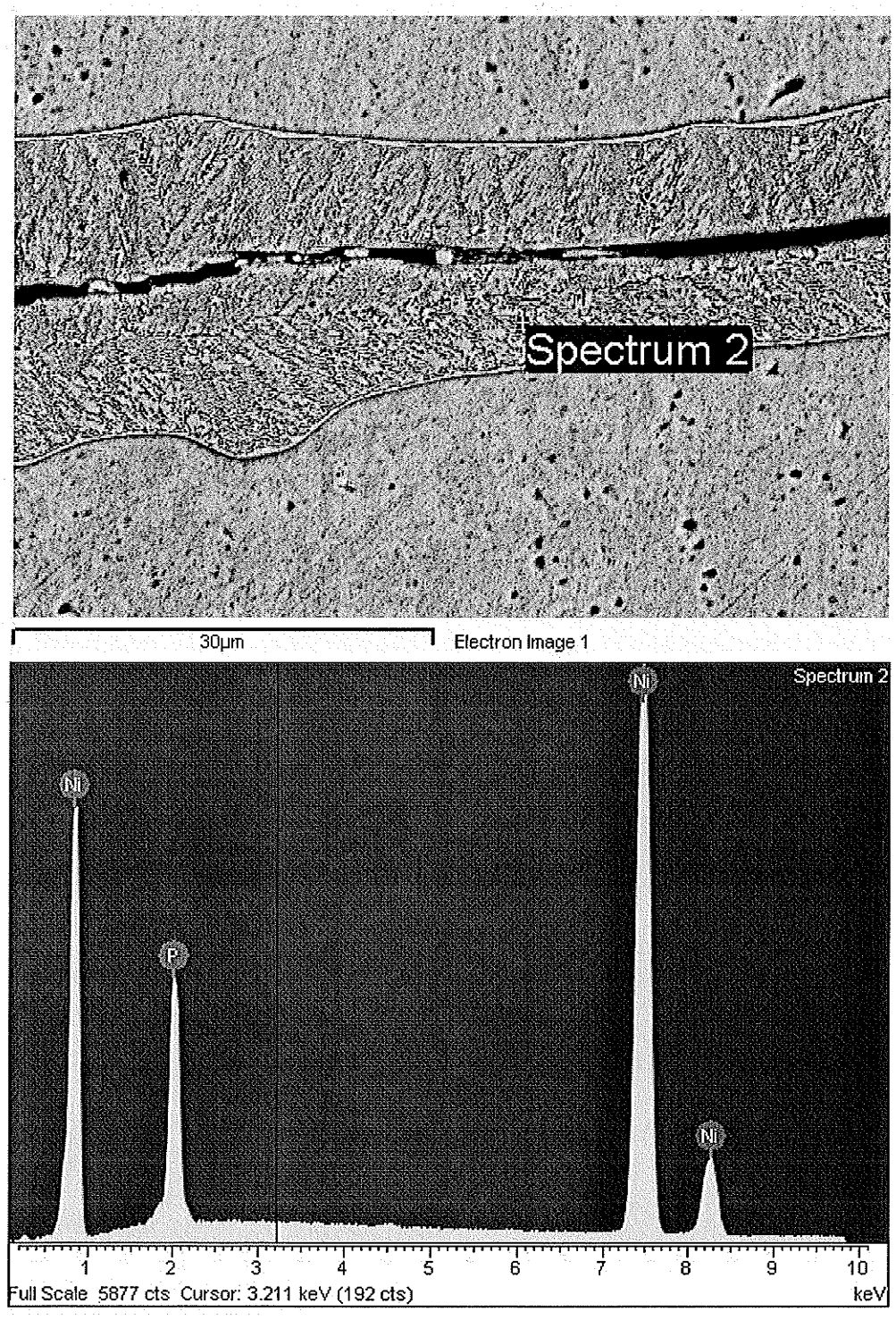

Figure 4.38: SEM EDS analysis of centerline eutectic

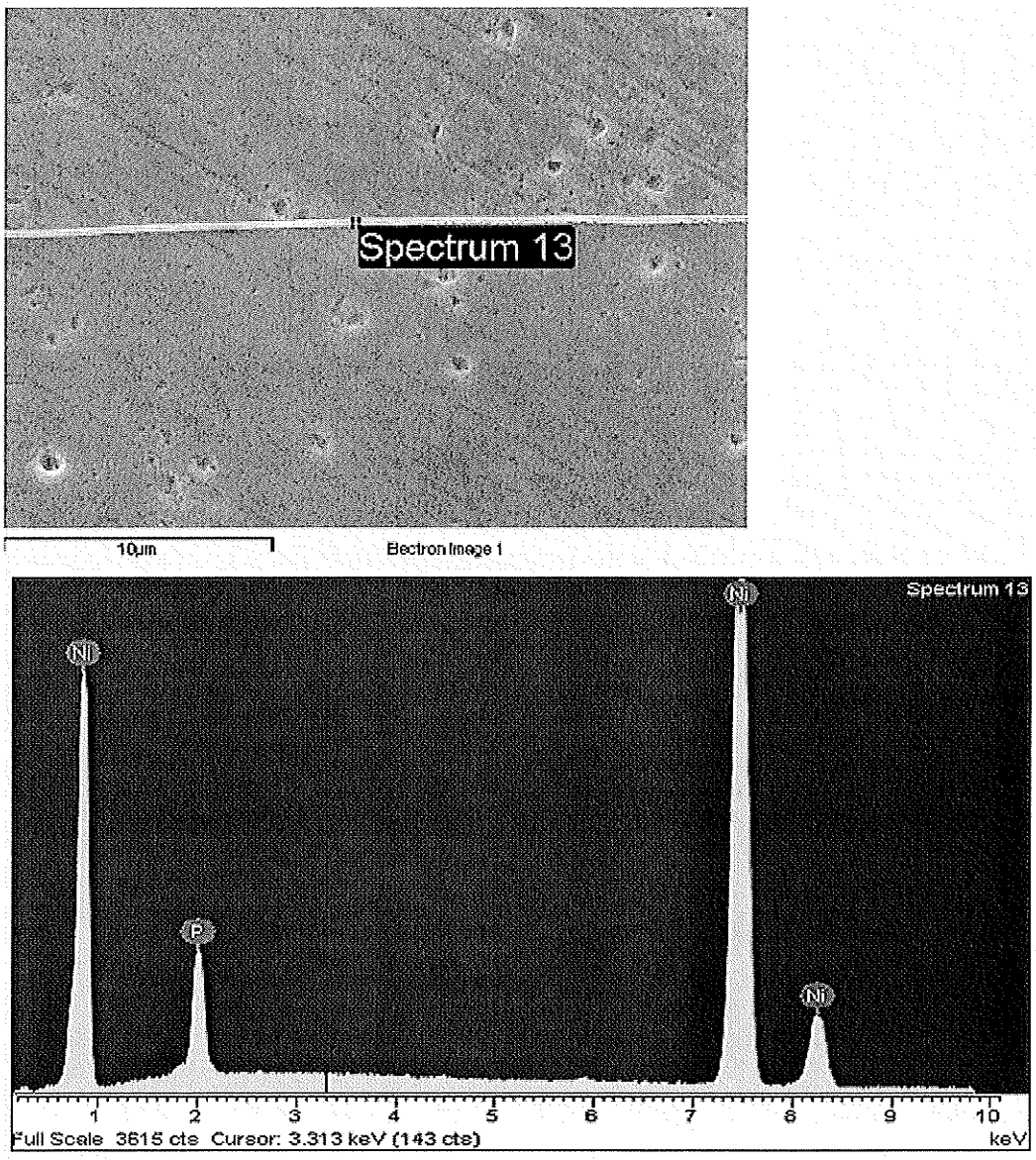

Figure 4.39: SEM EDS analysis of centerline eutectic in specimen bonded at 1100 °C for 24 hrs

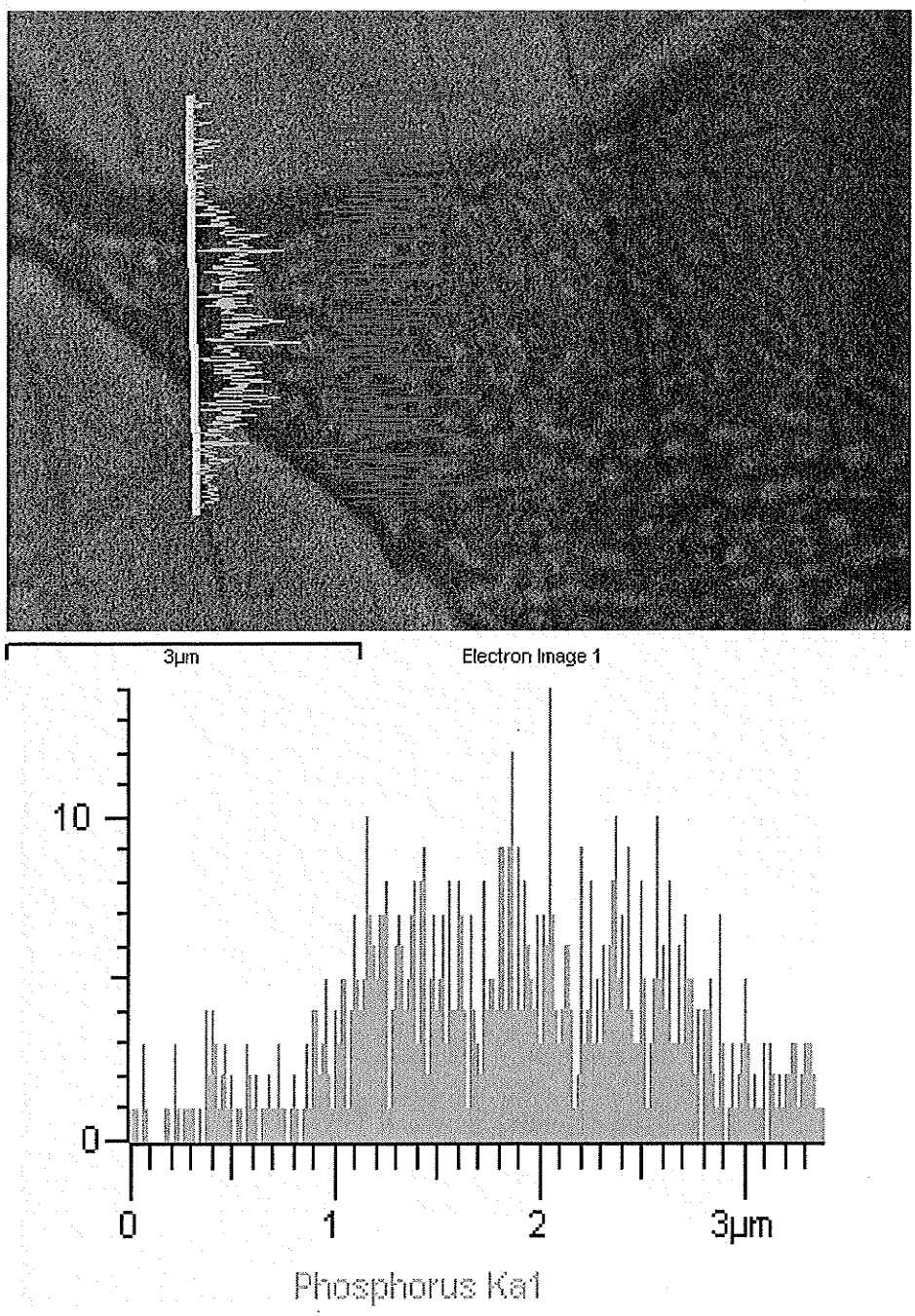

Figure 4.40: SEM EDS X-ray line scan across eutectic product

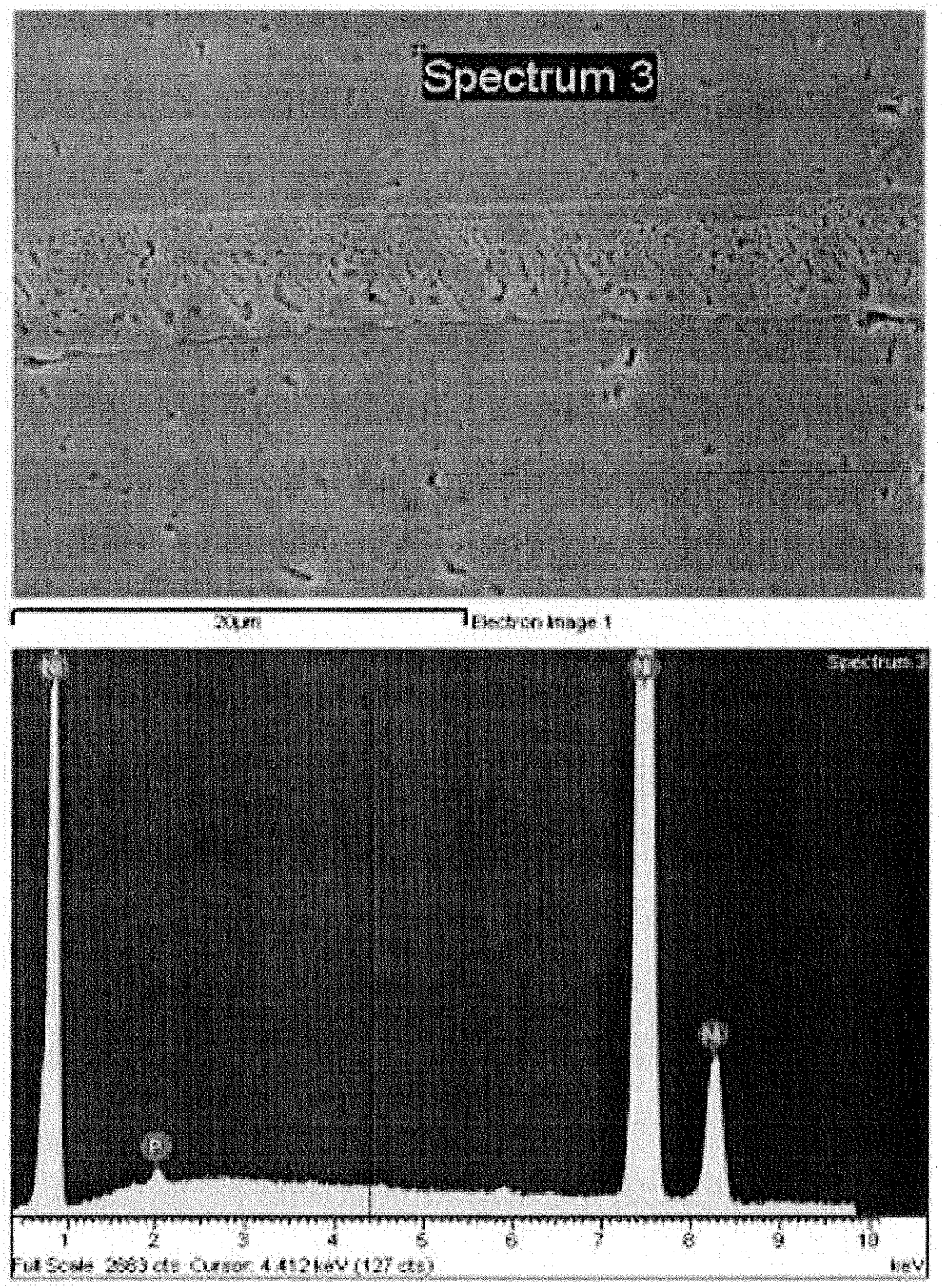

Figure 4.41: Spectrum of SEM EDS showing phosphorous peak in isothermally solidified region of TLP joint

As stated earlier, increase in holding time from 1 h to 24 hrs required for increased phosphorous diffusion at a constant temperature of 1100 °C, resulted in significant decrease in the width of the deleterious centerline eutectic from 22 μm to less than 1 μm.

4.10 Effect of Initial Filler Material Gap Size on Microstructure of TLP Bonded

To study the effect of filler gap size on microstructure of TLP bonded joint of the nickel base metal, 38 μm and 76 μm gap-sized specimens were bonded at 1180°C for 8 and 24 hours. The microstructure of the samples bonded for 8h, as obtained by the optical microscope, are shown in Figures 4.42 and 4.43. Both of the joints consisted of continuous centerline eutectic product. Nevertheless, an increase in average width of the eutectic constituent from 16.85 μm in the 38 μm specimen to 27 μm in the 76 μm specimen was observed. The formation of continuous centerline eutectic in the two specimens indicated that a complete isothermal solidification of the liquated insert was not achieved after 8 hrs of holding at 1180°C bonding temperature. Microstructural examination of joints prepared at the 1180°C bonding temperature for 24 hrs holding time showed that complete isothermal solidification was achieved in the 38 μm specimen while a continuous centerline eutectic with an average width of about 5.76 μm was formed in the 76 μm specimen due to incomplete isothermal solidification. The microstructure of the samples bonded for 24h, as obtained by SEM, are shown in Figures 4.44 and 4.45.

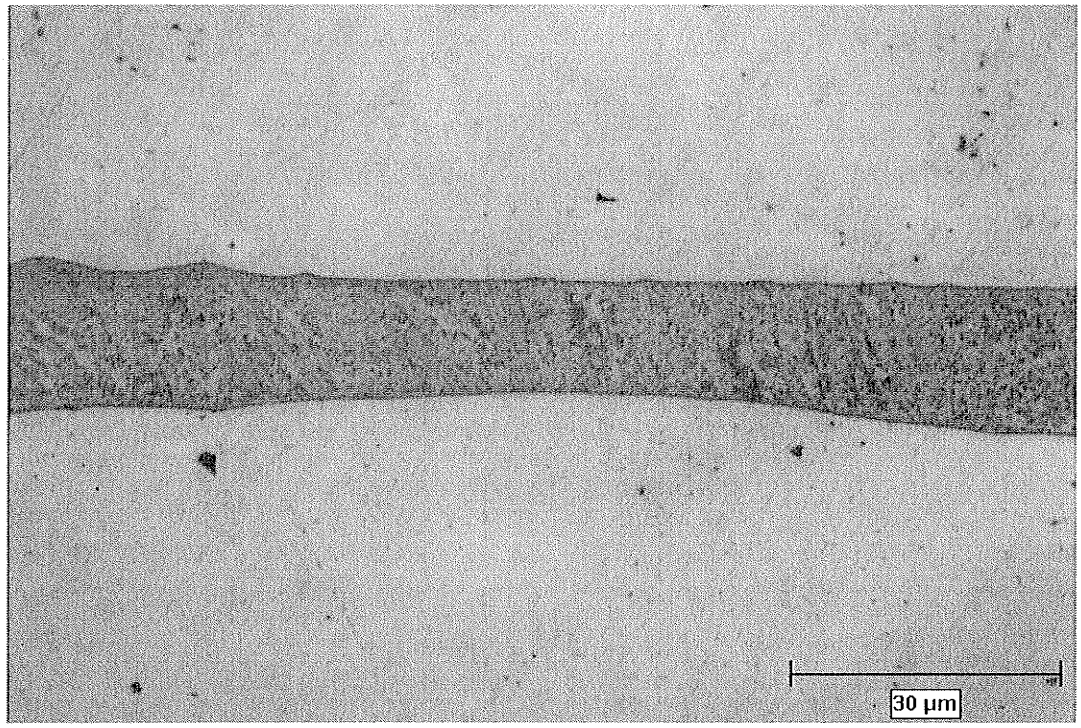

Figure 4.42: Microstructure obtained for test done at 1180 °C for 8 hrs using 38 µm Ni-P filler alloy (X 1000)

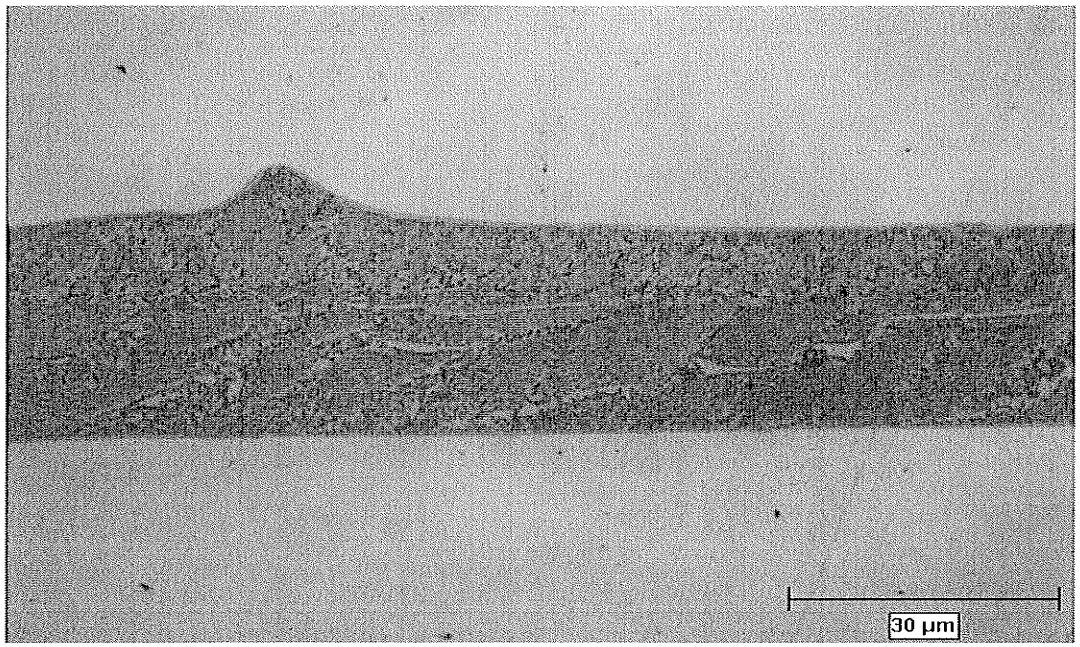

Figure 4.43: Microstructure obtained for test done at 1180 °C for 8 hrs using 76 µm Ni-P Filler alloy (X 1000)

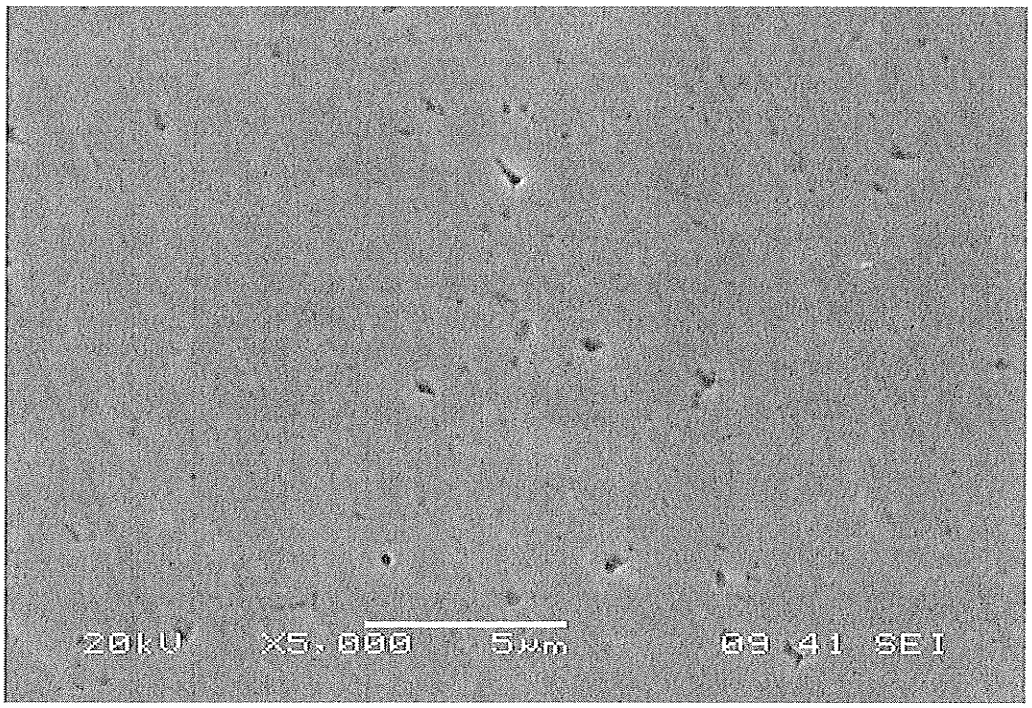

Figure 4.44: Microstructure obtained for test done at 1180 °C for 24 hrs using 38μm Ni-P filler alloy (X 5000)

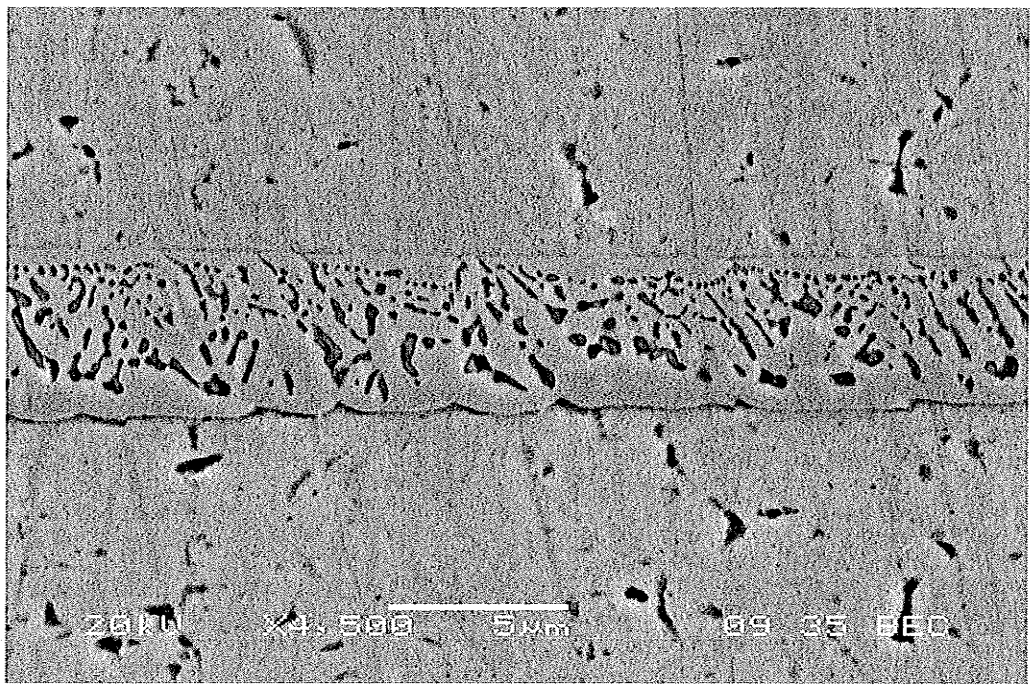

Figure 4.45: Microstructure obtained for test done at 1180 °C for 24 hrs using 76μm Ni-P filler alloy (X 4500)

As mentioned earlier, migration of solid-liquid interface, i.e. isothermal solidification of liquid insert during TLP bonding occurs by diffusion of melting point depressing solute (phosphorus in the present work) from the liquid into solid base alloy. At the constant temperature and holding time, the amount of phosphorus diffusion and, thus, extent of isothermal solidification would be the same in the two different gap size specimens. Therefore, the width of residual liquid, which transformed during cooling into centerline eutectic in both specimens, is expected to decrease with decrease in initial filler gap size, as was observed. This implies that longer time will be required to achieve complete isothermal solidification in larger gap size samples compared to smaller gap size samples. Models based on the diffusion induced solid-liquid interface motion [31, 48] have been used in estimating the time, t_f, that is required to produce a single phase microstructure during TLP bonding through a complete isothermal solidification of liquated insert. Generally, in these models, the time t_f can be approximated by

$$t_f^{1/2} = \frac{2h}{\gamma 4D^{1/2}} \qquad (4.7)$$

Where, D is diffusion coefficient of the melting point depressant in the sold base alloy, and 2 hrs is the maximum with of the insert following its equilibrium at solid-liquid interface, γ is a dimensionless parameter, which is estimated by solving equation 4.8 numerically.

$$\frac{C_\alpha - C_m}{C_\beta - C_\alpha} = \gamma\sqrt{\pi}\exp(\gamma^{1/2}(1+erf(\gamma))) \qquad (4.8)$$

Where, C_α and C_β are solute concentration in the solid and liquid phase at the migrating interface, respectively. Cm is the initial solute concentration in the base alloy. The maximum width, h, of the insert after equilibration depends strongly on the initial width (W) of interlayer employed. Thus, it can be seen from equation 4.7, and as indicated by

the present observation, that the time, t_f, for full migration of the solid-liquid interface to prevent formation of the centerline eutectic will increase with increase in gap size at any particular bonding temperature.

4.11 Effect of TLP Bonding Temperature on Microstructure of TLP Joint

As indicated previously, an important parameter in the consideration of TLP bonding for commercial applications is the holding time, t_f, required to complete the isothermal solidification process and, hence, prevent the formation of deleterious brittle microconstituents. This parameter is a function of solute diffusivity in the solid substrate and the phase relationships between the filler alloy and the base metal, both of which are dependent on bonding temperature. To study the effect of bonding temperature on the TLP joint's microstructure, 38 μm gap sized specimens were bonded at 1180°C for 1 and 24 hours and their microstructure was compared with those that were bonded for equivalent holding time at a lower temperature, 1100°C. Microstructure of the specimens bonded at 1180 °C for 1 h is presented in Figure 4.46. An incomplete isothermal solidification of the liquated insert occurred in the specimen, which resulted in the formation of continuous centerline eutectic. The average width of the eutectic, 32 μm, was, however, larger that that observed in the joint produced at 1100 °C for 1hr, which was 22 μm.

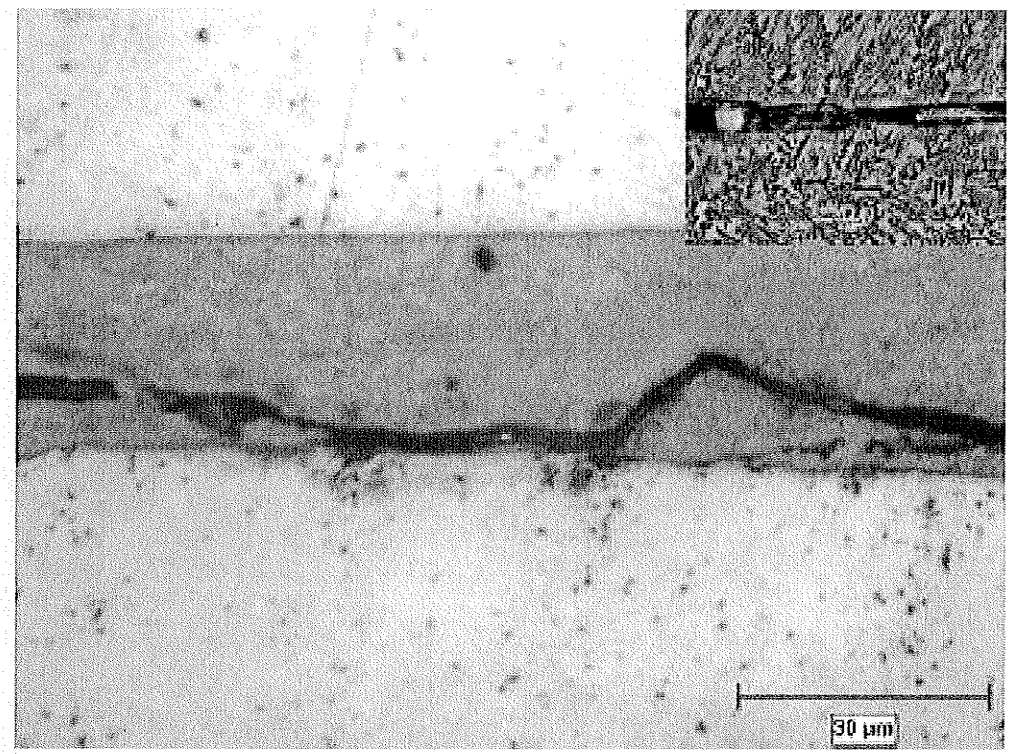

Figure 4.46: Optical micrograph of specimen bonded at 1180 °C for 1h: insert in micrograph shows higher magnification SEM image of crack through centerline eutectic product (X1000)

At a constant holding time, an increase in bonding temperature is expected to significantly increase solute diffusivity and reduce the width of the centerline eutectic reaction product. This is, however, at variance to what was observed in specimens bonded for 1 h at 1100 °C and 1180 °C. As stated earlier, the joint prepared at 1180 °C contained centerline eutectic width of 32 μm while 22 μm thick eutectic was observed the 1100 °C specimen. This difference can be attributed to the effect of base metal dissolution during the TLP bonding process. Subsequence to initial melting f the filler alloy, as the melting point depressing element diffuses into the base alloy, it reaches a high enough concentration near the substrate-filler interface to cause melting of the base alloy, also known as melt back or erosion.

Base metal dissolution during TLP bonding was examined by Nishimoto et. al. [52] based on a derivation of Nernst-Brunner theory [53]. Nishimoto et. al. [52] computed a dissolution parameter and showed that Nernst-Brunner theory could be used to explain dissolution during TLP bonding. It was determined that the dissolution rate is dependent on temperature with increase in temperature increasing the rate of dissolution as well as the size of equilibrium dissolution width. Hence, even though the starting thickness of the filler alloy used in the present work was the same for the two bonding temperatures 1100 °C and 1180 °C, the equilibrium dissolution width and thus, the size of liquated insert would be larger at 1180 °C than at 1100 °C. This increase in the size of the liquid interlayer prior to the commencement of isothermal solidification during bolding at 1180 °C could explain the larger eutectic width that was observed in the joint prepared at this temperature for 8 h.

Nonetheless, due to the considerable higher rate of solute diffusion in the solid substrate at 1180 °C, the effect of larger size of dissolution width would be insignificant after some extended holding time, such that, the time required to completely solidify the liquid and, thus, preclude the eutectic formation will be reduced relative to a lower temperature. This is supported by microstructural examination of specimens bonded at 1100°C and 1180°C for 24 hrs. After holding for 24 hrs at 1180°C, no eutectic constituent was observed along the TLP joint while continuous centerline eutectic less then 1 μm was formed from residual liquid in the joint prepared at 1100°C for the same 24 hrs holding time. These results, thus, show that increase in bonding temperature would be beneficial during TLP bonding only if sufficient holding time is allowed for complete isothermal solidification of liquated insert. Otherwise, increase in bonding temperature may instead result in formation of thicker deleterious eutectic micro-constituent along the TLP joint centerline.

Part III: Effect of Post-Braze Heat Treatment Process Parameters on The Microstructure of TLP Bonded Joints

4.12 Introduction

The use of filler alloys which contain MPD solutes that have low solubility and diffusivity in the base metal, such as phosphorous in nickel, can result in isothermal solidification completion times that are prohibitively long. In such cases, it has been suggested that short holding time can be used during TLP bonding and post-bond heat treatment can be applied to modify the joint's microstructure and eliminate/reduce the detrimental eutectic-type microconstituents that form due to incomplete isothermal solidification [54].

Successful application of post-braze heat treatment, however, requires proper selection of temperature and time. Limited work has been reported on post-bond heat treatment of nickel base superalloys. Therefore, the objective of this part of the thesis was to investigate the effect of post-bond holding time and temperature on microstructure of TLP joint in IN738 superalloy using MBF60(Ni-P) filler alloy.

4.13 Microstructure of TLP Joint in IN738 Using MPF60(Ni-P) Filler Alloy

IN738 was TLP bonded for 1 h at 1065 ^{o}C using 38 μm thick MBF60(Ni-P) filler. The microstructure of the joint produced is shown in Figure 4.47. A continuous eutectic product with an average width of 92 μm was formed along the centerline of the joint.

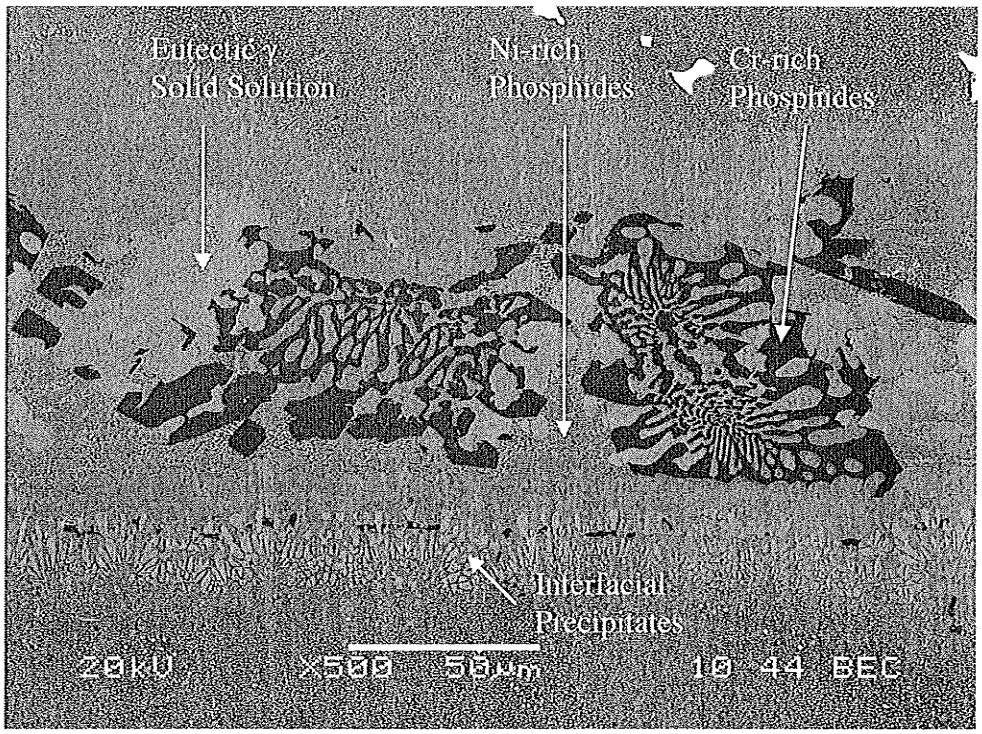

Figure 4.47: Microstructure of centerline eutectic of sample bonded at 1065 °C for 1 h

SEM-EDS semi-quantitative composition analysis of the eutectic (Table 4.1) suggests that it consisted of nickel base solid solution phase, a nickel rich and a chromium rich phosphide phases. In addition to the joint's centerline eutectic, precipitation of chromium and phosphorous rich particles, presumably, phosphides occurred in the base alloy grains and grain boundaries adjacent to the substrate-joint interface (Figure 4.47).

Analytical models of TLP bonding generally assumes that base metal dissolution and isothermal solidification stages occur sequentially. It is assumed that due to orders of magnitude difference in solute diffusivity on either side of liquid-solid interface, dissolution of the base metal into liquated interlayer occurs at a much faster rate than solid-state diffusion of MPD solute in the base metal. Accordingly, the filler alloy, upon melting, rapidly attains equilibrium with the solid substrate through base metal dissolution, following which solid-state diffusion of MPD solute commences. Under this condition, formation of intermediate second phase particles such as phosphides within the base alloy is unexpected since the process is assumed to progress under equilibrium condition following the rapid base-metal dissolution. Nevertheless, it has been suggested that base metal dissolution and solid-state diffusion of MPD solute could occur simultaneously rather than sequentially. In such a case, precipitation of phosphide particles can be expected in the base alloy region where solubility of phosphorous is exceeded due to continuous solid-state diffusion of phosphorous during base-metal dissolution.

Table 4.1: EDS metallic compositional analysis of phases in centerline eutectic

	Element Composition (wt.%)							
Phase	Al	Ti	Cr	P	Co	Si	Ta	Ni
γ Solid-Solution	1.47	0.94	11.13	0.38	5.80	0.66	—	79.61
Cr rich Phosphides	—	14.04	17.93	18.39	10.05	—	—	38.72
Ni-Rich Phosphides	—	0.53	5.95	11.17	3.19	—	—	82.35

Both the formation of centerline eutectic and interface second phase particles has been reported to degrade the mechanical properties of TLP bonded materials [2, 17, 19, 27, 30]. Therefore, the influence of post-bond heat treatment on these microconstituents was investigated in the present work as follows.

4.14 Post-Bond Heat Treatment of TLP Bonded Materials

Due to the relatively very high melting temperatures of intermetallic phosphide particles, it has been previously suggested that once these particles form in TLP joint, it becomes very difficult to eliminate or reduce their presence through liquated reaction by post-bond heat treatment. While these particles do have high melting temperature, the fact that they exist in close contact with other phases that they could react with to form liquid phase by eutectic–type reaction at temperatures significantly below their occurrence melting temperature suggests that the use of post-bond heat treatment may be feasible.

To investigate this possibility, post bond heat treatment of specimens bonded using the condition stated in section 4.13 was performed at 800 °C and 1000 °C, below and above the Ni-P binary eutectic temperature of 870 °C respectively, for 3 hrs and 24 hrs. Metallographic examination of heat treated specimens showed no significant change in the average width of the eutectic in the 800 °C specimens after 3 hrs and 24 hrs (Figure 4.48). In contrast, however, the average eutectic width reduced in the 1000 °C specimens to an average of 53μm after 24 hrs (Figure 4.49). In addition, the eutectic morphology in 800 °C specimens was essentially the same as that in the as-bonded specimen but a notable change in morphology was noted in 1000 °C specimens.

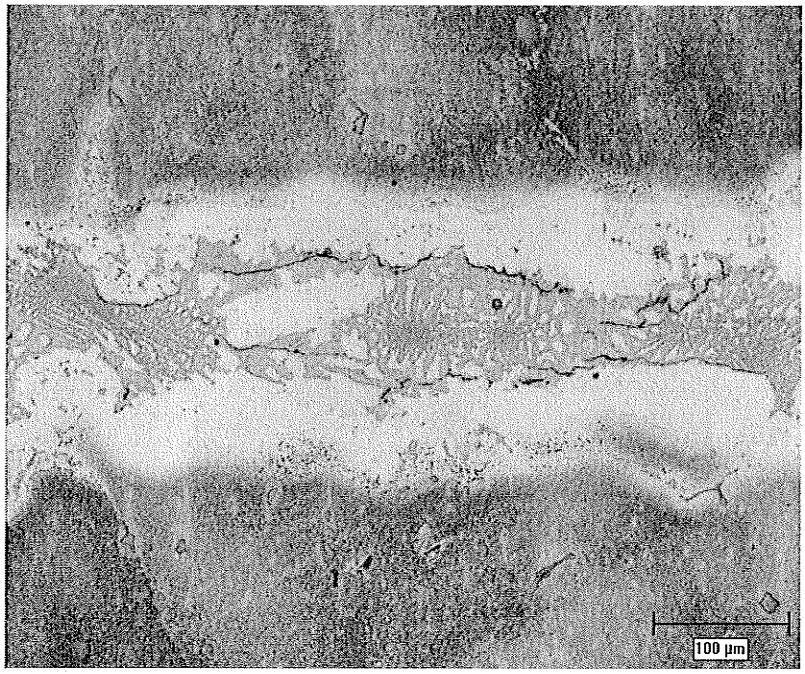

(a)

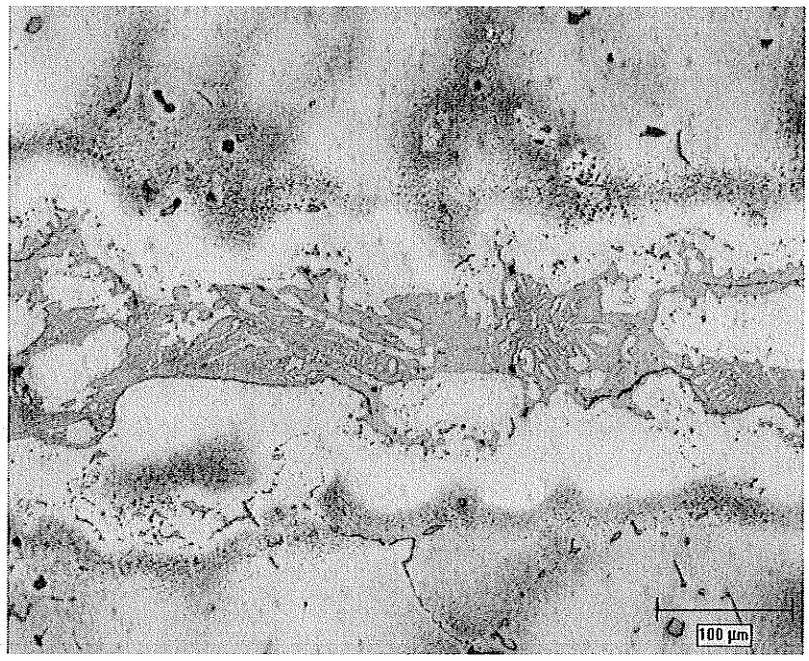

(b)

Figure 4.48: Microstructure of post-braze heat treated specimens at 800 °C for (a) 3 hrs and (b) 24 hrs (X200)

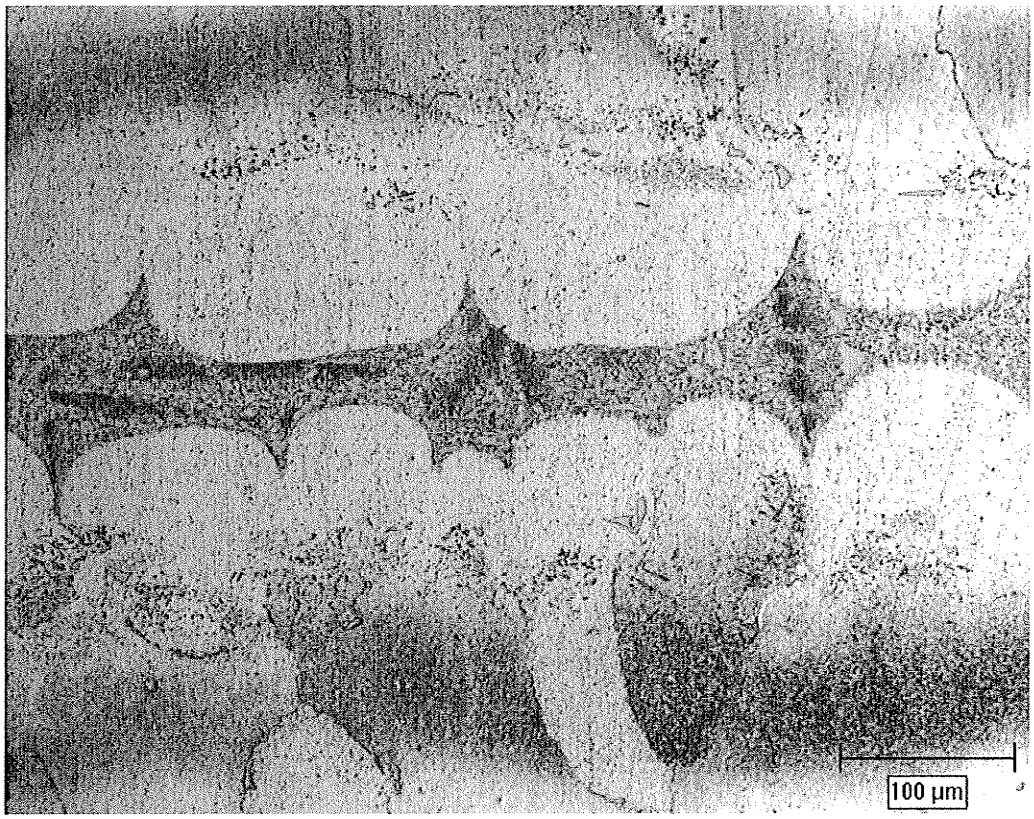

Figure 4.49: Microstructure of post-bond heat treated specimens at 1000 °C for 24 hrs (X200)

This suggests that heat treatment above the Ni-P eutectic temperature resulted in liquation of the centerline eutectic in 1000 °C specimens. Upon liquation, a sharp concentration gradient at solid-liquid interface can enhance diffusion of phosphorous away from the joint into the substrate. Continuous diffusion of phosphorous into the base alloy with increase in holding time would cause the volume of liquid that can be maintained at equilibrium to decrease resulting in isothermal solidification. Residual liquid present after holding time duration would transform into centerline eutectic during cooling and produce a decrease in centerline eutectic width as observed in the 1000 °C specimens. Since 800 °C is below the Ni-P eutectic temperature, any microstructural change to the centerline eutectic product at this temperature would occur exclusively by solid-state diffusional process, which is generally slow. This could explain the apparent no change in the eutectic width after 24 hrs of post-bond heat treatment at 800 °C.

The number density/volume fraction of the interface second particles did not change noticeably after 24 hrs of holding at both 800 °C and 1000 °C. In contrast to centerline eutectic, as stated previously, the interface second phase particles are likely formed by diffusion induced solid-state precipitation reaction; as such, microstructural modification by changes to these particles would likely occur by solid-state diffusion process, which may account for the negligible change in their number density after 24 hrs of holding time.

To further study the effect of post-bond heat treatment temperature, heat treatment of specimens bonded using the condition stated above was performed at 1100 °C and 1200 °C for 24h. Similar to the observations in 1000 °C specimens, the morphology of the

centerline eutectic changed and the eutectic width reduced considerably in 1100 °C ad 1200 °C specimens (Figures 4.50 and 4.51). According to the Arrhenius equation, diffusivity of phosphorous, D, in the base alloy increases with temperature as given by equation 4.9.

$$D = D_o \exp(-Q / RT) \qquad (4.9)$$

Where D_o is the frequency factor, Q is the activation energy, R is the gas constant and T is the absolute temperature. Taken that diffusivity of phosphorous in the base metal controls the isothermal solidification of liquated interlayer during post bond heat treatment temperature above Ni-P eutectic temperature, an increase in temperature from 1000 to 1100 and 1200 °C would accelerate the isothermal solidification and in effect reduce the eutectic width as observed.

Likewise, an increase in temperature was observed to produce significant reduction in the interface second phase precipitates, which is in contrast to the effect of increase in time at 800 °C and 1000 °C. An increase in temperature can significantly lower thermodynamic stability of the phases within the base alloy matrix which would result in the decrease in their number density, as observed in the 1100 °C and 1200 °C specimens.

As previously stated, formation of centerline eutectic and interface second phase particles do reduce mechanical properties of TLP joint in structural engineering materials. The results of this part of the thesis show that while post-bond heat treatment time can reduce the size of deleterious eutectic provided that heat treatment temperature is above eutectic temperature, holding time does not have such effect on interface precipitates. In contrast, however, an increase in post-bond heat treat treatment temperature can produce

significant reduction in both eutectic product and interface second phase particles. The variation in responses of these microconstituents to post-bond heat treatment parameters can be related to the nature of formation during TLP bonding. That is, centerline eutectic is formed from residual interlayer liquid during cooling, while interface precipitates are possibly formed by solid-state precipitation reaction at bonding temperature.

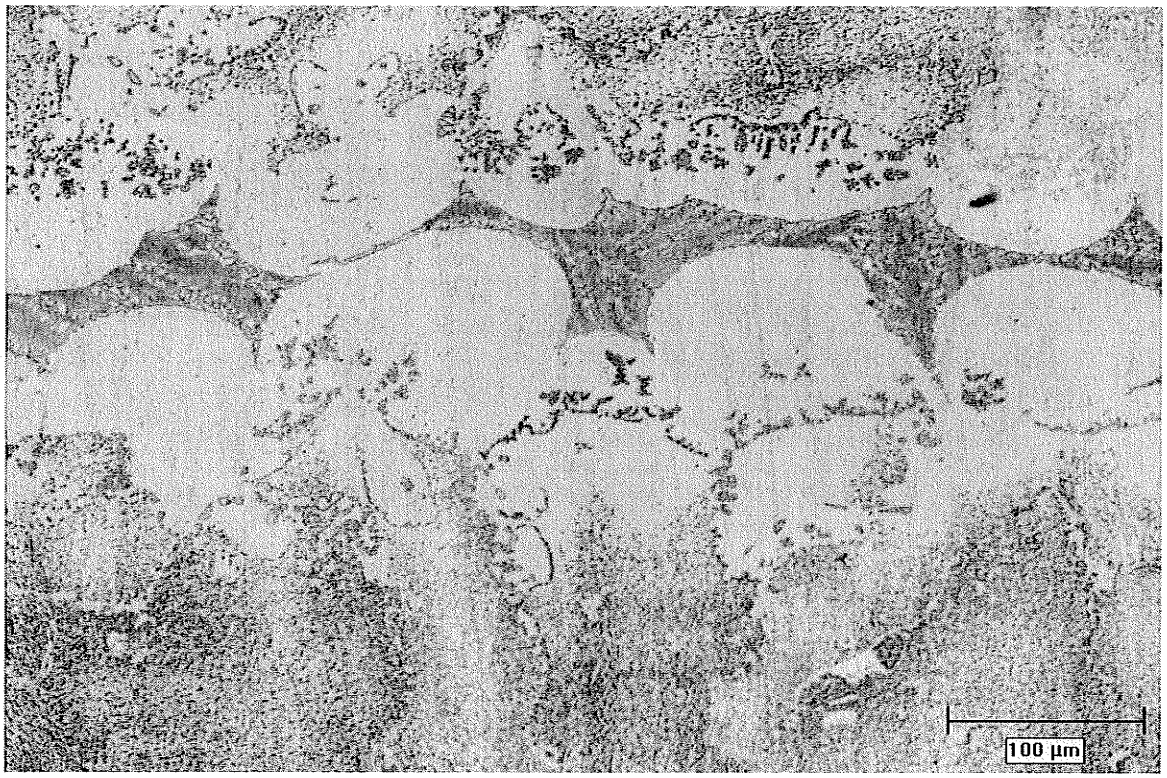

Figure 4.50: Microstructure of post-bond heat treated specimen at 1100 °C for 24 hrs (X200)

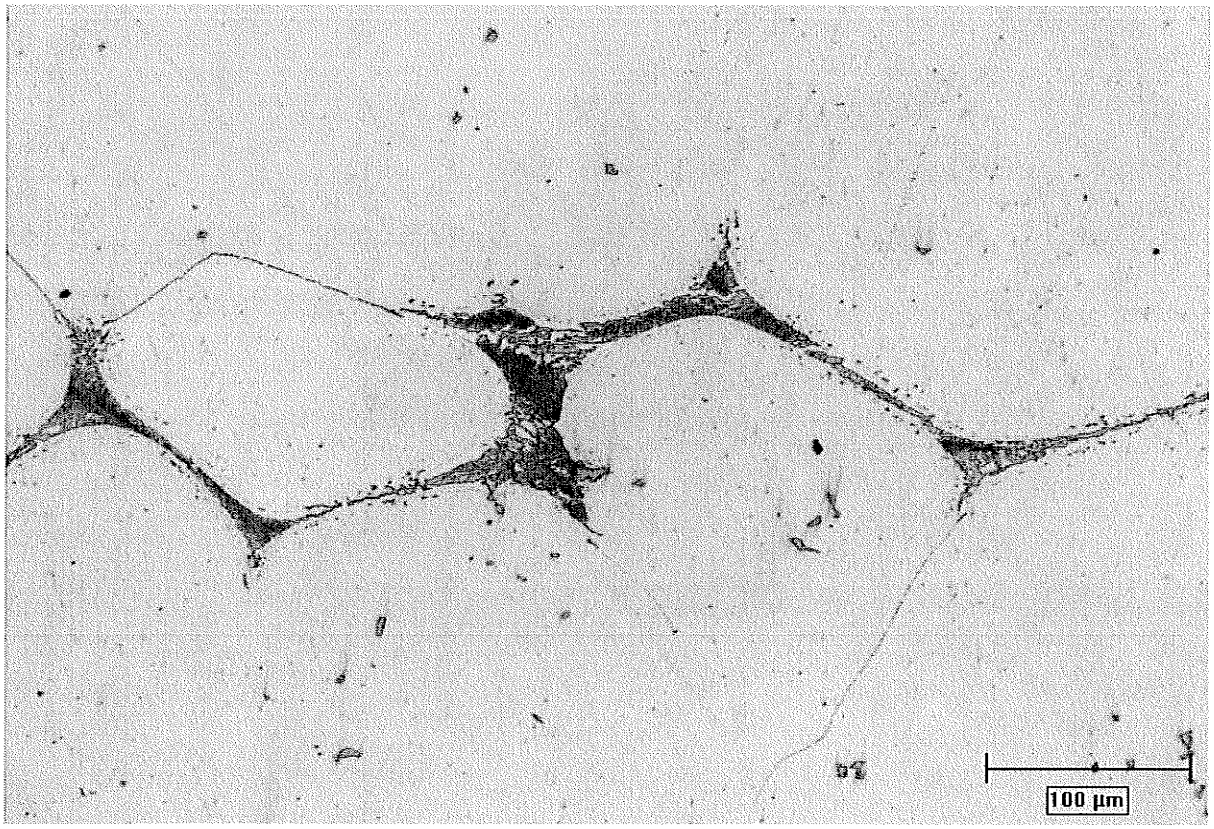

Figure 4.51: Microstructure of post-bond heat treated specimen at 1200 °C for 24 hrs (X200)

Chapter 5: Summary and Conclusions

The first part of this work reports the results of theoretical and experimental investigations carried out to better understand the causes of the anomalous behaviour of prolonged isothermal solidification completion time with increase in temperature during transient liquid phase (TLP) bonding. The study which was carried out using Inconel 738 superalloy as the base metal and MBF80 (Ni-Cr-B) as the filler alloy indicated that:

1) An increase in base metal dissolution due to increased TLP bonding temperature can not be solely used to explain increase in isothermal solidification completion time, t_f, with increase in temperature. Reduction in solute solubility with increase in temperature is a more dominant factor.

2) In contrast to standard analytical TLP bonding models, deviation from parabolic relationship, between displacement of solid-liquid interface and holding time, was observed experimentally during TLP bonding of IN738 superalloy using a Ni-Cr-B filler alloy. This deviation behavior can be duly rationalized by the application of implicit finite difference model to solve Fick's diffusion equation.

3) Deviation from the parabolic relationship is caused by reduction in solute concentration gradient ($\partial C/\partial x$) below a critical value $(\partial C/\partial x)_c$ due to continual diffusion of MPD solute from liquated interlayer in the base material during TLP bonding.

4) An increase in the size of the deviation zone with concomitant increase in the reduction of isothermal solidification rate occurs with increase in temperature.

This phenomenon was found to be a new alternate cause of increase in t_f with increase in temperature above T_c and it is reported for the first time in this work.

5) Based on the concept of deviation from parabolic behavior, salient factors that can have important influence on the occurrence of T_c are suggested to be :

   a) Thickness of filler alloy

   b) Initial concentration of MPD solute in filler alloy and base material

   c) Solubility of MPD solute in base material

   Proper optimization of these factors can improve the commercial appeal of TLP bonding technique by significantly reducing the processing time required to produce reliable high-temperature eutectic-free joint.

In certain applications where boron-bearing fillers are unsuitable, filler alloys containing alternative MPD solutes such as phosphorous or silicon must be used. The second part of this thesis focused on the effect of TLP bonding process parameters on the microstructure of TLP joint in commercial pure nickel by using a Ni-P filler alloy. The results of the study showed that:

1) The extent of isothermal solidification of liquated interlayer increased with holding time during TLP bonding of pure nickel with Ni-P filler material.
2) Incomplete isothermal solidification of the liquated insert resulted in transformation of residual liquid into phosphorous enriched continuous eutectic along the joint centerline region, which provided a preferential path for crack initiation and propagation.

3) The width of the deleterious non-equilibrium solidification eutectic product increased with increase in initial filler alloy thickness.
4) Two different observations regarding the influence of bonding temperature on the eutectic size was observed. After short holding times, thicker eutectic was observed at higher temperatures due to increased base metal dissolution. At longer times, however, the eutectic width decreased significantly owing to increased diffusivity of phosphorous with increase in temperature.

Due to the relatively slow diffusion of phosphorous in nickel-base materials during TLP bonding, prohibitively long holding times may be required to eliminate the deleterious microconstituents at the joint. Microstructural modification by post bond heat treatment is a possible approach for reducing the deleterious intermetallic phases that form during TLP bonding. Finally, the results of studying the influence of post-bond heat treatment on microstructure of TLP joint using IN738 base metal and Ni-P filler in the third part of this thesis showed that:

1) TLP bonding of IN738 at 1065 ^{o}C for 1h using a 76 μm thick Ni-P filler alloy resulted in formation of centerline eutectic that contained nickel based solid solution phase, a nickel rich and chromium rich phosphide phases.
2) In addition to the eutectic, phosphorous rich second phase particles, which were possibly formed by solid-state diffusion induced precipitation reaction were observed within the base alloy region adjacent to the substrate-joint interface.
3) While increase in post-bond heat treatment temperature and holding time produced significant reduction in the eutectic width at temperatures above Ni-P

eutectic temperature, 870 °C, reduction of the interface precipitates was observed only by increasing temperature.

4) The variation in the responses of centerline eutectic and interface precipitates to post-bond heat treatment temperature and time can be related to their mode of formation and thus dissolution reaction in which the eutectic involves a liquation reaction whereas the interface precipitates involves exclusively solid state reaction.

Chapter 6: Suggestions for Future Work

This study has resulted in the identification of a very interesting phenomenon, deviation from parabolic behavior that can have important influence on the processing time and thus the general appeal of TLP bonding technique for commercial applications. To investigate this phenomenon further, the following detailed studies are recommended toward optimization of the joining process to produce sound and reliable joint in practically accessible time.

1) Experimental investigation on the influence of initial concentration of MPD solute in filler alloy on isothermal solidification completion time at various temperatures and using different gap sizes to verify the suggestions made in this study. This could be combined with determination of variation of solute concentration gradient in the base material in order to aid the understanding of the underlying concept.
2) A study of the role of the mode of existence and distribution of MPD solute in base alloy prior to TLP joining on isothermal solidification kinetics using different MPD solutes. This is pertinent considering that MPD solutes can exist in either γ solid-solution form or in second phase precipitates in superalloys prior to bonding.
3) Development of numerical TLP bonding models that incorporate possible dependence of diffusion coefficient on concentration, non-planar liquid-solid interface and possible enhanced diffusion due to precipitation solute enriched second phase particles. This may enhance the accuracy of numerical simulations.

4) As shown in this work that post-bond heat treatment can be used to modify microstructure of TLP bonded materials, the influence of such microstructural changes on ambient and elevated temperature mechanical properties of bonded materials needs to be evaluated to ascertain the effectiveness of the approach.

Appendix A: Binary Phase Diagrams

A.1 Ni-B Phase Diagram [51]

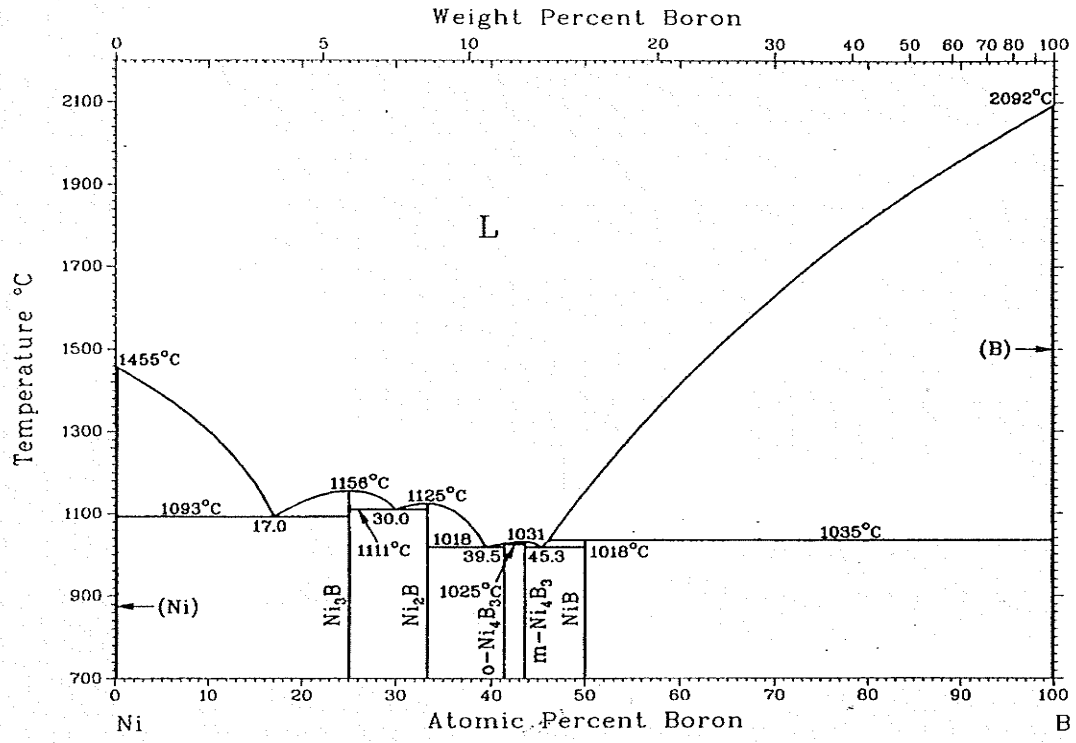

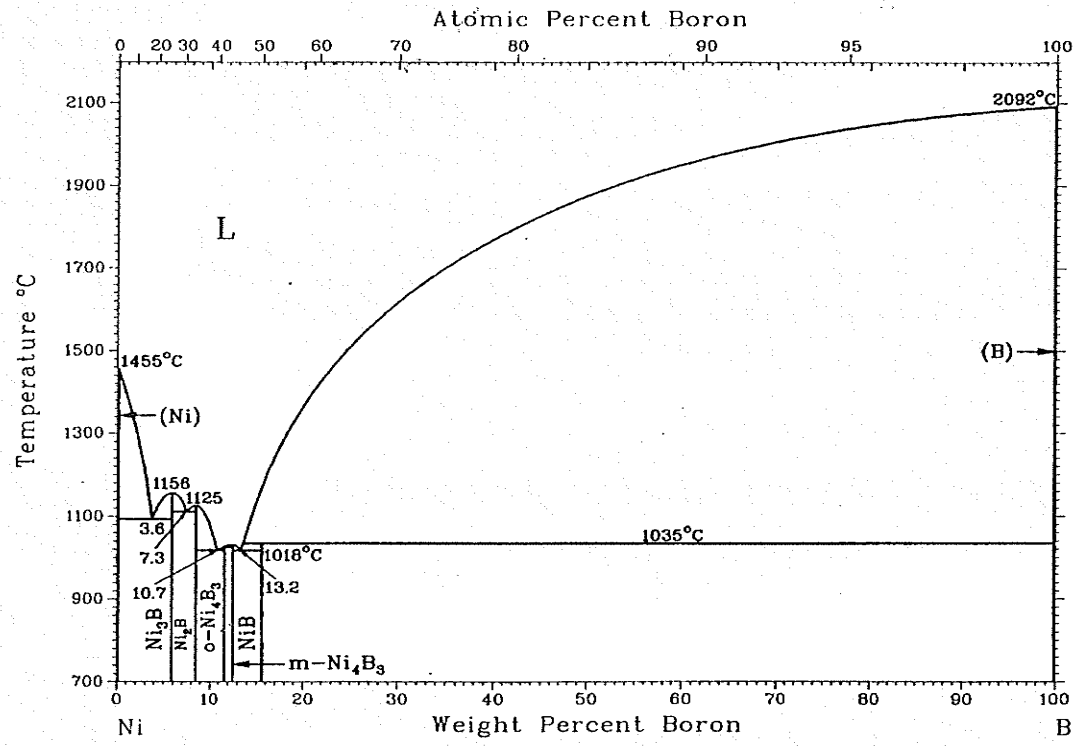

A.2 Ni-Si Phase Diagram [51]

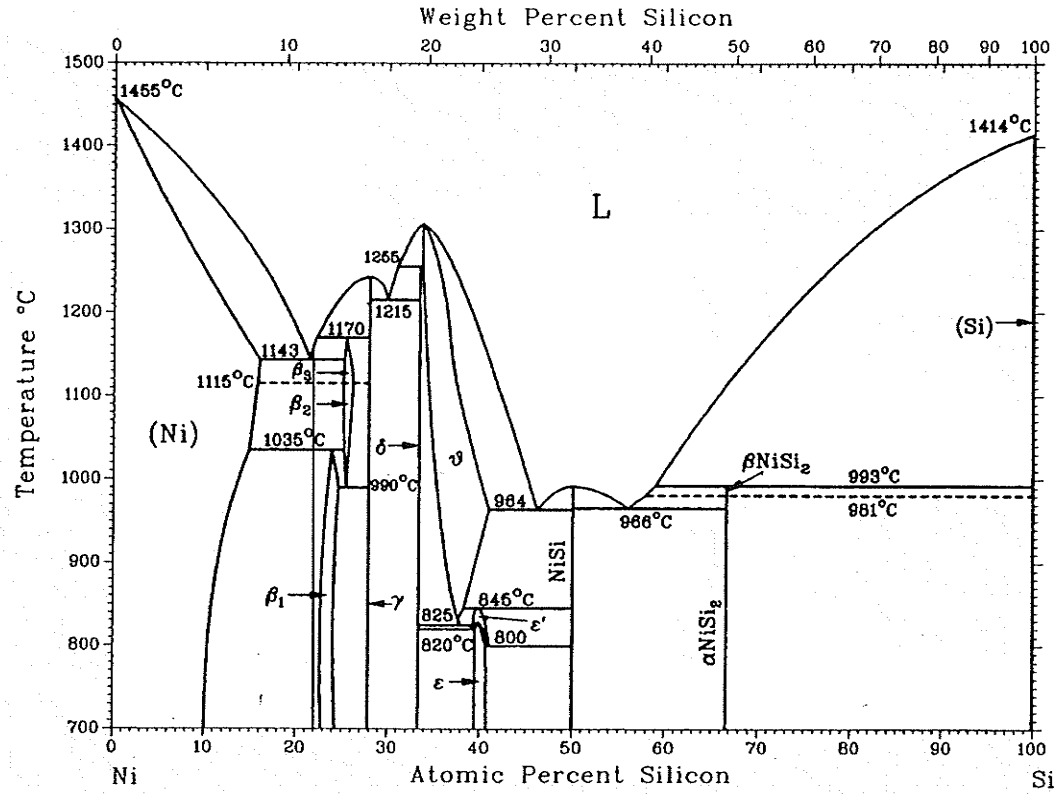

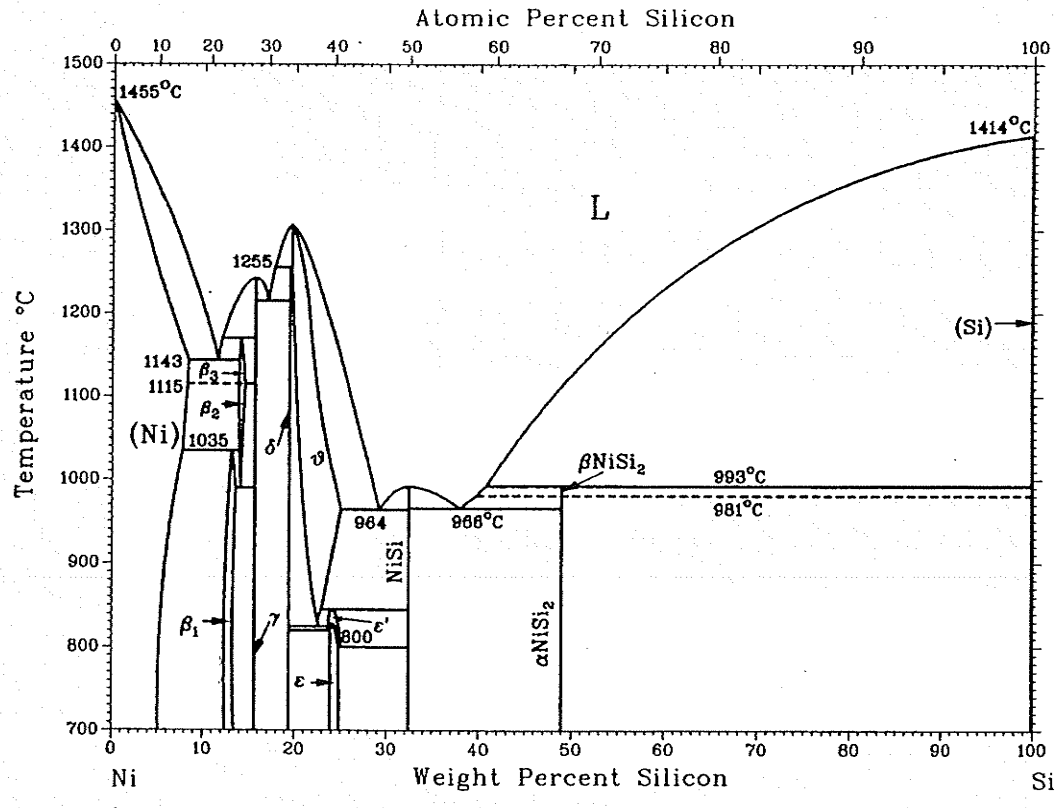

A.3 Ni-P Phase Diagram [51]

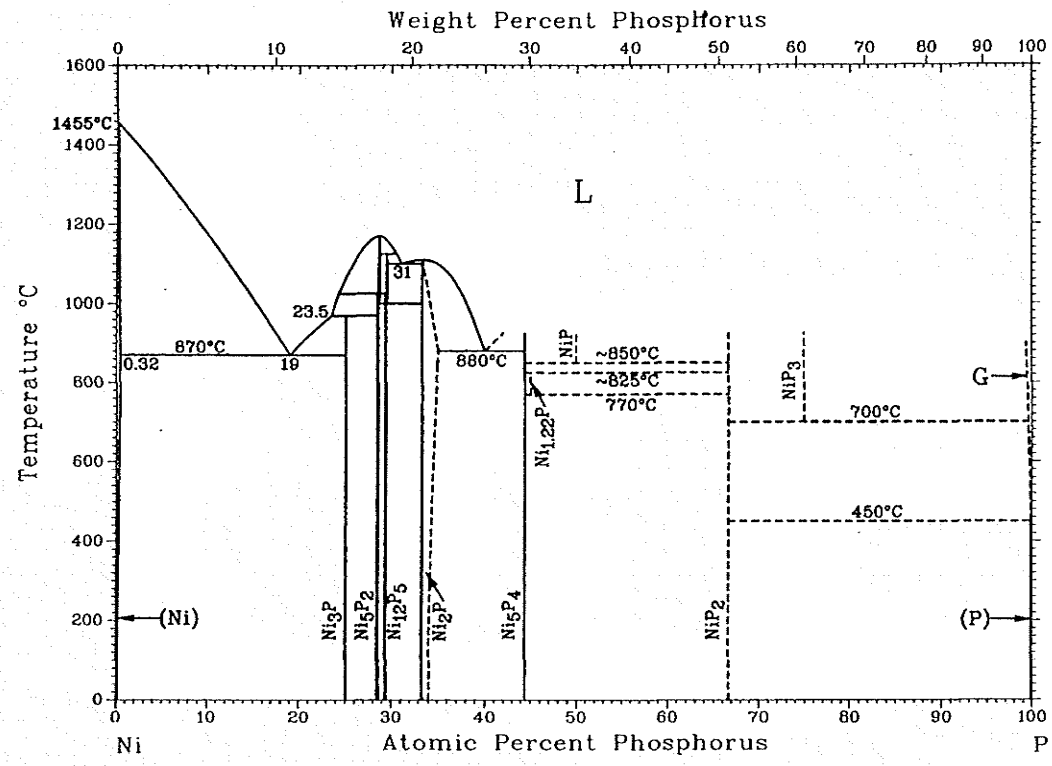

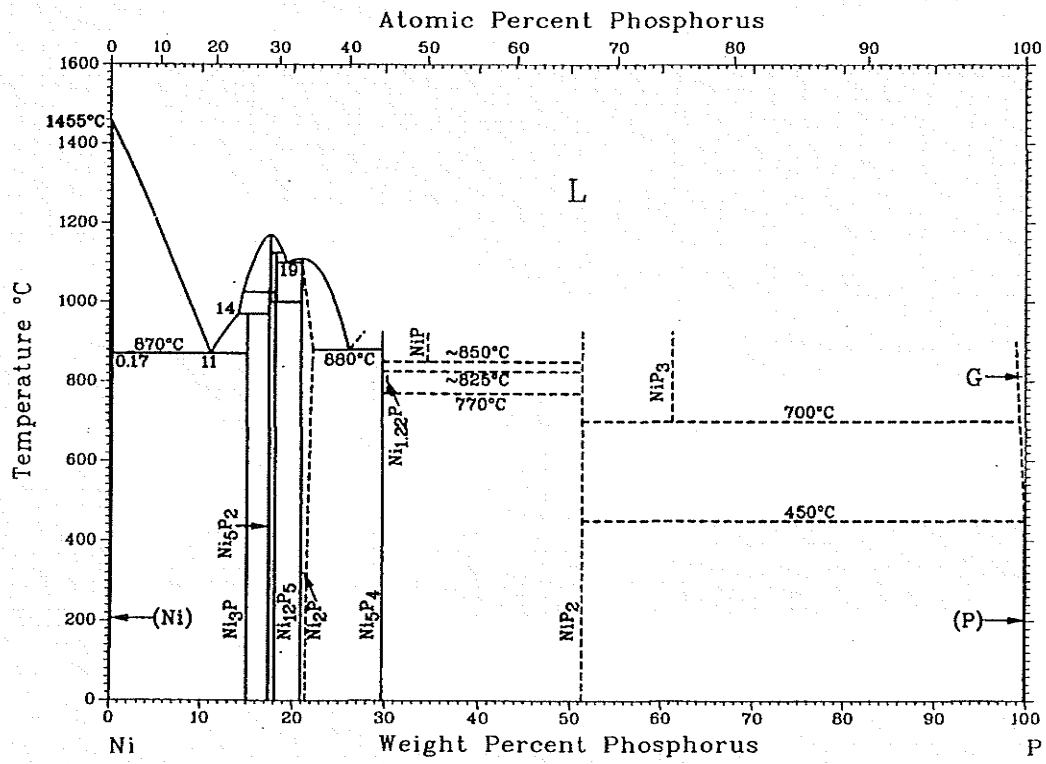

Appendix B: Analytical Modeling of TLP Bonding Program

B.1 Mathematical Implementation

The analytical modeling program obtains the solution for the time required to achieve complete isothermal solidification by solving for the constant K in equation B.1 derived by Ramirez and Liu [31], maximum dissolution width W_{max} using equation B.2 and diffusivity D from using equation B.3 then substituting the results into equation B.4 derived by Tua-Poku et. al. [28] to solve for isothermal solidification completion time t.

$$\frac{C_{\alpha L}-C_o}{C_{L\alpha}-C_{\alpha L}}=\sqrt{\pi}.\frac{K.(1+erf(K))}{\exp(-K^2)} \qquad \text{(B.1)}$$

$$W_{\max}=\frac{C_F.W_o}{C_{L\alpha}} \qquad \text{(B.2)}$$

$$D=D_o\exp(-Q/RT) \qquad \text{(B.3)}$$

$$t=\frac{W_{\max}^2}{16.K^2.D} \qquad \text{(B.4)}$$

The main challenge in solving for t is solving the error function in equation B.1. Generally, mathematical tables can be used to approximate the error function. The solutions obtained by this method, however, are not accurate and do not reflect the true analytical solution of the model. Therefore, a Newton-Raphson numerical root finding method is used to efficiently solve for K by approximating the error function by a Taylor series. This section outlines the steps undertaken to numerically obtain the solution of the analytical model.

The general iterative equation for the Newton-Raphson method is:

$$K_{i+1} = K_i - \frac{f(K_i)}{f'(K_i)} \qquad \text{for i = 0, 1, 2, ...} \qquad \text{(B.5)}$$

Obtaining an expression for $f(K)$:

$$f(K) = \left(\frac{C_{\alpha L} - C_o}{C_{L\alpha} - C_{\alpha L}}\right) - \left(\sqrt{\pi}.\frac{K(1+erf(K))}{\exp(-K^2)}\right) \qquad \text{(B.6)}$$

Using a Taylor series to approximate $erf(K)$:

$$erf(K) = \frac{2}{\sqrt{\pi}}\int_0^K e^{-u^2}\,du$$

$$erf(K) = \frac{2}{\sqrt{\pi}}\left(K - \frac{K^3}{3.1!} + \frac{K^5}{5.2!} - \frac{K^7}{7.3!} + ...\right) \qquad \text{(B.7)}$$

$$erf(K) = \frac{2}{\sqrt{\pi}}\sum_{n=0}^{\infty}\frac{(-1)^n K^{2n+1}}{(2n+1).n!} \qquad \text{(B.8)}$$

$f(K)$ becomes:

$$f(K) = \left(\frac{C_{\alpha L} - C_o}{C_{L\alpha} - C_{\alpha L}}\right) - \left(\sqrt{\pi}\,\frac{K\left[1 + \left(\frac{2}{\sqrt{\pi}}\sum_{n=0}^{\infty}\frac{(-1)^n K^{2n+1}}{(2n+1)n!}\right)\right]}{\exp(-K^2)}\right) \qquad \text{(B.9)}$$

Now an expression for $f'(K)$ is obtained by differentiating equation B.6:

$$f'(K) = -\sqrt{\pi}\left[\frac{\exp(-K^2)(1+Kerf'(K)+erf(K))+2K^2(1+erf(K))\exp(-K^2)}{\exp(-K^2)^2}\right]$$

(B.10)

Now an expression for $erf'(K)$ is obtained by differentiating equation B.7:

$$erf'(K) = \frac{2}{\sqrt{\pi}} + \frac{2}{\sqrt{\pi}}\left(-\frac{K^2}{1!}+\frac{K^4}{2!}-\frac{K^6}{3!}+.....\right)$$

$$erf'(K) = \frac{2}{\sqrt{\pi}} + \frac{2}{\sqrt{\pi}}\sum_{n=1}^{\infty}\frac{(-1)^n K^{2n}}{n!} \qquad \text{(B.11)}$$

Equation B.10 becomes:

$$f'(K) = -\sqrt{\pi}.\frac{\exp(-K^2)(1+K.(\frac{2}{\sqrt{\pi}}+\frac{2}{\sqrt{\pi}}\sum_{n=1}^{\infty}\frac{(-1)^n K^{2n}}{n!})+(\frac{2}{\sqrt{\pi}}\sum_{n=0}^{\infty}\frac{(-1)^n K^{2n+1}}{(2n+1).n!}))+2K^2(1+(\frac{2}{\sqrt{\pi}}\sum_{n=0}^{\infty}\frac{(-1)^n K^{2n+1}}{(2n+1).n!}))\exp(-K^2)}{\exp(-K^2)^2}$$

(B.12)

Substituting equations B.9 and B.12 back into B.4 and considering the first 10 terms of the Taylor series yields:

$$K_{i+1} = K_i - (\frac{C_{\alpha L}-C_o}{C_{L\alpha}-C_{\alpha L}}) - \left(\sqrt{\pi}.\frac{K_i(1+\left(\frac{2}{\sqrt{\pi}}\sum_{n=0}^{10}\frac{(-1)^n K_i^{2n+1}}{(2n+1).n!}\right))}{\exp(-K_i^2)}\right)$$

$$+\frac{}{\sqrt{\pi}.\frac{\exp(-K_i^2)(1+K_i.(\frac{2}{\sqrt{\pi}}+\frac{2}{\sqrt{\pi}}\sum_{n=1}^{11}\frac{(-1)^n K_i^{2n}}{n!})+(\frac{2}{\sqrt{\pi}}\sum_{n=0}^{10}\frac{(-1)^n K_i^{2n+1}}{(2n+1).n!}))+2K^2(1+(\frac{2}{\sqrt{\pi}}\sum_{n=0}^{10}\frac{(-1)^n K_i^{2n+1}}{(2n+1).n!}))\exp(-K_i^2)}{\exp(-K_i^2)^2}}$$

(B.13)

Equation B.13 is iteratively solved until a converged answer is obtained. Due to the much faster convergence of Newton-Raphson method compared to linearly convergent methods, a converged solution for K is usually obtained in five or less iterations only. Once K is determined equations B2 to B.4 can be solved easily.

B.2 User's Guide to the Analytical Modeling Program

To perform analytical simulations of TLP bonding using the written program follow the following steps:

1) Install the program into your hard drive by double clicking on **setup.exe**
2) Once the program is open click on **Start Program** button
3) Enter the data related to the TLP bonding condition at which the simulation is to be performed.
4) Under **Iteration Settings**, enter the desired number of iterations and level of accuracy desired.
5) Click on the **Calculate** button in the left side of the screen.
6) The iterative solutions are shown in the list box and final calculations are shown in red. To clear data from the list box click on the **Clear List** button. The **Clear** button clears all solutions and the **Reset All** button resets data to default settings.

To study the effect of varying process parameters follow the steps 1 to 4 outlined above then do the following:

1) Choose the process parameter you would like to study from the list in the top right side of the screen.

2) Enter the number of increment value and number of increments by which the parameter being studied is increased from its original value.

3) Click the **Analyze Process Parameter Effects** button in the top right part of the screen.

4) The solutions are then listed in the right list box. To save the solutions in a text file click on **Save Data** button. To append new solutions to existing data in a text file make sure that the **Append data** check box is checked before clicking on **Save Data** button.

5) To study the effect of varying bonding temperature on the analytical solution temperatures and their corresponding MPD solute's solidus, $C_{\alpha L}$, and liquidus, $C_{L\alpha}$, solubilities in the base metal must be specified. Then click on the **Analyze Temperature Effects** button at the bottom right side of the screen. Boxes under **Studying the Effect of Varying Temperature** must be filled by a zero if they are not being used for analysis.

B.3 Capabilities and Limitations of the Analytical Modeling Program

The analytical modeling of TLP bonding program has a number of attractive capabilities which can be summarized as follows:

- The program does not require a complier to run and it is available as an executable program that can be downloaded and can operate in Windows XP or Vista environments.
- The program is capable of running multiple simulations to study the effect of varying multiple TLP bonding process parameters such as:
    - Bonding temperature

- Initial thickness of filler alloy
- Initial solute concentration in filler and base metal
- Diffusivity of MPD solute in the base metal
- Solubility of the MPD solute in the base metal

- The graphical user interface used allow for a more user friendly program where the user has control over the number of iterations and accuracy of converged solution.
- The program can save a report of obtained solutions as a text file which can be easily used to interact with graphing programs such as Microsoft Excel or MatLAB.

Limitations of the analytical modeling program can be summarized as follows:

- It can only be used to obtain an analytical solution for binary systems.
- It can not be used in operating systems older the Microsoft XP.
- Graphing and plotting capabilities were not implemented in the program. Therefore, Microsoft Excel or MatLAB might need to be used along side the program.
- Although the program was written in a manner to avoid debugging issues, certain issues might arise if meaningless inputs are inserted by the user.

Appendix C: Numerical Simulation of TLP Bonding Program

C.1 Mathematical Implementation & Algorithm Solution

Using a finite difference approach based on Landau transformation Illingworth et. al. [32] derived equations C.1 to C.3 ensuring solute conservation and developed an algorithm for obtaining a numerical solution. Equation C.1 provides an expression for the total amount of solute at time t^j where j is the time step. Equations C.2 and C.3 provides expressions for future compositions in phase A and phase B, respectively. The Landau transformation introduces new positional variables for which the interval [0,1] corresponds to the extent of each phase. Fixed discritization of these variables will, therefore, correspond to points whose position in real space can be considered to automatically adjust to accommodate the motion of the interface.

Equations C.1 to C.3 must be solved simultaneously since the concentration profiles and interface motion form a strongly coupled problem. Additionally, since the system of simultaneous equations is non-linear, an iterative solution method must be used. Equations C.1 to C.3 are expressed in a manner which allows for obtaining a solution using an explicit scheme ($\sigma = 0$), Crank-Nicolson scheme ($\sigma = ½$), or an implicit scheme ($\sigma = 1$). Explicit solutions can result in instability of the solution and unphysical oscillations. If Crank-Nicolson scheme is used to descretize discontinuous composition profiles, unphysical oscillations will result which limits the time step used. On the other hand, fully implicit schemes predict monotonic concentration profiles independent of the time step used which means that a stable numerical solution can be obtained.

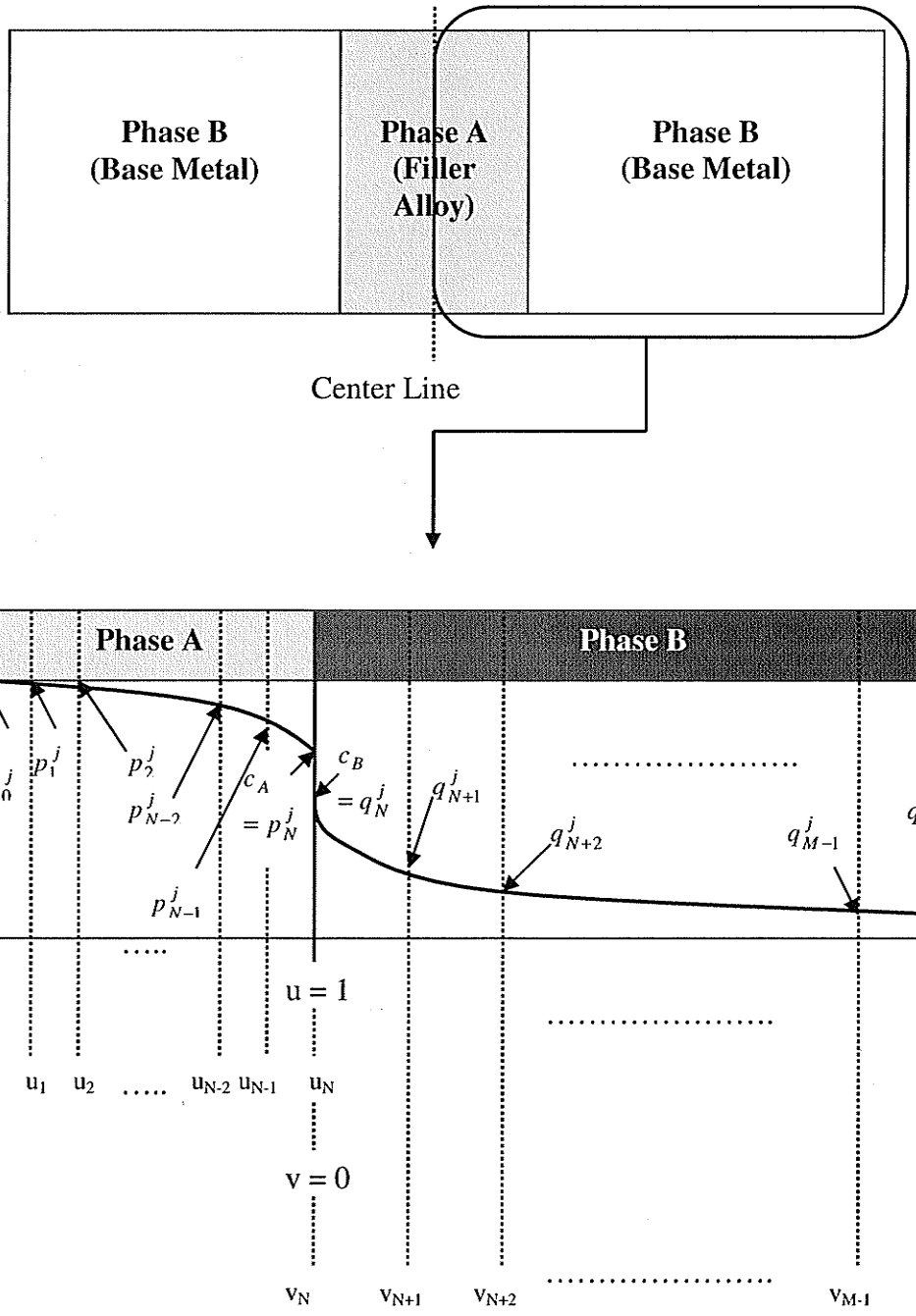
Phase B
(Base Metal)
Phase A
(Filler
Alloy)
Phase B
(Base Metal)
Center Line
Phase A
Phase B
p_0^j
p_1^j
p_2^j
p_{N-2}^j
p_{N-1}^j
c_A
$= p_N^j$
c_B
$= q_N^j$
q_{N+1}^j
q_{N+2}^j
q_{M-1}^j
q_M^j
u = 0
u = 1
u_o u_1 u_2 ..... u_{N-2} u_{N-1} u_N
v = 0
v = 1
v_N v_{N+1} v_{N+2} v_{M-1} v_M

$$\frac{D_B \delta t}{L - s^{j+\sigma}}\left(\frac{q_1^{j+\sigma} - c_B}{v_1}\right) - \frac{D_A \delta t}{s^{j+\sigma}}\left(\frac{c_A - p_{N-2}^{j+\sigma}}{1 - u_{N-2}}\right)$$
$$= (s^{j+1} - s^j)\left[\frac{1 + u_{N-2}}{2} p_{N-1-1/2}^{j+\sigma} + \frac{1 - u_{N-2}}{2} c_A - (1 - \frac{v_1}{2}) q_{1/2}^{j+\sigma} - \frac{v_1}{2} c_B\right] \tag{C.1}$$

$$\left[p_i^{j+1} s^{j+1} - p_i^j s^j\right]\left[u_{i+1/2} - u_{i-1/2}\right] = \frac{\delta t}{s^{j+\sigma}}\left[(D_A)_{i+1/2}^{j+\sigma} \frac{p_{i+1}^{j+\sigma} - p_i^{j+\sigma}}{u_{i+1} - u_i} - (D_A)_{i-1/2}^{j+\sigma} \frac{p_i^{j+\sigma} - p_{i-1}^{j+\sigma}}{u_i - u_{i-1}}\right]$$
$$+ (s^{j+1} - s^j)\left[p_{i+1/2}^{j+\sigma} u_{i+1/2} - p_{i-1/2}^{j+\sigma} u_{i-1/2}\right] \tag{C.2}$$

$$\left[q_i^{j+1}(L - s^{j+1}) - q_i^j (L - s^j)\right](v_{i+1/2} - v_{1-1/2}) = \frac{\delta t}{L - s^{j+\sigma}}\left[(D_B)\frac{q_{i+1}^{j+\sigma} - q_i^{j+\sigma}}{v_{i+1} - v_i} - (D_B)\frac{q_i^{j+\sigma} - q_{i-1}^{j+\sigma}}{v_i - v_{i-1}}\right]$$
$$+ (s^{j+1} - s^j)\left[q_{i+1/2}^{j+\sigma}(1 - v_{i+1/2}) - q_{i-1/2}^{j+\sigma}(1 - v_{i-1/2})\right] \tag{C.3}$$

Where:

δt : Time step

s^j : Future interface position in time step j

p_i^j : Concentration in phase A in position i in time step j

q_i^j : Concentration in phase B in position i in time step j

L : Thickness of phase B plus half-thickness of phase A

u: Proportional position in phase A

v: Proportional position in phase B

M, N: Number of discretisation points

D_A: Diffusion coefficient in phase A

D_B: Diffusion coefficient in phase B

c_A: Equilibrium concentration of phase A in contact with B

c_B: Equilibrium concentration of phase B in contact with A

σ: A constant between 0 and 1

The algorithm needed to solve the three equations is outlined as follows [32]:

1) Take s^j, p_i^j and q_i^j as initial values for $s^{j+\sigma}$, $p_i^{j+\sigma}$ and $q_i^{j+\sigma}$ and calculate intermediate concentration profiles $p_{i+1/2}^{j+\sigma}$ and $q_{i+1/2}^{j+\sigma}$.
2) Calculate the future interface position s^{j+1} using equation B.1.
1) Using the new value for s^{j+1}, update the estimate for $s^{j+\sigma}$.
2) Calculate the future interface positions, p_i^{j+1} and q_i^{j+1} for all i using equations B.2 and B.3 and the boundary conditions.
3) Estimates for $p_i^{j+\sigma}$ and $q_i^{j+\sigma}$ are updated using the values for p_i^{j+1} and q_i^{j+1}. Intermediate concentration profiles $p_{i+1/2}^{j+\sigma}$ and $q_{i+1/2}^{j+\sigma}$ are then calculated.
4) Steps 2 to 5 are repeated until successive estimates of the interface position s^{j+1} differ by less than some fixed tolerance. A converged answer corresponds to a solution of the implicit set of descretized equations.

Due to non-monotonic (oscillating) tendencies which can result in solutions obtained using second-order center-difference schemes, Illingworth et. al. [32] suggested using fully implicit up/down-wind approximations which approximates intermediate concentration profiles depending on the interfacial velocity. Using these approximations, equations C.2 and C.3 are re-expressed in an implicit manner depending on the velocity

of the interface. Irregularly spaced discretization has been found to have better convergence for a planar geometry. Further increase in the special discretization was found to have no major effects on the accuracy of the solution and inaccuracies in the numerical solution are mostly due to coarse discretization of time [55]. The procedure used to solve equations C.1 to C.3 and to solve the algorithm necessary to obtain a numerical solution is outlined next.

Initial Approximation of Interface Location

Taking s^j, p_i^j and q_i^j as initial values for $s^{j+\sigma}$, $p_i^{j+\sigma}$ and $q_i^{j+\sigma}$ and calculating intermediate concentration profiles $p_{i+1/2}^{j+\sigma}$ and $q_{i+1/2}^{j+\sigma}$, equation B.1 becomes:

$$s^{j+1} = s^j + \frac{\dfrac{D_B \delta t}{L - s^j}\left(\dfrac{q_1^j - c_B}{v_1}\right) - \dfrac{D_A \delta t}{s^j}\left(\dfrac{c_A - p_{N-2}^j}{1 - u_{N-2}}\right)}{\left[\dfrac{1+u_{N-2}}{2} p_{N-1-1/2}^j + \dfrac{1-u_{N-2}}{2} c_A - (1 - \dfrac{v_1}{2}) q_{1/2}^j - \dfrac{v_1}{2} c_B\right]} \qquad \text{(C.4)}$$

Positive Interfacial Velocity:

$$s^{j+1} > s^j,\ p_{i+1/2}^{j+\sigma} = p_{i+1}^{j+1},\ p_{i-1/2}^{j+\sigma} = p_i^{j+1}$$

Equation C.4 becomes:

$$s^{j+1} = s^j + \frac{\dfrac{D_B \delta t}{L - s^j}\left(\dfrac{q_1^j - c_B}{v_1}\right) - \dfrac{D_A \delta t}{s^j}\left(\dfrac{c_A - p_{N-2}^j}{1 - u_{N-2}}\right)}{\left[c_A - (1 - \dfrac{v_1}{2}) q_{1/2}^j - \dfrac{v_1}{2} c_B\right]} \qquad \text{(C.5)}$$

Negative Interfacial Velocity:

$$s^{j+1} < s^{j},\ p_{i+1/2}^{j+\sigma} = p_{i}^{j+1},\ p_{i-1/2}^{j+\sigma} = p_{i-1}^{j+1}$$

Equation C.4 becomes:

$$s^{j+1} = s^{j} + \frac{\dfrac{D_B \delta t}{L - s^{j}}\left(\dfrac{q_1^{j} - c_B}{v_1}\right) - \dfrac{D_A \delta t}{s^{j}}\left(\dfrac{c_A - p_{N-2}^{j}}{1 - u_{N-2}}\right)}{\left[\dfrac{1 + u_{N-2}}{2} p_{N-1-1/2}^{j} + \dfrac{1 - u_{N-2}}{2} c_A - c_B\right]} \qquad \text{(C.6)}$$

Equations C.5 and C.6 can be easily solved noting the following:

- Initial estimation for s^j is the initial position of the phase A/B interface.
- In addition to the position of the element in phase A having to be user specified, initial estimations of concentrations at each element must also be specified.

  So for N = 32

  u = [0 0.063.....0.995 0.998 1]

  p = [C_F C_F C_F ..... C_F C_F C_A]

  Where C_F is the initial concentrations of the MPD in phase A, and C_A is the concentration in phase A at the boundary (interface).
- Similarly, initial position and initial concentrations at Phase B must also be specified.

  So for M = 64

  v = [0 0.0002 0.001... 0.937 0.968 1]

  q = [C_B C_m C_m .....C_m C_m C_m]

  Where C_B is the concentration in phase B at the boundary (interface) and C_m is the initial concentrations of the MPD in phase B.

Calculation of Future Solute Concentrations in Phases A and B

Phase A:

Positive Interfacial Velocity:

$$s^{j+1} > s^{j} \;.\; p_{i+1/2}^{j+\sigma} = p_{i+1}^{j+1} \;,\; p_{i-1/2}^{j+\sigma} = p_{i}^{j+1}$$

Equation C.2 becomes:

$$-p_{i-1}^{j+1}\left[(\frac{\delta t.D_A}{s^{j+1}}).(\frac{1}{u_i - u_{i-1}})\right]$$
$$+p_{i}^{j+1}\left[s^{j+1}(u_{i+1/2}-u_{i-1/2})+(\frac{\delta t.D_A}{s^{j+1}}).(\frac{1}{u_{i+1}-u_i}+\frac{1}{u_i-u_{i-1}})-u_{i-1/2}(s^{j+1}-s^{j})\right]$$
$$-p_{i+1}^{j+1}\left[(\frac{\delta t.D_A}{s^{j+1}}).(\frac{1}{u_{i+1}-u_i})+(s^{j+1}-s^{j})u_{i+1/2}\right]=p_i^{j}s^{j}(u_{i+1/2}-u_{i-1/2})$$

(C.7)

Negative Interfacial Velocity:

$$s^{j+1} < s^{j} \;,\; p_{i+1/2}^{j+\sigma} = p_{i}^{j+1} \;,\; p_{i-1/2}^{j+\sigma} = p_{i-1}^{j+1}$$

Equation C.2 becomes:

$$-p_{i-1}^{j+1}\left[(\frac{\delta t.D_A}{s^{j+1}}).(\frac{1}{u_i - u_{i-1}})-u_{i-1/2}(s^{j+1}-s^{j})\right]$$
$$+p_{i}^{j+1}\left[s^{j+1}(u_{i+1/2})+(\frac{\delta t.D_A}{s^{j+1}}).(\frac{1}{u_{i+1}-u_i}+\frac{1}{u_i-u_{i-1}})-u_{i+1/2}(s^{j+1}-s^{j})\right]$$
$$-p_{i+1}^{j+1}\left[(\frac{\delta t.D_A}{s^{j+1}}).(\frac{1}{u_{i+1}-u_i})\right]=p_i^{j}s^{j}(u_{i+1/2}-u_{i-1/2})$$

(C.8)

Phase B:

Positive Interfacial Velocity:

$$s^{j+1} > s^{j},\ q_{i+1/2}^{j+\sigma} = q_{i+1}^{j+1},\ q_{i-1/2}^{j+\sigma} = q_{i}^{j+1}$$

Equation C.3 becomes:

$$-q_{i-1}^{j+1}\left[\left(\frac{\delta t.D_B}{L-s^{j+1}}\right).\left(\frac{1}{v_i - v_{i-1}}\right)\right]$$
$$+q_{i}^{j+1}\left[(L-s^{j+1})(v_{i+1/2}-v_{i-1/2}) + \left(\frac{\delta t.D_B}{L-s^{j+1}}\right).\left(\frac{1}{v_{i+1}-v_i}+\frac{1}{v_i-v_{i-1}}\right) + (1-v_{i-1/2})(s^{j+1}-s^{j})\right]$$
$$-q_{i+1}^{j+1}\left[\left(\frac{\delta t.D_B}{L-s^{j+1}}\right).\left(\frac{1}{v_{i+1}-v_i}\right) + (1+v_{i+1/2})(s^{j+1}-s^{j})\right] = q_i^{j}(L-s^{j})(v_{i+1/2}-v_{i-1/2})$$

(C.9)

Negative Interfacial Velocity:

$$s^{j+1} < s^{j},\ q_{i+1/2}^{j+\sigma} = q_{i}^{j+1},\ q_{i-1/2}^{j+\sigma} = q_{i-1}^{j+1}$$

Equation C.3 becomes:

$$-q_{i-1}^{j+1}\left[\left(\frac{\delta t.D_B}{L-s^{j+1}}\right).\left(\frac{1}{v_i - v_{i-1}}\right) - (1-v_{i-1/2})(s^{j+1}-s^{j})\right]$$
$$+q_{i}^{j+1}\left[(L-s^{j+1})(v_{i+1/2}-v_{i-1/2}) + \left(\frac{\delta t.D_B}{L-s^{j+1}}\right).\left(\frac{1}{v_{i+1}-v_i}+\frac{1}{v_i-v_{i-1}}\right) - (1-v_{i+1/2})(s^{j+1}-s^{j})\right]$$
$$-q_{i+1}^{j+1}\left[\left(\frac{\delta t.D_B}{L-s^{j+1}}\right).\left(\frac{1}{v_{i+1}-v_i}\right)\right] = q_i^{j}(L-s^{j})(v_{i+1/2}-v_{i-1/2})$$

(C.10)

Equations C.7 and C.8 are now ready to be solved iteratively. To do so, the equations can be re-expressed in the form:

$$-A_i.p_{i-1}^{j+1} + B_i p_i^{j+1} - C_i p_{i+1}^{j+1} = D_i$$

This yields the following tri-diagonal matrix:

$$\begin{bmatrix} B_1 & C_1 & 0 & 0 & \ldots\ldots & 0 & 0 \\ A_2 & B_2 & C_2 & 0 & \ldots\ldots & 0 & 0 \\ 0 & A_3 & B_3 & C_3 & \ldots\ldots & 0 & 0 \\ . & . & . & . & \ldots\ldots & . & . \\ . & . & . & . & \ldots\ldots & . & . \\ . & . & . & . & \ldots\ldots & . & . \\ . & . & . & . & \ldots\ldots & . & . \\ . & . & . & . & \ldots\ldots & . & . \\ . & . & . & . & \ldots\ldots & . & . \\ . & . & \ldots\ldots & & A_{N-1} & B_{N-1} & C_{N-1} \\ 0 & 0 & \ldots\ldots & & & A_N & B_N \end{bmatrix} \begin{bmatrix} p_1^{j+1} \\ p_2^{j+1} \\ p_3^{j+1} \\ . \\ . \\ . \\ . \\ . \\ p_{N-1}^{j+1} \\ p_N^{j+1} \end{bmatrix} = \begin{bmatrix} D_1 + A_1(p_0^{j+1}) \\ D_2 \\ D_3 \\ . \\ . \\ . \\ . \\ . \\ D_{N-1} \\ D_N + C_N(c_A) \end{bmatrix}$$

Similarly, equations C.9 and C.10 can be re-expressed in the form:

$$-E_i.q_{i-1}^{j+1} + F_i q_i^{j+1} - G_i q_{i+1}^{j+1} = H_i$$

This yields the following tri-diagonal matrix:

$$\begin{bmatrix} F_1 & G_1 & 0 & 0 & \ldots\ldots & 0 & 0 \\ E_2 & F_2 & G_2 & 0 & \ldots\ldots & 0 & 0 \\ 0 & E_3 & F_3 & G_3 & \ldots\ldots & 0 & 0 \\ . & . & . & . & \ldots\ldots & . & . \\ . & . & . & . & \ldots\ldots & . & . \\ . & . & . & . & \ldots\ldots & . & . \\ . & . & . & . & \ldots\ldots & . & . \\ . & . & . & . & \ldots\ldots & . & . \\ . & . & . & . & \ldots\ldots & . & . \\ . & . & \ldots\ldots & & E_{M-1} & F_{M-1} & G_{M-1} \\ 0 & 0 & \ldots\ldots & & & E_M & F_M \end{bmatrix} \begin{bmatrix} q_1^{j+1} \\ q_2^{j+1} \\ q_3^{j+1} \\ . \\ . \\ . \\ . \\ . \\ q_{M-1}^{j+1} \\ q_M^{j+1} \end{bmatrix} = \begin{bmatrix} H_1 + E_1(c_B) \\ H_2 \\ H_3 \\ . \\ . \\ . \\ . \\ . \\ H_{M-1} \\ H_M + G_M(q_{M+1}^{j+1}) \end{bmatrix}$$

The tri-diagonal matrices can now be solved to calculate future concentrations p_i^{j+1} in phase A at all i:

$$K_1 = \frac{C_1}{B_1}, \qquad L_1 = \frac{D_1}{B_1}$$

For i = 2 to N calculate S_i and W_i:

$$K_i = \frac{C_i}{B_2 - A_2 K_{i-1}}$$

$$L_i = \frac{A_2 L_{i-1} + D_2}{B_2 - A_2 K_{i-1}}$$

Knowing that:

$$p_N^{j+1} = L_N$$

Phase B future concentrations can then be calculated recursively using:

$$p_i^{j+1} = K_i p_{i+1}^{j+1} + L_i$$

Similarly, the tri-diagonal matrices can now be solved to calculate future concentrations q_i^{j+1} in phase B for all i:

$$S_1 = \frac{G_1}{F_1}, \qquad W_1 = \frac{H_1}{F_1}$$

For i = 2 to M calculate S_i and W_i:

$$S_i = \frac{G_i}{F_2 - E_2 S_{i-1}}$$

$$W_i = \frac{E_2 W_{i-1} + H_2}{F_2 - E_2 S_{i-1}}$$

Knowing that:

$$q_M^{j+1} = W_M$$

Phase B future concentrations can then be calculated recursively using:

$$q_i^{j+1} = S_i q_{i+1}^{j+1} + W_i$$

Calculation of Future Interface Position:

Using the concentration profiles calculated by solving the tri-diagonal matrices for p_i^{j+1} and q_i^{j+1}, the future interface location can be calculated using the implicit scheme as follows:

Positive Interfacial Velocity:

$$s^{j+1} > s^j,\ p_{i+1/2}^{j+\sigma} = p_{i+1}^{j+1},\ p_{i-1/2}^{j+\sigma} = p_i^{j+1}$$

Equation C.4 becomes:

$$s^{j+1} = s^j + \frac{\frac{D_B \delta t}{L - s^j}\left(\frac{q_1^{j+1} - c_B}{v_1}\right) - \frac{D_A \delta t}{s^j}\left(\frac{c_A - p_{N-2}^{j+1}}{1 - u_{N-2}}\right)}{\left[c_A - (1 - \frac{v_1}{2})q_{1/2}^{j+1} - \frac{v_1}{2}c_B\right]}$$

Negative Interfacial Velocity:

$$s^{j+1} < s^j,\ p_{i+1/2}^{j+\sigma} = p_i^{j+1},\ p_{i-1/2}^{j+\sigma} = p_{i-1}^{j+1}$$

Equation C.4 becomes:

$$s^{j+1} = s^{j} + \frac{\dfrac{D_B \delta t}{L - s^{j}}\left(\dfrac{q_1^{j+1} - c_B}{v_1}\right) - \dfrac{D_A \delta t}{s^{j}}\left(\dfrac{c_A - p_{N-2}^{j+1}}{1 - u_{N-2}}\right)}{\left[\dfrac{1 + u_{N-2}}{2} p_{N-1-1/2}^{j+1} + \dfrac{1 - u_{N-2}}{2} c_A - c_B\right]}$$

If successive estimations of the future interface position s^{j+1} differ by less than some fixed tolerance, then the converged estimate corresponds to a solution of the descretised equations. Once a solution has been obtained for a single time step j, the whole procedure is then repeated to obtain an approximate solution for the next time step and so on.

C.2 User Guide for the Numerical Modeling Program

The program has been written in MatLAB and consists of three sub-programs/functions (Simulator.m, trimatrix1.m and trimatrix2.m) and a main program (TLP.m). User defined inputs are inserted in the main program which calls the function programs. The Simulator.m provides the code required to obtain a numerical solution while the other two functions trimatrix1.m and trimatrix2.m provides the code required to solve the tri-diagonal matrices obtained for phases A and B, respectively.

Similar to the analytical modeling program, boundary conditions must be defined which include the initial concentration of the MPD solute in the filler alloy and the base metal, and the liquidus (c_A) and solidus (c_B) concentrations at the interface. Duration of each time step and the total number of time steps must be defined in addition to the half thickness of the filler alloy and the thickness of the base metal. To run the numerical program the following steps must be followed:

1) Open MatLAB and set the working directory to where the numerical simulation program is installed. All the four m-files of the simulation program must be in the same working directory.

2) Open the TLP.m file and update the user defined inputs as desired in lines 4 to 26 of the code. If the effect of varying process parameters is to be tested then update the variables as desired in lines 61 to 80 of the code as desired. If the effect of varying temperature is to be tested then update variables as desired in lines 89 to 125 of the code as desired.

3) Once desired inputs have been changed save the file and go to the MatLAB command window then type "TLP".

4) Choose a number from 1 to 5 which corresponds to the desired activity shown in the menu.

5) Once simulations are run, results are plotted which can be saved as desired.

C.3 Capabilities and Limitations of the Numerical Modeling Program

The written program has some attractive capabilities which include:

- Multiple simulations can be automatically run which is very useful in testing the effect of varying process parameters such as temperature, filler alloy thickness, base metal thickness and initial concentrations of the MPD solute in the filler alloy and the base metal.
- Once simulations are complete, the program automatically plots three graphs namely: holding time vs. half-width of liquated region, square root of time vs.

half-width of liquated region, and percentage of base metal thickness vs. solute concentration.

- Due to the implicit manner used in solving the algorithm, a stable solution is obtained regardless of the size of the time step used.

Limitations of the numerical modeling program can be summarized as follows:

- MatLAB must be used to run the codes.
- Solutions obtained for slow diffusing MPD solutes or one with low solubility in the base metal such as phosphorous in nickel might require longer computational times.
- Large time steps can affect the accuracy of the numerical solution and can lead to slight truncation errors at the initial stages of simulation. Illingworth et. al. [55] reported that the accuracy of the numerical solution improves by a factor of approximately two as the time step is reduced by half.

References

[1] Beiber G.C., Hihalisin R.J, 2nd International Conference on the Strength of Metals and Alloys, Asilomer, ASM, Vol.4, 1966, p. 1031

[2] Duvall D.S., Oczarski W.A., Weld. J., Vol. 46, No, 9, 1967, p.423

[3] Duvall D.S., Owczarki W.A., Paulonis D.F., Weld. J., Vol. 53, No. 4, 1974, p. 203

[4] Lugsscheider E., Schmoor H., "High Temeprature Brazing and Diffusion Welding", Germany, 1995, p.259

[5] Pouranvari M., Ekrami A., Kokabi A.H., Mat. Sci. Eng., 2008, In Press

[6] "Alloy IN-738: Technical Data", INCO, New York, p.1-11

[7] Sims C., Stoloff N., Hagel W., "Super Alloys II", John Wiley & Sons, New York, 1987, p. 97 – 118

[8] Jena A.K., Chaturvedi M.C., J. Mat. Sci., Vol. 19, 1984, p. 3121

[9] Hagel W.C., Beattie H.J., Iron and Steel Institute Special Report, London, Vol. 64, p. 64

[10] Donachie M.J., Donachie S.J., "Superalloys – A Technical Guide", 2nd ed., ASM International, 2002

[11] Kotval P.S., Venables J.D., Calder R.W., Met. Trans., Vol. 3, 1972, p. 453

[12] Collins H.E, Quigg R.J., Trans. ASM, Vol. 61, 1968, p. 139

[13] Smith W.F., "Structure and Properties of Engineering Alloys", 2nd ed., McGraw-Hill Inc., USA, 1993, p. 487 – 491

[14] Kou S., "Welding Metallurgy", 2nd ed., Wiley & Sons Inc., USA, 2003, p. 3 - 32

[15] Schwartz M., "Brazing", 2nd ed., ASM International, USA, 2003, p. 4 – 61, 341

[16] Jacobson D.M., Humpston G., "Principles of Brazing", ASM International, 2005, p. 3 – 45

[17] Gale W.F., Butts D.A., Science and Technology of Welding and Joining, Vol 9, No. 4, 2004, p. 283-300

[18] Duvall D. S., Owczarski W.A., Paulonis D.F., Weld. J., 1974, Vol. 53, p. 203 – 214

[19] Tuah-Poku I., Dollar M., Massalski T. B., Metall. Trans., 1988, Vol. 19A, p. 675 – 686

[20] MacDonald W.D., Eager T.W., Annu. Rev. Mater. Sci., 1992, Vol. 22, p. 23 – 46

[21] Niemann J. T., Garret R. A., Weld. J., Vol. 52, 1974, p. 175-184

[22] Zhou Y., Gale W.F., North T.H., Inter. Mat. Rev., Vol. 40, No. 5, 1995, p. 181 – 196

[23] Kuntz, Ph.D. Thesis, University of Toronto, 2006

[24] Nakao Y., Nishimoto K., Shinozaki K,, Kang C., International Institute for Welding, Document no. IA-334-86-OE, UK, 1986

[25] Nakao Y., Nishimoto K., Shinozaki K,, Kang C., Schweissen und Scneiden, Germany, Vol. 44, No.2, 1992, p. 87

[26] Gale W.F., Wallach E.R., Met. Trans., Vol. 22 A, 1991, p. 2451 – 2457

[27] Zhou Y., J. Mat. Sci. Let., Vol. 20, 2001, p. 841-844

[28] Tuah-Poku I., Dollar M., Massalski T.B., Metall. Trans., Vol 19A, 1988, p. 675

[29] Lesoult G., Center for Joining of Materials Report, Carnegie Mellon University, Pittsburgh, PA, 1976

[30] Sakamoto A., Fujiwara C., Hattori T. Sakai S., Weld. J., Vol. 68, 1989, p. 63

[31] Ramirez J., Liu S., Weld. J., Vol. 71, 1992, p. 365s

[32] Illingworth T.C., Golosnoy I.O., Gergely V., Clyne T.W., J. Mat. Sci., Vol 40, 2005, p. 2505 – 2511

[33] Zhou Y., North T.H., Mater. Sci. Eng., Vol. 1, No. 4, 1003, p. 505

[34] Shinmura T., Ohsasa K., Narita, Mat. Trans. JIM, Vol. 42, No. 2, 2001, 292

[35] Tanzilli R.A., Heckel R.W., Trans. A.I.M.E. Vol. 242, 1968, p. 2312

[36] Campell C.E., Boettinger W.J., Metall. Mater. Trans., Vol. 31A, 2000, p. 2835

[37] Sinclair C.W., J. Phase Diagram, Vol. 20, No. 4, 1999, p. 361

[38] Sinclair C.W., Purdy G.R., Morell J.E., Metall. Trans. Vol. 31A, 2000, p. 1187

[39] Ikeuchi K., Zhou Y., Kokawa H., North T.H., Metall. Trans. A, Vol. 23A, 1992, p. 2905

[40] Nakagawa H., Lee C.H., North T.H., Metall. Trans A., Vol. 22A, 1991, p. 543-555

[41] Saida K., Zhou Y., North T.H., J. Mater. Sci., Volume 28, 1993, p. 6427

[42] Zorc B., Kosec L., Rev. Metal. Madrid, Vol. 36, 2000, p. 100 – 107

[43] Nakao Y., Nishimoto K., Shinozaki K., Kang C., Advanced Joining Technologies, Chapman & Hall, London, 1990, p. 133-134

[44] Burachynsky V., Cahoon J.R., Metall. Mat. Trans. A, Vol. 28A, 1997, p. 576

[45] MacDonald W.D., Eager T.W., Metall. Mat. Trans. A, Vol. 29A, 1998, p. 315-325

[46] Idowu O.A., Richards N.L., Chaturvedi M.C., Mat. Sci. Eng., A 397, 2005, p. 98 – 112

[47] Tokoro K., Wikstrom N.P., Ojo O.A., Chaturvedi M.C., Mat. Sci. Eng., A 477, 2008, p. 311-318

[48] Ojo O.A., Richards N.L., Chaturvedi M.C., Sci. Tech. W. Join., Vol. 9, No. 6, 2004, p.532 – 540

[49] Ohasa K., Shinmura T., Narita T., J. Phase Equilib., Vol. 20, 1999, p. 199

[50] Tung S.K., Kim L.C., Lai M.O., Scr. Mater., Vol. 34, 1996, p. 763

[51] Liao P.K., Spear K.E. Bull. Alloy Phase Diagr., Vol. 7, No. 3, 1986, p. 550

[52] Nishmoto K., Saida K., Kim D., Nakao Y., ISIJ Int., Vol. 35, No. 10, 1995, p. 1298-1306

[53] Moelwyn-Hughes E. A.: "The kinetics of reaction in solution", Oxford, Clarredon Press, 1947, p. 374

[54] Ekrami A., Moeinifar S., Kokabi A.H., Mat. Sci. Eng A 456, 2007, p. 93-98

[55] Illingworth T.C., Golosnoy I.O, J. Comp. Phy., Vol. 209, 2005, p. 207-225